Damage tolerance of cemented carbides under service-like conditions

A dissertation submitted to partial fulfilment of the requirements for the degree of Doctor of Philosophy by

José Maria Tarragó

Department of Materials Science and Metallurgical Engineering
Doctorate program in Materials Science and Engineering
Universitat Politècnica de Catalunya – Barcelona Tech

Advisor: Luis Miguel Llanes

Barcelona, Spain
September 2016

Cover photo: FESEM micrograph corresponding to unstable crack growth under monotonic loading for Co-base hardmetals. The image corresponds to a serial section obtained with the FIB/FESEM system.

Back cover photo: FESEM micrograph corresponding to stable crack growth under cyclic loads for Co-base hardmetals. The image corresponds to a serial section obtained with the FIB/FESEM system.

UNIVERSITAT POLITÈCNICA DE CATALUNYA
BARCELONATECH
Escola de Doctorat

Acta de qualificació de tesi doctoral

Curs acadèmic:

Nom i cognoms

Programa de doctorat

Unitat estructural responsable del programa

Resolució del Tribunal

Reunit el Tribunal designat a l'efecte, el doctorand / la doctoranda exposa el tema de la seva tesi doctoral titulada "*Damage tolerance of cemented carbides under service-like conditions*"_____

_____.

Acabada la lectura i després de donar resposta a les qüestions formulades pels membres titulars del tribunal, aquest atorga la qualificació:

☐ NO APTE ☐ APROVAT ☐ NOTABLE ☐ EXCEL·LENT

(Nom, cognoms i signatura) President/a		(Nom, cognoms i signatura) Secretari/ària
(Nom, cognoms i signatura) Vocal	(Nom, cognoms i signatura) Vocal	(Nom, cognoms i signatura) Vocal

_____, _____ d'/de _____ de _____

El resultat de l'escrutini dels vots emesos pels membres titulars del tribunal, efectuat per l'Escola de Doctorat, a instància de la Comissió de Doctorat de la UPC, atorga la MENCIÓ CUM LAUDE:

☐ SÍ ☐ NO

(Nom, cognoms i signatura) President de la Comissió Permanent de l'Escola de Doctorat	(Nom, cognoms i signatura) Secretari de la Comissió Permanent de l'Escola de Doctorat

Barcelona, _____ d'/de _____ de _____

Abstract

Cemented carbides, also referred to as hardmetals, are liquid-phase sintered composite materials consisting of at least one hard and wear-resistant phase (WC in the majority of cases) embedded in a soft and ductile metallic one from the iron group (being Co and its alloys the most widely used), acting as a binder. Hardmetals exhibit an outstanding combination of hardness, wear resistance, strength and toughness as a consequence of their fully interpenetrated two-phase structure. This unique combination of properties has established cemented carbides at the forefront of a wide range of engineering and tooling applications operating under extremely demanding service conditions. The key to success of cemented carbides resides in their microstructure, which can be tailored to meet individual requirements for such a range of applications; being the composition, content, size and distribution of the constituents the principal microstructural parameters.

The current situation of hardmetal industry is strongly struggled by the high and volatile prices of raw materials, owing that principal ore mines are located at places hardly accessible to the “industrial world”. At this juncture, producers and end-users are deeply concerned in: (1) increasing the performance and enhancing service-life and reliability of engineering products; (2) improving the efficiency of recycling processes; and (3) replacing current constituents by alternative and less critical materials. Within this context, premature and unexpected fracture, together with wear, is the main damage phenomenon limiting the life in most cemented carbide applications. In the vast majority of cases such ruptures stem from the combination of high monotonic and cyclic stresses, together with different damage-related features associated with harsh service conditions, such as corrosion, impacts and thermal shock. Therefore, relevant consideration of fracture toughness and fatigue resistance is required if reliability (i.e. lower probability of premature and unexpected failures) and lifetime of hardmetal engineering tools and components is to be increased. Following the above ideas, **the purpose of this thesis is to improve the performance and increase the reliability of cemented carbides in rupture-limited applications on the basis of enhanced damage tolerance and reduced fatigue sensitivity through an optimal microstructural design.** Within this framework, this investigation is composed of three main subjects covering different aspects related to the performance of hardmetals under service-like

conditions. The first two sections are devoted to conduct a comprehensive study on the influence of the microstructure on fracture and fatigue behaviour of hardmetals. The aim of the third section is to evaluate microstructural effects on the tolerance of cemented carbides to service-like damage, induced either by localised corrosion or thermal shock.

Main contribution to toughness in cemented carbides derives from plastic stretching of crack-bridging ductile enclaves at the crack wake, referred to as the multiligament zone [1,2]. Hence, the development of a multiligament zone implies the existence of a rising crack growth resistance (R-curve) behaviour, the size of which is dependent on the width and strength of the ligaments; and thus, on the microstructural arrangement. In toughened materials, damage tolerance is successfully promoted with the development of R-curve behaviour. Therefore, higher reliability and strength enhancement can be attained by building microstructures capable of developing toughening mechanisms so that strength becomes less sensitive to flaw size [3]. The main advantage of such strategy is that it permits to allocate appreciable service-damage without compromising the structural integrity of the component. In this regard, **the first section of this thesis is dedicated to carry out a detailed investigation of fracture mechanics and mechanisms in cemented carbides, and to propose a relation to capture microstructural effects on the R-curve characteristics of these materials.** This section also includes a study on the uniaxial compression behaviour of micropillars consisting of Co-binder ligaments constrained by their surrounding WC carbides milled with focused ion beam (FIB). Main purpose of this work is to bring insights on the mechanical deformation and failure behaviour of the constrained ductile metallic ligaments and the carbide/binder interface as key features for determining effective toughening in cemented carbides.

Strength reduction of hardmetals under the application of cyclic stresses is intimately related to the inhibition of the crack-tip bridging mechanism [4]. For WC–Co cemented carbides, the degradation of bridging ligaments is mainly associated with an accumulation of the fcc to hcp fatigue-induced martensitic phase transformation [5]. However, this mechanism does not apply for Ni binders [6,7]; therefore, it remains unclear if effective fatigue susceptibility of Co-base hardmetals is comparable to that of cemented carbides consisting of alternative binders. Moreover, hardmetals exhibit crack-deflection as an additional toughening mechanism, but contrary to the case of crack-bridging, it is immune to fatigue loads [8]. The effective action of this toughening mechanism is speculated to increase with rising carbide mean grain size. Accordingly, it is also the goal of this thesis to assess the microstructural influence on the effective toughening derived from crack-deflection in cemented carbides. Hence, **the second part of this thesis is devoted to study and understand the fatigue sensitivity of cemented carbides consisting of binders with deformation mechanisms beyond phase transformation as well as medium/coarse microstructures.**

As mentioned above, cemented carbides applications are generally subjected to harsh working conditions. These derive in different damage mechanisms that limit their service-life. Within this context, **the third section of this thesis consists of a systematic study on the influence of the microstructure on damage-related features induced by either thermal shock or corrosion, in order to set out guidelines for optimal microstructural design.** In doing so, (1) the structural integrity of damaged cemented carbides is assessed on the basis of residual strength; (2) microstructural effects on damage tolerance are captured by means of considering induced damage level as a critical parameter; and (3) toughness and R-curve characteristics (previously determined) are assumed to be dominant properties for enhanced performance. In addition, thermal shock resistance parameters for studied materials are estimated and invoked as figures of merit for rationalizing structural design of cemented carbides applications subjected to thermal shock.

Keywords: cemented carbides; alternative binders; fracture mechanics; fracture mechanisms; R-curve behaviour; fatigue crack growth; fatigue life; fatigue mechanisms; crack-deflection; corrosion; thermal shock; residual strength; damage tolerance; FIB/FESEM tomography; fractography

Preface

This dissertation includes the research work conducted by the author for obtaining the degree of Doctor of Philosophy at the Universitat Politècnica de Catalunya – Barcelona Tech during the period from the 5th of March 2012 to the 14th of September 2016. This Ph.D. thesis was carried out under the supervision of Prof. Luis Miguel Llanes Pitarch at the Centre d'Integritat Estructural i Fiabilitat dels Materials (CIEFMA) group from the Departament de Ciència dels Materials i Enginyeria Metal·lúrgica (CMEM) of the Universitat Politècnica de Catalunya (UPC). The presented work is original, unless otherwise detailed references are provided.

This Ph.D. thesis is presented as a compendium of published articles and contains eight chapters, which are described hereafter. Chapter 1 describes the state of the art on cemented carbides and their behaviour under service-like conditions. Chapter 2 summarizes the aims and scope of the thesis. Experimental details are described in respective articles but some additional details on the microstructural and mechanical characterization of studied materials as well as on the 3D FIB/FESEM tomography technique are included in Chapter 3. In Chapter 4 the eight articles presented in this thesis are introduced and classified in three main subject areas: (1) fracture behaviour of cemented carbides; (2) fatigue mechanics and mechanisms of cemented carbides; and (3) structural integrity of cemented carbides subjected to service-like damage induced either by corrosion or thermal shock. Full articles are included in Chapters 5 to 7 according to their areas of study. Finally, the summary of the results, the conclusions and the impact and future perspectives of the work are detailed in Chapter 8.

List of publications

This Ph.D. thesis consists of a compendium of the articles presented in the following list. The term IF refers to the impact factor, whereas Q indicates the quartile.

Article I. Tarragó JM, Jimenez-Piqué E, Turón-Viñas M, Rivero L, Al-Dawery I, Schneider L, Llanes L. *Fracture and fatigue behavior of cemented carbides: 3D Focused Ion Beam Tomography of crack-microstructure interactions.* International Journal of Powder Metallurgy 50, 1–10 (2014). IF 0.409, Q4 (58/74) in the category: "Metallurgy and Metallurgical Engineering".

Article II. Tarragó JM, Roa JJ, Jiménez-Piqué E, Keown E, Fair J, Llanes L. *Mechanical deformation of WC–Co composite micropillars under uniaxial compression*. International Journal of Refractory Metals and Hard Materials 54, 70–74 (2016). DOI: 10.1016/j.ijrmhm.2015.07.015. IF 1.989, Q2 (86/260) in the category: "Materials Science, Multidisciplinary" and Q1 (7/74) in the category: "Metallurgy and Metallurgical Engineering".

Article III. Tarragó JM, Jiménez-Piqué E, Schneider L, Casellas D, Torres Y, Llanes L. *FIB/FESEM experimental and analytical assessment of R-curve behavior of WC–Co cemented carbides*. Materials Science & Engineering A 645, 142–149 (2015). DOI: 10.1016/j.msea.2015.07.090. IF 2.567, Q1 (58/260) in the category: "Materials Science, Multidisciplinary", Q1 (5/74) in the category: "Metallurgy & Metallurgical Engineering" and Q2 (36/80) in the category: "Nanoscience & Nanotechnology".

Article IV. Tarragó JM, Coureaux D, Torres Y, Casellas D, Al-Dawery I, Schneider L and Llanes L, *Microstructural effects on the R-curve behavior of WC–Co cemented carbides*, Materials & Design 97, 492–501 (2016). DOI: 10.1016/j.matdes.2016.02.115. IF 3.501, Q1 (43/260) in the category: "Materials Science, Multidisciplinary".

Article V. Tarragó JM, Ferrari C, Reig B, Coureaux D, Schneider L, Llanes L. *Mechanics and mechanisms of fatigue in a WC–Ni hardmetal and a comparative study with respect to WC–Co hardmetals*. International Journal of Fatigue 70, 252–257 (2015). DOI: 10.1016/j.ijfatigue.2014.09.011. IF 2.275, Q1 (12/130) in the category: "Engineering, Mechanical" and Q2 (68/260) in the category: "Materials Science, Multidisciplinary".

Article VI. Tarragó JM, Roa JJ, Valle V, Marshall JM, Llanes L. *Fracture and fatigue behavior of WC–Co and WC–CoNi cemented carbides*. International Journal of Refractory Metals and Hard Materials 49, 184–191 (2015). DOI: 10.1016/j.ijrmhm.2014.07.027. IF 1.989, Q2 (86/260) in the category: "Materials Science, Multidisciplinary" and Q1 (7/74) in the category: "Metallurgy and Metallurgical Engineering".

Article VII. Tarragó JM, Fargas G, Jimenez-Piqué E, Felip A, Isern L, Coureaux D, Roa JJ, Al-Dawery I, Fair J, Llanes L. *Corrosion damage in WC–Co cemented carbides: residual strength assessment and 3D FIB-FESEM tomography characterisation*. Powder Metallurgy 57, 324–330 (2014). DOI: 10.1179/1743290114Y.0000000115. IF 0.772, Q3 (38/74) in the category: "Metallurgy and Metallurgical Engineering".

Article VIII. Tarragó JM, Dorvlo S, Esteve J, Llanes L. *Influence of the microstructure on the thermal shock behavior of cemented carbides.* Ceramics International 42, 12701–12708 (2016). DOI: 10.1016/j.ceramint.2016.05.024. IF 2.605, Q1 (4/26) in the category: "Materials Science, Ceramics".

Contents

List of figures and tables

Figures

Tables

Glossary of symbols and abbreviations

Glossary of symbols

a	Crack length
a_c	Critical crack length
C	Constant of proportionality on the Paris-Erdogan equation
C_{WC}	Contiguity of the carbide phase
d_{WC}	Carbide mean grain size
E	Elastic modulus
$HV30$	Vickers hardness under the application of 30 kgf
K_{Ic}	Plain strain fracture toughness
K_{max}	Maximum crack-tip stress intensity factor
K_{min}	Minimum crack-tip stress intensity factor
K_R	Crack-tip resistance stress intensity factor for crack propagation (R-curve)
K_t	Critical crack-tip stress intensity factor required for crack initiation
K_{th}	Fatigue crack growth threshold
m	Weibull modulus
m'	Exponent of the Paris-Erdogan equation
N	Number of cycles
$N_{WC/binder}$	Number of carbide/ binder interfaces
$N_{WC/WC}$	Number of carbide/carbide interfaces

p	Exponent of the modified Paris-Erdogan equation corresponding to K_{max}
P_f	Probability of failure
q	Exponent of the modified Paris-Erdogan equation corresponding to ΔK
R	First Hasselman's thermal shock resistance parameter referring to crack nucleation
r	Load ratio
R'	Second Hasselman's thermal shock resistance parameter referring to crack nucleation
R''''	Fourth Hasselman's thermal shock resistance parameter referring to crack propagation
S	Stress
S'	Shape factor
t	Crack length normalising parameter for the description of R-curve behaviour
V	Specimen volume
V_0	Normalising volume
V_{binder}	Binder volume content
V_{WC}	Carbide volume content
V^{wt}_{binder}	Binder weight content
α	Carbide phase
α_{CTE}	Coefficient of thermal expansion
β	Binder phase
Δa	Subcritical crack growth under the application of monotonic loads
ΔK	Stress intensity factor range
ΔT_c	Critical temperature difference
η	Eta phase
λ	Heat conductivity
λ_{binder}	Binder mean free path
ρ_c	Composite density
ρ_{WC}	Density of the carbide phase
σ_0	Weibull characteristic strength
σ_{app}	Applied strength

σ_f	Fatigue limit
σ_r	Fracture strength
υ	Poisson ratio

Glossary of abbreviations

FIB	Focused ion beam
SEM	Scanning electron microscopy
FESEM	Field emission scanning electron microscopy
fcc	Face centred cubic
hcp	Hexagonal close packed
PM	Powder metallurgy
REACH	European program for registration, evaluation, authorisation and restriction of chemical substances
NPT	U.S. national toxicology program
EDM	Electrical discharge machining
EBSD	Electron backscatter diffraction
TEM	Transmission electron microscopy
FCG	Fatigue crack growth
SEPB	Single edge pre-cracked beam

Chapter 1

Introduction

1.1. Introduction to cemented carbides

Cemented carbides, also called hardmetals, are a group of powder metallurgy (PM) liquid-phase-sintered materials consisting of brittle refractory carbides of the transition metals (e.g. WC, TiC, TaC and NbC) embedded in a metallic matrix that acts as a binder. The preferential choice for the binder is cobalt. However, alternative binders, principally nickel and iron alloys, have also attracted considerable attention as cobalt substitutes in certain applications. The key to success of cemented carbides resides in their outstanding combination of strength, toughness and wear-resistance. Such remarkable mechanical properties result from the extremely different properties of their two interpenetrating constitutive phases: hard, brittle carbides and a soft, ductile metallic binder (e.g. Refs. [9–11]). As a consequence, they are forefront materials in a wide range of extremely demanding applications, where high tribomechanical performance and improved reliability are required, such as metal cutting, mining, rock drilling, metal forming and wear parts [12].

1.1.1. History and current status of hardmetal industry

The starting point for the use of hardmetals in engineering applications dates from 1923, when Karl Schröter successfully sintered for the first time a WC–Co hardmetal. Schröter's main purpose was to replace diamond in drawing dies to produce tungsten wires for incandescent lamps [13,14]. Three years later, Krupp brought sintered carbides onto the market under the name of "WIDIA". In short time afterwards, cemented carbides started to replace high speed steels in cutting tools due to its superior hot hardness and improved wear resistance [14,15]. This fact involved a drastically increase in cutting speeds, resulting in important savings for machine tool industry. From that moment on, the field of application of cemented carbides rapidly expanded; and in consequence worldwide hardmetal production has steady increased during the last century, as can be seen in **Figure 1.1** [14]. In 2008 world hardmetal production

was about 60,000 tons and was estimated to be worth more than 10 billion euros [16]. Indeed, in 2011 worldwide tungsten consumption for cemented carbides reached 62,000 tons, which represent almost the 60% of worldwide tungsten consumption (including recycled material) [17]. Concretely, tungsten consumption is growing extremely fast in China and nowadays it accounts for almost the 60% of world consumption [17]. Stone working and machining of wood and plastics are the largest fields of application, followed by metal cutting, wear applications and chipless forming. In contrast, metal cutting group accounts for a 65% of the turnover (due to its high degree of innovation and added value), compared to the other hardmetal sectors [18], as shown in **Figure 1.2**.

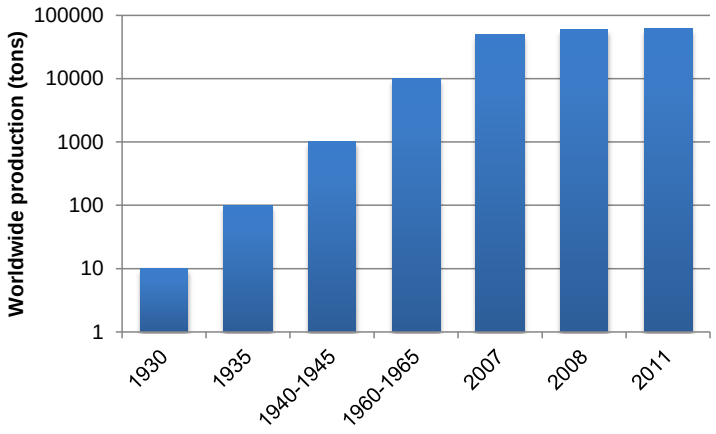

Figure 1.1. Estimated worldwide production of hardmetals in the years from 1930 to 2011 [14,17]. Adapted image from [14].

Since the discovery of the first WC–Co cemented carbide, performance enhancement has been continuous and some of the most outstanding advances of the hardmetal industry are reflected in **Table 1.1** [13]. Current developments in the field of hard materials are mainly related to the scarcity of raw materials that results in high and volatile prices due that main ore mines are located in areas of difficult access to the "industrial world" [16,17]. In addition, hardmetal industry has encountered an important challenge from the health perspective. In fact, the European program for Registration, Evaluation, Authorisation and Restriction of Chemical substances (REACH) [19] and the U.S. National Toxicology Program (NTP) [20] have considered cobalt dust as a toxic and carcinogenic material [17]. Therefore, significant efforts are being devoted to: minimize the use and/or replace raw materials, increase the efficiency of recycling processes, and improve the performance and enhance the lifetime of cemented carbide tools and components [17].

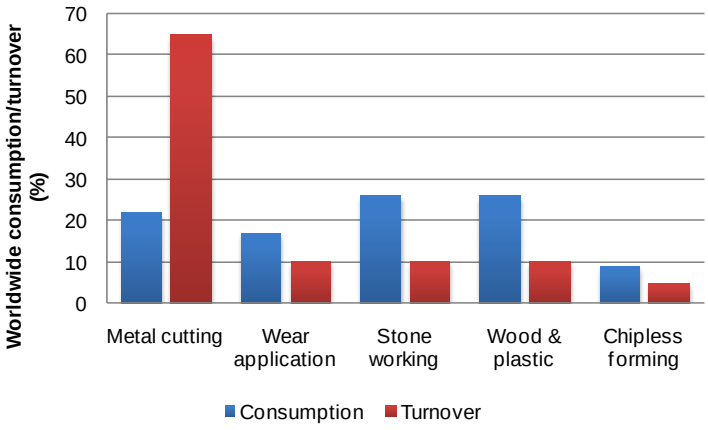

Figure 1.2. General application areas of cemented carbides by worldwide consumption and by turnover; note the significant differences in share due to the strong differences in the degree of added value. Adapted image from [18].

Year	**Event**
1923-1925	Invention of the first WC–Co tool
1929-1931	Development of WC–TiC–Co and WC–TaC(VC,NbC) –Co grades
1938	WC–Cr_3C_2–Co
1948-1970	Manufacturing of submicron WC–Co hardmetals
1965-1975	Hot Isostatic Pressing (HIP)
1965-1978	Application of CVD coatings on hardmetals tools like TiC, TiN and Al_2O_3
1969-1971	Thermochemical surface hardening
1970-1990	Powders recycled by the zinc process
1974-1977	Polycrystalline diamond on WC–base hardmetal
1981	Many thin coatings with AlON layers
1981-2015	Functionally graded cemented carbides
1983-1992	HIP sintering
1985	“CALPHAD” for phase diagram modifications
1990-2010	Fine-grained cemented carbides
1992-1995	Plasma CVD diamond coating
1993-1995	Coatings with complex carbonitrides
1994	Nanocrystalline cemented carbides
2012-	Cemented carbides by additive manufacturing

Table 1.1. Principal developments in the cemented carbide industry from the invention of the first WC–Co tool [13,14,21,22].

1.1.2. Structure of cemented carbides

Tungsten carbide-cobalt (i.e. WC–Co) system is by far the most common hardmetal and its typical microstructure is shown in **Figure 1.3a**. WC–Co is considered as a pseudo-binary section in a three component system W, C and Co. However, if during the manufacturing process the carbon balance is not properly controlled, additional and undesirable phases appear in the structure as can be seen in the vertical section of the W–C–Co phase diagram calculated for a WC–10%$_{wt.}$Co cemented carbide (**Figure 1.3b)** [23]. Then, high C contents result in the presence of graphite, whereas low C contents lead to η-phase (i.e. M_6C or $M_{12}C$, where M is generally Co_nW_n) [24]. Therefore, the principal metallurgical phases found in cemented carbides are the carbide (α) and binder (β) phases.

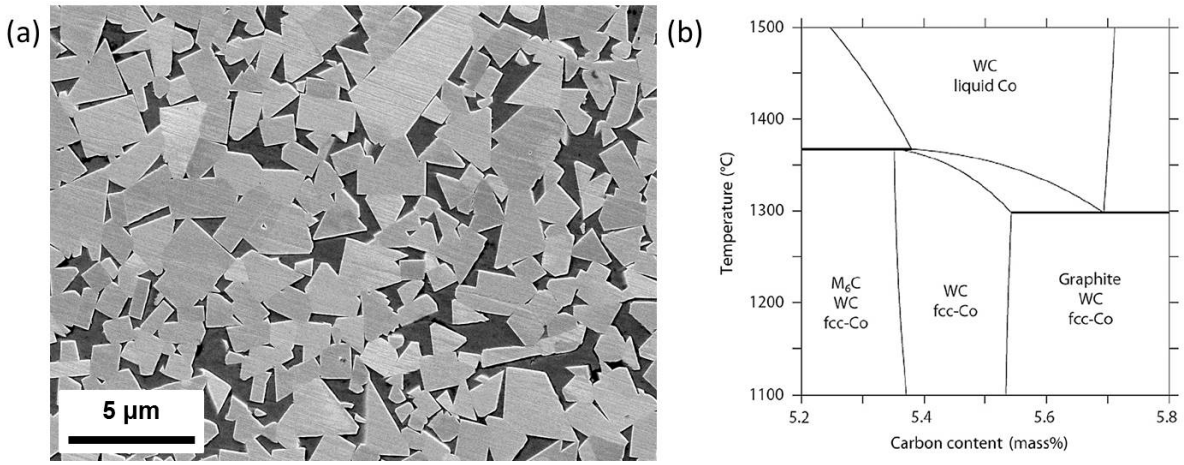

Figure 1.3. (a) Example of the microstructure of a WC–10%$_{wt.}$Co hardmetal and (b) vertical section of the W–C–Co phase diagram calculated for a WC–10%$_{wt.}$Co cemented carbide [23]. Image from [12].

Carbide phase

Generally the carbide phase represents between 65 and 97% in volume of the composite material. In the W–C binary system there exist three different types of carbides: stoichiometric monocarbide WC, subcarbide W_2C and cubic substoichiometric γ–WC_{1-x}. Nevertheless, tungsten monocarbide is the principal hard phase existing in cemented carbides at room temperature. Tungsten carbide exhibits a hexagonal close packed (hcp) structure and its lattice parameters are a = 0.2906 nm and c = 0.2837 nm (**Figure 1.4a**) [9,25]. WC crystals basically grow on the prismatic and basal surfaces, and present three different types of facets, one basal {0001} and two prismatic {1010} [9]. Consequently, they exhibit a marked anisotropy. WC grains have a faceted structure and experiment a tendency to form an equilibrium shape with truncated corners [9,16], as illustrated in the schematic representation of a WC grain shape shown in **Figure 1.4b** [26].

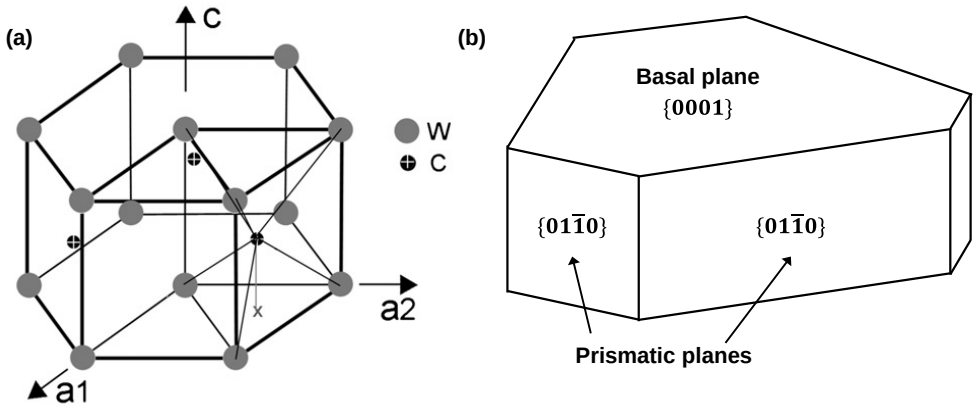

Figure 1.4. (a) WC unit cell with unit lattice vectors: a_1 = 1/3[2-1-10], a_2 = 1/3[-12-10], and c = [0001]. Each tungsten atom is bounded to the six nearest carbon atoms forming two mirror-like triangular prisms [25] and (b) schematic WC grain shape [26].

In addition to WC, MC cubic carbide additions are frequently incorporated in certain applications to enhance hardness and wear resistance at high temperatures, such as in cutting tools for high-speed machining of steels [27]. Concretely, the metals of the IV (Ti, Zr, Hf) and V (V, Nb, Ta) groups are widely considered because they form harder carbides than WC [9]. Among them, TiC is the most used, due to its extremely hot hardness, and the main selection in industrial applications is based on WC–TiC carbides with (Ta,Nb)C additions [27].

Binder phase

Despite of its relative expensive price, cobalt has been the traditional choice for the binder phase in WC based cemented carbides. There are several reasons behind this choice. First, the especially favourable chemical bonding between the WC–Co couple that leads to a very low interfacial energy, nearly perfect wetting and a very good adhesion. That results in products with an outstanding compromise between strength, hardness and toughness. Second, the sintering process is well-known and easily controlled due to the temperature dependent solubility of W and C on cobalt. Third, the fact that cobalt is a ferromagnetic binder that allows non-destructive quality control through the assessment of their magnetic properties, i.e. coercitivity and magnetic saturation [9,12].

Cobalt has a hcp crystallographic structure as the most stable phase at room temperature [16]. However, in cemented carbides the high temperature face centred cubic (fcc) phase is partially stabilized at room temperature. The relative amount of fcc/hcp phases is determined by the W and C content dissolved in the binder, the cooling rate, the plastic strain induced after cooling and the size of the physical domains [28]. Indeed, the fcc structure is frequently the predominant Co phase within the binder,

although some hcp lamellas are also often encountered within binder pools. The binder phase is fully interconnected and Co grains tend to extend over much larger areas than the carbide mean grain size and to enclose several WC particles (e.g. **Figure 1.5**) [29]. The size of the cobalt grains is significantly influenced by the amount of W dissolved in the binder and by the microstructural parameters, i.e. carbide mean grain size and binder content [27,29–31].

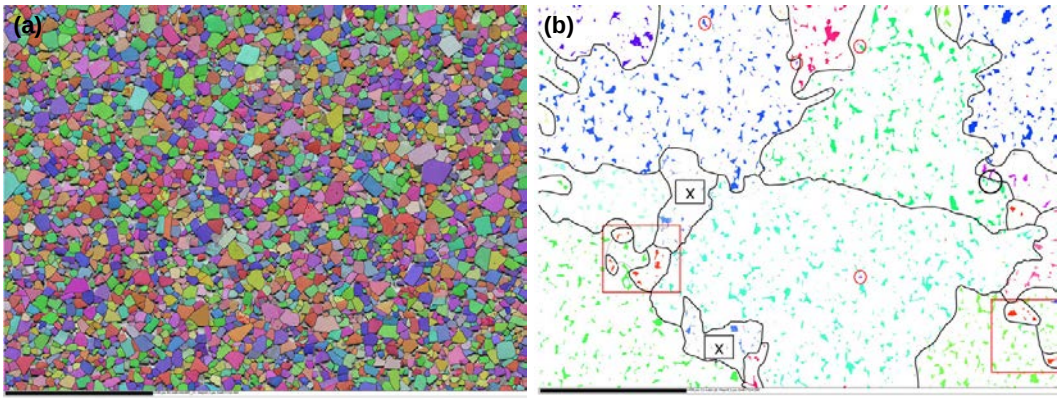

Figure 1.5. Electron Backscattered Scanning Diffraction (EBSD) micrograph of (a) carbide and (b) binder phases of a WC–11%$_{wt.}$Co cemented carbide. Images from [27].

In certain applications Ni and Fe alloys are the preferential binder choice, instead of Co, aiming to increase some specific properties. Concretely, nickel binder is selected in applications involving high corrosive environments, whereas iron-based binders are rather used in small and specific niches of application such as wood-working [12,32]. The special attention received by nickel as an alternative binder to cobalt comes from its similarity in structure and properties, besides its good corrosion resistance. Both, cobalt and nickel exhibit good wettability with WC, and fully dense hardmetals without anomalous porosity can be produced [32]. The principal difference between them is the higher stacking-fault energy of Ni that results in lower hardening rates [17]. Thus, hardness and strength of WC–Co grades tend to be superior to those exhibited by WC–Ni ones. However, the mechanical properties of WC–Ni hardmetals can be enhanced by using solid solution strengthening and dispersion hardening techniques [12], with elements such as Cr [32] and Si [33]. Furthermore, Cr additions result in a large increase of the corrosion resistance of WC–Ni hardmetals [34]. An additional inconvenience for the use of Ni- and Fe-based hardmetals is the reduction of the size of the carbon window for avoiding graphite and eta-phase, in comparison with that of the WC–Co system. It difficult carbon control for a proper sintering process [12,32].

1.1.3. Microstructure of WC–Co/Ni cemented carbides

Mechanical and tribological performance of cemented carbides is closely related to their particular microstructure, being the content and physical dimensions of each constituent phase the most common features for defining them (e.g. Refs. [10,35]). Thus, to understand the mechanical behaviour of cemented carbides it is necessary to study the composition, distribution and size of each of the phases constituting the material. Within this context, the principal parameters used to characterize the microstructure of hardmetals are the average grain size of WC particles (d_{WC}) and the binder volume content. However, both parameters are frequently varied simultaneously, and correlation between property and microstructure requires of additional two-phase normalizing parameters. Among them, the contiguity of the carbide phase, C_{WC}, and the binder mean free path, λ_{binder}, clearly stand out (e.g. Refs. [9,10,13,27]). The former describes the interface area fraction of WC carbides that is shared between them [36], whereas the latter refers to the mean size of the metallic phase. In addition to these key parameters, there are other microstructural aspects that strongly influence the properties of cemented carbides, such as the binder chemical nature [12], the amount of W and C dissolved in the binder [28] and the shape [37] and grain size distribution [38] of the carbides, to name a few. Although the influence of such variables on the performance of hardmetals is widely recognized, normally they are not taken into account when analysing mechanical property-microstructure relations [10].

1.1.3.1. Mean grain size of the carbide phase

The carbide mean grain size is a statistical concept which refers to the average size of the WC particles that compose the hardmetal. WC carbides in hardmetals can have different sizes, going from ultrafine up to extra coarse carbides (**Table 1.2**). The growth of these crystals in each grade depends upon mean size and size distribution of the starting powders, milling and sintering conditions, and composition of the binder [27]. It is interesting to remark that high carbon contents generally promote the growth of tungsten carbides grains. Grain growth inhibitors, such as chromium carbide (Cr_3C_2) and vanadium carbide (VC), are generally required in the finer microstructures to reduce grain growth and to keep a narrow grain size distribution.

Grain size (μm)	Designation
< 0,2	Nano
0.2 – 0.5	Ultrafine
0.5 – 0.8	Submicron
0.8 – 1.3	Fine
1.3 – 2.5	Medium
2.5 – 6	Coarse
> 6	Extra coarse

Table 1.2. Grain size classification of cemented carbides [12].

Binder content

As explained before, the relative content of each phase plays a major role in determining the mechanical properties of cemented carbides. The binder content is usually given in weight percentage but it can be easily converted to volume content by applying the following expression:

$$V_{binder} = \frac{1 + \frac{1-V_{binder}^{wt}}{V_{binder}^{wt}\rho_{WC}}(\rho_{WC} - \rho_c)}{1 + \frac{1-V_{binder}^{wt}}{V_{binder}^{wt}}} \qquad (1.1)$$

where V_{binder} is the binder content in volume, V^{wt}_{binder} is the binder content in weight, ρ_{WC} is the tungsten carbide density (15.65 g/cm^3) and, ρ_c is the experimental density of the composite.

Carbide contiguity

The contiguity of the carbide phase is a key two-phase microstructural parameter that defines the ratio between the grain boundary area occupied by WC/WC interfaces to the total interface area of carbide grains [36]. Similar to grain size, contiguity can be also estimated using the linear intercept method according to the following expression [9,10,39]:

$$C_{WC} = \frac{2N_{WC/WC}}{2N_{WC/WC} + N_{WC/binder}} \qquad (1.2)$$

where $N_{WC/WC}$ and $N_{WC/Binder}$ are the number of carbide/carbide and carbide/binder intercepted interfaces. Roebuck and Bennett [39] studied the contiguity as a function of the binder content for a series of hardmetals and proposed the following empirical relation:

$$C_{WC}(V_{binder})^n = D \tag{1.3}$$

where the best-fitting is obtained when n and D constants take values of 0.45 and 0.2, respectively. However, they pointed out a significant dispersion of C_{WC} values for each specific binder content, associated with different mean sizes and distributions of the carbide phase and to the difficulty to properly interpret all interfaces [10,38,39]. Furthermore, contiguity depends on additional factors such as the carbide particle shape [37,40] or the manufacturing conditions, including sintering time and temperature [41]. Within this context, the author of this thesis and co-authors proposed another empirical relation that considers the simultaneous effect of binder content and carbide mean grain size for contiguity determination in hardmetals based on an extensive data collection from open literature [42]. It is described by the following equation:

$$C_{WC} = 0.036 + 0.973 * exp\left(\frac{-d_{WC}}{3.901}\right) * exp\left(\frac{-V_{binder}}{0.249}\right) \tag{1.4}$$

Binder mean free path

The binder mean free path is a measure of the mean distance between the aggregate carbide grains within the binder material; in other words, it represents the size of the cobalt region in cemented carbides [9]. It constitutes the most important parameter for the characterization of the geometry of the binder phase. In composite materials with a homogeneous distribution of the phases, the equation to estimate the binder mean free path size is given by the expression:

$$\frac{\lambda_{binder}}{V_{binder}} = \frac{d_{WC}}{V_{WC}} \tag{1.5}$$

where V_{WC} is the WC volume content. However, in structures with one predominant phase the mean free path is given by the following equation [39]:

$$\lambda_{binder} = \frac{1}{1 - C_{WC}} \frac{V_{binder}}{V_{WC}} d_{WC} \tag{1.6}$$

The binder mean free path is the appropriate microstructural parameter to relate some specific behaviour with respect to microstructure when both, grain size and binder content, are simultaneously varied. It rises when increasing the carbide mean grain size and/or the volume fraction of the binder. Thus, an increase of the binder mean free path implies a rise of the fracture toughness of the material at the expense of a decrease in hardness [10].

1.1.4. Microstructure-property relations and applications

As already mentioned in previous paragraphs, the microstructure of cemented carbides plays a major role in defining their mechanical properties. In general terms, it can be stated that high binder contents and coarse grain sizes are the proper microstructural selection in applications requiring a high relevance of toughness and enhanced damage tolerance; whereas low binder contents and fine grain sizes are the best choice in those materials demanding wear resistance and high hardness levels. In **Figure 1.6** the dependence of hardness, wear resistance, compressive strength and fracture toughness on binder content is shown for different WC mean grain sizes [43].

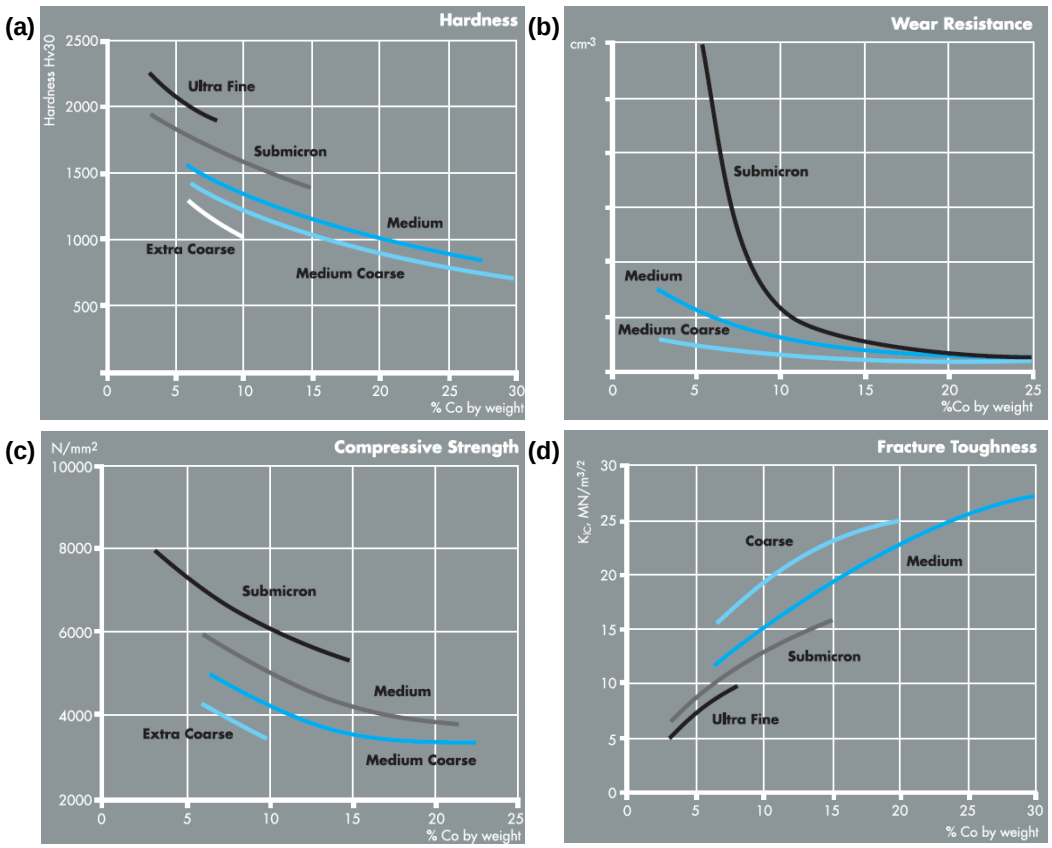

Figure 1.6. Influence of the microstructure on the mechanical properties of cemented carbides: (a) hardness, (b) wear resistance, (c) compressive strength and (d) fracture toughness of cemented carbides as a function of the binder content for different carbide mean grain sizes. Image from [43].

Besides their outstanding combination of mechanical properties, cemented carbides exhibit additional properties that made of them the best choice in a wide range of extremely demanding applications. To name a few, hardmetals exhibit high stiffness and hot hardness values, are extremely good thermal conductors and have a relevant resistance against impacts, thermal shock and corrosion [44]. Accordingly, cemented carbides are forefront materials in the tooling industry and are used in a large number of applications such as: metal cutting, plastic and metal forming, mining, rock drilling, drawing dies, structural components and wear parts [12]. Within this context, the microstructure of cemented carbides can be tailored to reach the best property compromise to maximise the performance according to the in-service conditions to which they are subjected. The application range of cemented carbides as a function of their microstructure is illustrated in **Figure 1.7** [43].

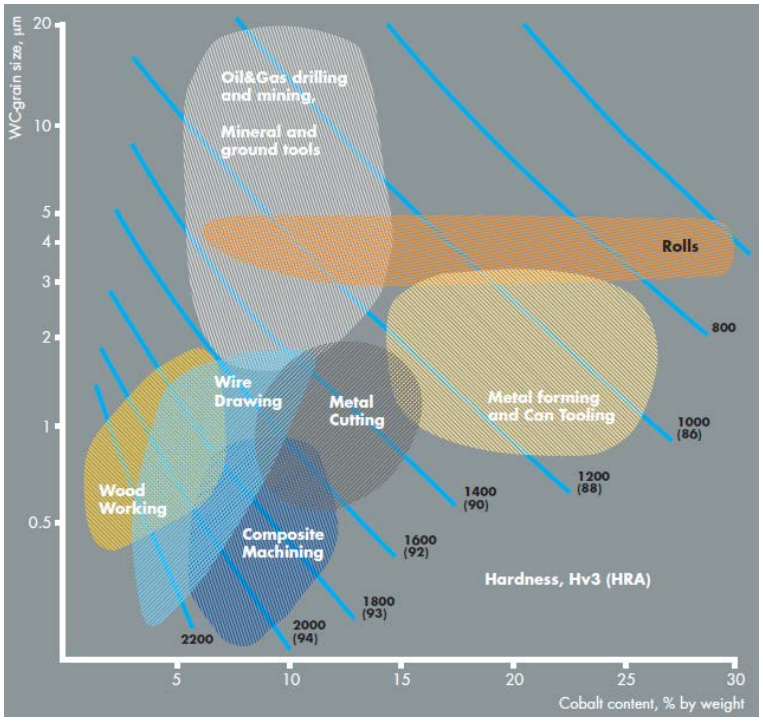

Figure 1.7. Application range of cemented carbides as a function of their WC grain size and cobalt content. Image from [43].

1.2. Fracture behaviour of cemented carbides

Almost all engineering and tooling applications require hard (wear resistant) and tough (damage tolerant) materials. However, in general these properties are mutually exclusive. Within this context, and as already pointed out in the previous section, hard microstructures are characterized by large carbide contents and small carbide mean grain sizes. Meanwhile, the opposite microstructural trend is found in applications demanding high toughness levels [10,12]. Therefore, the majority of hardmetals applications

are microstructurally designed to achieve the best compromise between both properties. Brittle fracture is one of the most common failure mechanisms in the use of cemented carbides, particularly in the implementation of them as either forming tools or structural components [11]. Indeed, such applications are generally submitted to high mechanical forces and contact loads; and thus, are rather rupture-limited. Premature and unexpected failures of components involves important costs, not only for the direct expenses associated with the replacement of the failed piece but also for the downtime to either replace the broken tool or set out the entire engineering system for which the failed component was a single structural element. Thus, such applications require of a higher relevance of toughness for increasing their reliability.

1.2.1. Fracture mechanics and mechanisms

Brittle fracture of cemented carbides, as for other ceramic materials, is governed by unstable propagation of pre-existing flaws which may be processing-, shaping- or service- induced defects (e.g. Refs. [10,45–50]). Therefore, linear elastic fracture mechanics (LEFM) theory has been widely recognized as the theoretical mathematical framework to rationalize their fracture behaviour (e.g. Refs. [45,51–53]). Through the simple application of the Irwin-Griffith criterion, LEFM failure criterion relates the fracture strength (σ_r) with the critical flaw size (a_c) and the plane strain fracture toughness of the material (K_{Ic}) according to the expression [54]:

$$K_{Ic} = Y\sigma_r\sqrt{a_c} \qquad (1.7)$$

where Y is a dimensionless crack/specimen geometric factor. Fracture toughness physically represents the material's resistance to fracture, and is measured as the critical value of the crack-driving force required to propagate a pre-existing crack [55]. This model sustains a failure process consisting on crack initiation from critical defects, and subsequent catastrophic failure without stable subcritical crack growth extension (Δa) before fracture [11].

Within the above framework, hardmetal producers and end-users are concerned in the design of materials combining high strength levels with enhanced reliabilities, especially in the application of cemented carbides as structural components and forming tools [12]. Accordingly, two main strategies may be followed to achieve this objective: flaw control and toughening [3]. On the one hand, the principal purpose of the first approach is to homogenize the size of processing flaws and to minimize the presence of large defects, as the strength of cemented carbides is strongly sensitive to them [11]. On the other hand, the toughening approach attempts to design microstructures capable of providing sufficient fracture resistance such that strength of the material becomes not affected by the size of their flaws. The latter has

the obvious benefit, over flaw control approach, of being able to tolerate appreciable processing flaws and in-service damage without compromising the structural integrity of the material [3].

Toughening in materials can be developed in terms of intrinsic and extrinsic mechanisms [55]. Intrinsic toughening is the predominant mechanism in metallic materials and is mainly related to the generation of a plastic zone ahead of the crack-tip. On the other hand, extrinsic toughening is given by crack-tip shielding mechanisms, acting mostly behind the crack-tip to inhibit crack propagation. There exist a large diversity of extrinsic toughening mechanisms, such as crack-bridging by unbroken fibres or ductile phases in composite materials, transformation toughening, crack-deflection and oxide wedging, among others [55]. Regarding cemented carbides, crack-bridging by strongly bonded metallic reinforcements is the principal toughening mechanism [1,2,56–61], although crack-deflection also plays a significant role [8]. As a consequence, the outstanding fracture toughness levels exhibited by hardmetals are mainly associated with toughening derived from plastic stretching of crack-bridging ductile ligaments [59–61]. Within this context, cracks propagate throughout the composite assembly, leaving isolated metallic ligaments behind the crack-tip. As first described by Evans *et al.* [56], cracks open with increasing applied load, and a multiligament zone develops at the crack wake [1,2,58]. For WC–Co cemented carbides, this zone is reported to measure about five times the microstructural length scale (i.e. the addition of carbide mean grain size and binder mean free path) and to consist of between 2 and 4 ligaments in the direction of crack propagation [1,2]. Accordingly, the energy required to plastically deform the constrained ductile ligaments is the main contribution to toughness of these materials [1,2,56–62]. The deformation behaviour of binder ligaments considerably differs to that of the bulk material, since they are severely constrained by the surrounding carbides. Contrary to the behaviour of a tensile test bar, in which the elongation in the direction of applied load is compensated with a contraction in the perpendicular direction; lateral contraction of binder ligaments is impeded by the surrounding carbides, and their elongation must be compensated with the formation of microcavities inside the ligament to uphold volume constancy [1,2,62]. Using finite element calculations, it was demonstrated that binder sites exposed to a high local plastic strain and stress triaxiality are critical zones for microvoid nucleation [62]. First void will be followed by others along the plane linking the adjacent cracks in the carbide phase, and finally the ligament fractures by void growth and coalescence (**Figure 1.8**) [1,2,57,58,62,63]. Fracture close to the carbide-binder interface proceeds in a similar manner to that in the binder, i.e. by nucleation, growth and coalescence of microcavities. However, in this case shallow and closely spaced microvoids are evidenced running parallel to the binder/carbide interface but within the metallic phase. Fischmeister *et al.* [62] attributed the formation of such finer dimple structure to the fulfilment of high triaxiality conditions in these regions.

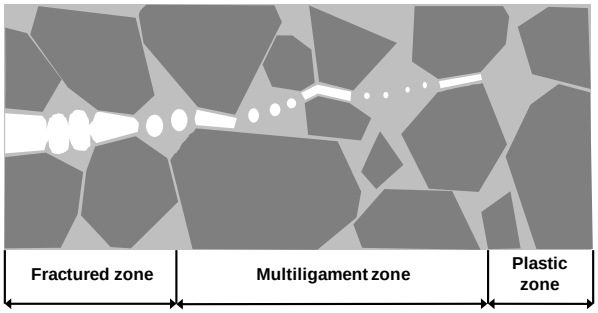

Figure 1.8. Nucleation, growth and coalescence of microcavities within the binder phase during crack unstable propagation. Adapted image from [2].

As in the case for brittle solids reinforced with a ductile phase (e.g. Refs. [64,65]), the development of such multiligament zone implies the existence of a rising crack growth resistance (R-curve) behaviour in hardmetals [8,66–69]. The size of such R-curve is dependent on the width and strength of the ligaments [61,67,70]; and thus, on the microstructural arrangement of the composites under consideration. R-curve behaviour may be described as the ability of a microstructure to develop toughening mechanisms on an advancing crack, which can be done, for example, by screening the crack-tip from the far-field driving force [65,71,72]. In the case of ceramics toughened by ductile reinforcements, the magnitude of these stresses increases with crack extension due to the formation of new bridges at the crack wake until a plateau is reached (i.e. steady-state value corresponding to plane-stress fracture toughness) [63]. The existence of such rising R-curve behaviour implies beneficial effects on reducing strength scatter (i.e. increasing strength reliability) and enhancing damage tolerance [3,71].

Contrary to LEFM failure criterion, one of the particularities of materials exhibiting R-curve behaviour is that cracks may grow stably before reaching a critical size where unstable crack extension takes place [65,73]. In this case, subcritical crack growth propagation before fracture is defined by the instability criterion, i.e. when tangency conditions are satisfied [65]:

$$\begin{aligned} K_{app} &= K_R \\ \frac{dK_{app}}{da} &= \frac{dK_R}{da} \end{aligned} \tag{1.8}$$

where K_{app} is the applied stress intensity factor, K_R is the crack-tip resistance stress intensity factor and a is the crack length. Both variables may be related to the applied strength (σ_{app}), according to LEFM basic equation [54]:

$$K_{app} = Y\sigma_{app}\sqrt{a} \tag{1.9}$$

In **Figure 1.9** a schematic representation of crack-growth resistance curves for a material with flat and a rising R-curve is shown [71]. The condition required for unstable fracture is fulfilled when the driving force for crack propagation increases faster than the material resistance to fracture; i.e. when the driving force as a function of the crack size is tangent to the crack growth resistance curve. A material exhibiting a flat R-curve curve always fractures at the same crack-tip resistance stress intensity factor level, i.e. there is a unique toughness value that unambiguously characterizes the material. On the other hand, materials having a rising R-curve behaviour develop different toughness levels (K_{eff}) depending on both, R-curve shape and initial crack size (a_0). Moreover, materials whit a flat R-curve does not experience stable subcritical crack growth and the initial crack size is the same as the critical one. However, in rising R-curve materials cracks grow stably before reaching the critical size for triggering unstable crack extension [71].

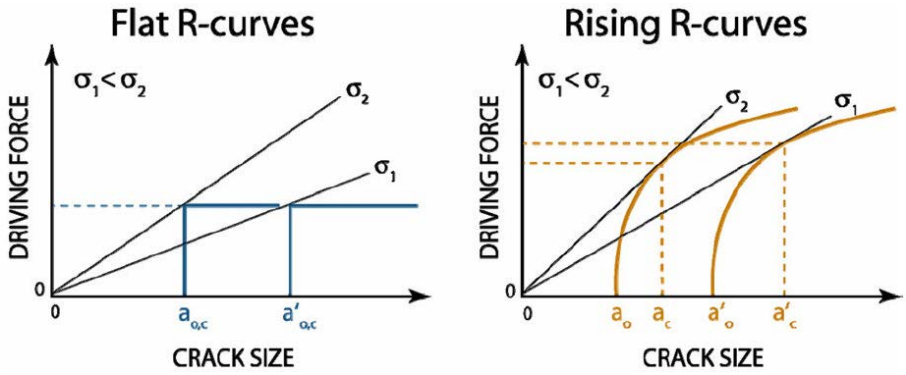

Figure 1.9. A schematic representation of crack-growth resistance curves for a material exhibiting a flat and a rising R-curve. Image from [71].

Two important factors must be contemplated when studying the fracture behaviour of cemented carbides. First, failure of hardmetals is intimately related to the propagation of pre-existing flaws. Second, they exhibit a marked R-curve behaviour. Therefore, in high-strength materials exhibiting R-curve behaviour, critical flaws are longer than processing defects but they are still “short cracks”. Under these considerations, multiligament zone does not get fully developed at rupture, and crack-tip resistance steady-state level is not reached [65,68]. Within this failure scenario, both R-curve shape and initial defect size (a_0) significantly influence the effective developed toughness level (K_{eff}) as well as the subcritical crack length reached before fracture. Consequently, the strength of cemented carbides is notably influenced by the R-curve characteristics and the defect population distribution.

1.2.2. Fracture behaviour within the framework of Weibull statistics theory

As previously commented, fracture behaviour of cemented carbides is of stochastic nature as it originates from the propagation of pre-existing defects [15,45,46,74–76]. Therefore, the strength of cemented carbides depends on the size, position, orientation and nature of the major flaw and exhibit wide scatters, due to the variability associated with defects size probability distribution. Consequently, strength is size-dependent as the probability of finding a major flaw increases when rising specimen size. Therefore, probabilistic failure mechanics are essential for proper design with this brittle-like material [73,77]. Within this context, Weibull statistics are claimed as the suitable approach to rationalize not only the rupture strength of hardmetals, but also their strength scatter. The latter is a parameter of enormous importance when designing with brittle materials [78].

This statistical approach is based on the theory of the weakest link, which establishes that the component or sample breaks when the weakest element fails. The application of Weibull statistics to rupture strength of materials describes the probability of failure (P_f) of specimens of a given volume, V, subjected to a homogeneous applied tensile stress state, σ_{app}, to cause fracture according to the expression [79]:

$$P_f(\sigma, V) = 1 - exp\left[\frac{V}{V_0}\left(\frac{\sigma_{app}}{\sigma_0}\right)^m\right] \qquad (1.10)$$

where V_0 is a normalising volume, and m and σ_0 are the Weibull modulus and characteristic strength, respectively. The former describes the strength scatter (i.e. m rises when decreasing the strength scatter), and the latter represents the stress state required for having a 63.3% probability of failure.

According to Weibull distribution standards [80], the range of failure probabilities covered by the experimental assessment of the Weibull curve increases with the dimension of the sample (i.e. the number of tested specimens). However, due to high specimen's costs, the number of specimens is usually limited and careful attention must be paid when extrapolating strength values to really low probabilities of failure and/or to different effective loaded volumes [81].

1.3. Fatigue behaviour of cemented carbides

The great majority of hardmetals applications are subjected to cyclic and repetitive loads; and consequently fatigue represents, together with wear and corrosion, one of the principal failure mechanisms. In addition, similar to the case of brittle fracture, fatigue failures are generally premature

and unexpected. Therefore, they often require of an overall stop of the engineering system, bringing high additional costs [82]. Hence, the resistance against fatigue becomes a critical design parameter in the majority of cemented carbides applications. From the above information it is clear that an accurate description and understanding of the fatigue behaviour of hardmetals is required if the performance of engineering parts made of these materials are to be optimized. However, literature devoted to study the influence of the microstructure on the fatigue behaviour of cemented carbides is rather scarce and almost limited to the straight WC–Co system [82].

1.3.1. Strength degradation under the application of cyclic loads

Fatigue can be defined as a progressive and localized damage that occurs when a material is subjected to cyclic loading. It involves initiation and evolution of cracks at loads that are too low to cause failure under monotonic loading. The most common method for evaluating the fatigue behaviour of structural materials is the applied stress–fatigue life approach (*S–N* curve), also known as the Whöler plot. This curve consists on a graph where the cyclic stress (*S*) is plotted against the number of cycles to failure (*N*), the latter in a logarithmic scale. This test methodology includes an interesting parameter, the endurance limit, which refers to the maximum stress level for specimen survival under a given number of cycles. Moreover, if for a given cycling stress state the material has an "infinite fatigue life", usually in the range between 10^6 to 10^8 cycles, the endurance limit can be also referred to as the fatigue limit (σ_f) [82,83].

The susceptibility of cemented carbides to be degraded under the application of cyclic loads is a fact known since 1941 [84]. However, the vast majority of published investigations devoted to study the fatigue behaviour of hardmetals are concentrated from the 80s until now [82]. From them, it is noteworthy the systematic and extensive investigation reported by Sockel's group following the S–N testing approach (e.g. **Figure 1.10a**) and complemented with a comprehensive study of fatigue micromechanisms based on Scanning Electron Microscopy (SEM) and Transmission Electron Microscopy (TEM) [5,85–91].

Hardmetals are extremely susceptible to the application of cyclic loads, and fatigue limit values up to 30-40% of the corresponding bending strength have been reported [5,85,86,90,91]. This fatigue susceptibility is mainly associated with the degradation of the metallic phase [5–7,85,86,89–91]. Therefore, a relevant influence of the microstructure on the susceptibility of cemented carbides to strength degradation (i.e. fatigue sensitivity) is to be expected. In fact, binder content and composition are the main parameters influencing fatigue response, even though the carbide mean grain size also plays a significant role [86,90,91]. Sockel's group investigated such fatigue susceptibility on the basis of the

Whöler plots slope, which is merely indicative of the ratio between the monotonic strength and the fatigue limit [5,85,86,90,91]. In such a way, they were able to determine an increase of fatigue sensitivity with binder mean free path, as shown in **Figure 1.10b** [85]. They also discerned a significant influence of the binder chemical nature on fatigue sensitivity, concluding that plain Co binder has a higher susceptibility to be degraded under cyclic loads than NiCo, FeCoNi and FeNi binders [90,91]. As already pointed out by Krawitz and co-workers [7], Co binder fatigue degradation was rationalized on the basis of the accumulation of a fatigue-induced fcc to hcp phase transformation [5,90,91]. This deformation micromechanism restricts significantly the ductility of the metallic binder, recognized as the main toughening phase in cemented carbides [1,2,58,92]. However, the prevalence of this deformation mechanism diminishes and/or disappears when replacing cobalt by alternative binders, such as Ni and Fe [6,7,90,91].

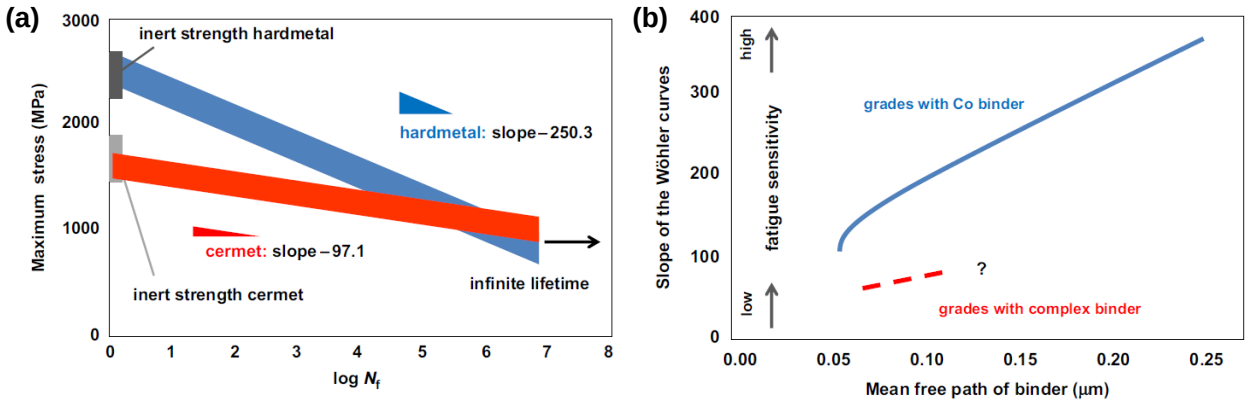

Figure 1.10. (a) *S–N* curves for a representative hardmetal and cermet grades, and (b) correlation of the slope of the *S–N* plots, as a measurement of fatigue sensitivity, with the mean free path of binder [85]. Images from [82].

1.3.2. Fatigue crack growth behaviour

The above described *S–N* approach is the classic and most widely used method to study the fatigue behaviour of structural materials. However fracture mechanics theory also offers an extensively accepted framework to evaluate the fatigue response of materials. This approach is based on assessing the number of loading cycles required to propagate the largest pre-existing flaw to failure [82]. Thus, it describes the fatigue crack growth (FCG) rates as a function of the range (ΔK) and/or the maximum (K_{max}) stress intensity factor. Although the *S–N* approach is simpler than the fracture mechanics one, the latter offers three obvious benefits over the former: (1) it is invariably more conservative, as this theory is defect tolerant and considers that the structures are inherently flawed; (2) it enables a quantitative evaluation of the damaging effect of flaws or defects within the material; and (3) it provides a rational basis for quality control of the product [82,83,93]. Thus, on the basis of the well-established assumption indicating that

subcritical crack growth of pre-existing defects is the controlling stage for fatigue failure in cemented carbides [5,85,86], the description of the FCG rates as a function of ΔK and/or K_{max} appears as a suitable methodology for evaluating the fatigue behaviour of these materials.

Nowadays it is fully accepted that the FCG behaviour of cemented carbides obeys a Paris-Erdogan equation:

$$\frac{da}{dN} = C\Delta K^{m\prime} \qquad (1.11)$$

where *da/dN* is the crack growth per cycle and *C* and *m'* are microstructurally dependent constants. However, contrary to the case of metals alloys having *m'* values lying between 2 and 4 [94], cemented carbides exhibit FCG rates with an extremely large powder-dependence on ΔK, as indicated by the high *m'* values within the 10 to 20 range [4,8,95–98].

Similar to the extensive investigation on hardmetals fatigue behaviour carried out by Sockel's group following the *S–N* approach, a large research program was conducted by Llanes group with the purpose of acquiring a deep knowledge on FCG mechanics and mechanisms of cemented carbides [4,8,97–99]. Within this context, special effort was devoted to evaluate the influence of the microstructure on the relative dominance between the static and cyclic failure modes as well as on the fatigue sensitivity of cemented carbides, this parameter being defined for pre-cracked specimens as the ratio between the FCG threshold (K_{th}) and fracture toughness [82].

Research program conducted by Llanes's group elucidated several aspects on the fatigue behaviour of cemented carbides, the main being summarized hereafter. First, as already postulated by Fry and Garret [96], a predominance of static over dynamic failure modes was evidenced, i.e. FCG rates were found to exhibit a higher dependence on K_{max} than on ΔK [4,97]. Furthermore, a modified Paris-Erdogan equation of type $da/dN = CK_{max}^{p}\Delta K^{q}$ was proposed for assessing the relative dominance of K_{max} over ΔK on the basis of the *p/q* ratio. In doing so, a decreasing prevalence of static over dynamic failure modes was discerned when increasing the binder mean free path (**Figure 1.11**) [4,82,97]. Second, a strong microstructural influence on fatigue sensitivity of hardmetals, depending on the compromising role played by the metallic binder as both toughening and fatigue susceptible agent, was evidenced (**Figure 1.11**) [4]. Third, Torres *et al.* proposed and validated the fatigue crack growth threshold as the effective toughness under cyclic loading [97,98]. This was done on the basis of: (1) considering subcritical crack growth of pre-existing flaws as the controlling stage for fatigue failure; and (2) assuming that fracture behaviour of hardmetals can be successfully rationalized within fracture mechanics framework.

Therefore, this methodology allowed correlating FCG and fatigue limits approaches, within an infinite life framework. Fourth, in accordance with previous published data [96], mean stress effects (i.e. associated with the applied load ratio, $r = K_{min}/K_{max}$) on the fatigue limit were discerned [97]. Hence, mean stress effects may be described according to a Goodman-like curve whose slope corresponds to the fatigue sensitivity under zero mean stress conditions (i.e. $r = -1$) [97].

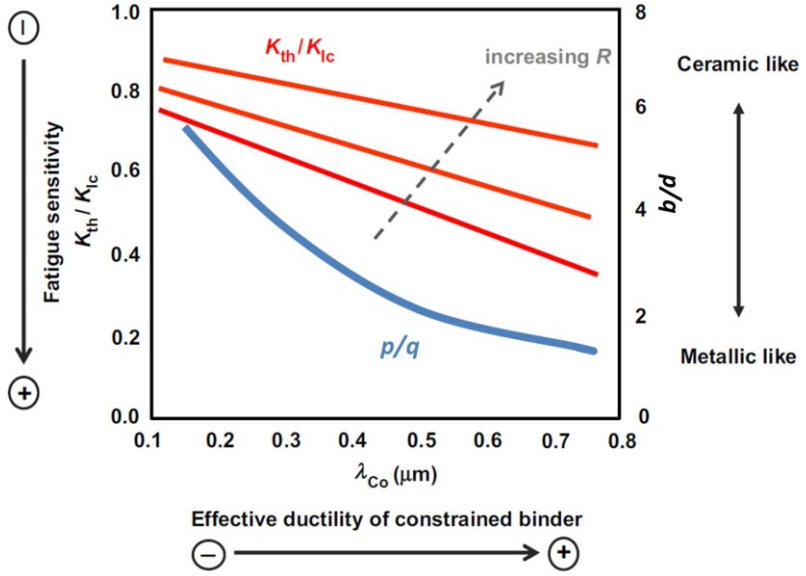

Figure 1.11. Fatigue sensitivity and *p/q* ratio evolution as a function of the binder mean free path for WC–Co cemented carbides [4]. Image from [82].

1.4. Service-like damage in cemented carbides

Hardmetals are found at the forefront of a wide range of engineering products that operate under harsh working conditions. Indeed, cemented carbides are the preferential choice in almost all the applications where the best solution to wear, impact, corrosion and thermal shock is sought [12]. However, despite their outstanding combination of properties, hardmetals suffer from different in-service degradation phenomena that seriously affect the performance and service-life of engineering structural parts. Among them, corrosion and thermal shock are two of the principals and are found in a large number of applications. The former is found in applications exposed to chemically aggressive media, including a wide variety of corrosive environments, such as lubricants, chemical and petrochemical products, and mine and sea waters, among others (e.g. Ref. [48,100–102]). Thus, areas of application where corrosion resistance is one of the main criteria for the choice of a suitable grade include: wear parts, particularly in the oil industry and for submarine applications; tools and die industry; and wood-machining parts, to name a few [12]. Thermal shock, although receiving less attention than corrosion, is

also encountered in several applications. Hence, thermal cracking and thermal fatigue [12,13,82,103,104] are recognized as common modes of failure of cemented carbide tools in different applications, such as: intermittent cutting [104,105], rock drilling [100] and some wear parts [12].

1.4.1. Corrosion behaviour

In acidic and neutral pH solutions, hardmetal corrosion process consists on a galvanic couple where the binder is selectively attacked due to its anodic role [106–108], whereas WC particles are cathodically protected [108,109] (**Figure 1.12**). In addition, due to the larger surface area covered by ceramic particles, corrosion in anodic sites gets enhanced [108]. The opposite trend is found in basic solutions, where ceramic particles dissolve and the binder phase passivates [110,111]. Corrosion mechanisms in cemented carbides are really complex and depend on a large number of factors such as surface state, corrosive media, hardmetal microstructure and binder chemical nature. Furthermore, corrosion system is in constant evolution due to the continuous changes produced by the cathodic and anodic reactions taking place at the surface [108].

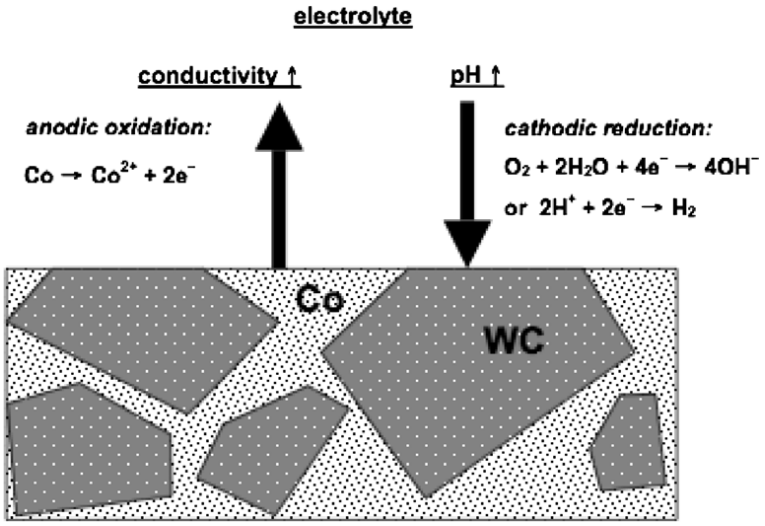

Figure 1.12. Schematic presentation of the reactions taking place on the WC–Co surface. Image from [108].

Since the metallic binder is the most susceptible phase to corrosion in acidic and neutral media, major efforts for improving the corrosion resistance of hardmetals have been focused on mitigating the dissolution of the binder phase. Within this context, the total or partial substitution of cobalt binder by alternative alloys, which have inherently a higher corrosion-resistance, significantly improves the corrosion performance of hardmetals in a large variety of neutral and acidic environments [12,106,107,112–114]. Furthermore, alloying the metal binder with small additions of Cr, up to the

solubility limit of the binder, dramatically decreases corrosion rates [12,107,109,112,114–116]. In fact, Cr_3C_2 is frequently added in cemented carbides with grain-refining purposes [13,117–119]. During sintering, main part of the chromium dissolves into the binder and that results in a beneficial effect against corrosion due to the formation of a passivating Cr_2O_3 film at the binder surface [109,111,116]. Similar to chromium carbide, Mo_2C is added for inhibiting grain growth and improving the wettability between the binder-WC couple [120], but also rises corrosion resistance due to the formation of a MoO_3 layer that enhances pitting corrosion resistance [121].

The potential of the system plays a critical role in defining corrosion mechanisms of cemented carbides. In acidic and neutral solutions, at low potentials the binder phase dissolves while the WC grains remain catholically protected [108,122]. Anodic polarization curve exhibits a pseudopassive region at intermediate potentials, due to the formation of a non-adhered layer at the surface consisting of corrosion products that difficult the diffusion of cobalt ion [113,123]. In the third region, corresponding to high applied potentials, the WC phase is oxidized [106–109,113,123] and a surface WO_3 layer is formed [113,123]. Further, during the anodic polarization, Co dissolves and forms an inner CoO layer and a $Co_{3-x}O_4$ outer layer, whose composition depends on the pH and passivation potential [113]. An example consisting of two polarization curves measured for two different WC–Co cemented carbides is shown in **Figure 1.13** [122].

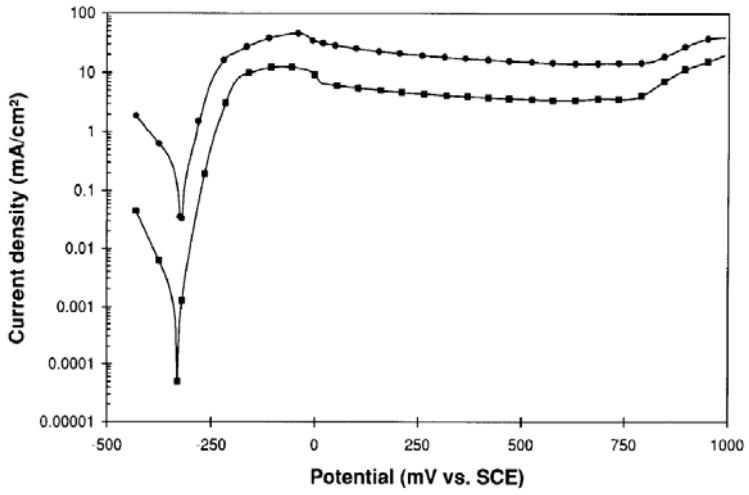

Figure 1.13. Examples of full polarization scans measured for WC–6Co%$_{wt.}$ (square) and WC–16.5Co%$_{wt.}$ (circles) cemented carbides. Image from [122].

In-service performance of cemented carbides is not only dependent on their intrinsic mechanical properties but also is highly influenced by their resistance to the aggressive medium to which are exposed. Within this context, corrosion attack exposes WC grains, resulting in a noticeable increase of wear rates. Accordingly, several studies have been focused on studying the synergic effects between

erosion/abrasion and corrosion on the wear rates of cemented carbides (e.g. Ref. [110,124–126]). Furthermore, corrosion damage may also induce a detrimental effect on the fracture strength and fatigue resistance of hardmetals, promoting a premature and un-expected failure [48,82,102,127]. However, to the best knowledge of the authors, only two studies have been addressed to correlate strength reduction and corrosion damage in cemented carbides. Both of them pointed out relevant strength degradation due to the stress raising effects produced by localized corrosion damage in the form of pits [48,102]. Thus, from a structural integrity perspective, it is essential to understand the detrimental impact that corrosion damage may induce in the performance of cemented carbides components.

1.4.2. Thermal shock resistance

Despite the exceptional thermal conductivity and excellent fracture toughness of hardmetals in comparison with ceramic materials, WC–Co cemented carbides are sensitive to thermal shock due to its brittle-like nature behaviour [128,129]. Thus, sudden temperature changes may result in the apparition of subcritical microcracks or even in the catastrophic failure of the structural component. However, studies devoted to investigate the thermal shock resistance of hardmetals are relatively scarce [128–134], and only a few of them correlate induced damage by thermal shock with resulting remnant properties [128,130].

The measurement of the retained strength after a quench test is the most widely used method for evaluating thermal shock resistance of ceramics. The test consists in determining the critical thermal shock temperature differential (ΔT_c) above which the residual strength is reduced up to values of 70% the average strength measured at room temperature [135]. Within this context, when the microstructure plays a critical role in defining thermal shock resistance, Hasselman theory is frequently invoked to rationalize thermal shock behaviour. This theory consists of several parameters (i.e. *R* parameters) defining the resistance of the material to either crack initiation or propagation due to thermal shock [136–139]. First Hasselman thermal shock parameter (i.e. the *R* parameter) was described by Kingery [137] in the middle 50's. However, it was not until a few years afterwards that Hasselman introduced the *R''''* parameter [138], and later on he proposed the unified thermal shock theory [139]. First Hasselman parameter is defined as follows:

$$R = \frac{\sigma_r(1-\nu)}{E\alpha_{CTE}} \tag{1.12}$$

where ν is the Poisson ratio, E is the elastic modulus and α_{CTE} is the coefficient of thermal expansion. However, in the case of a poor surface heat transfer, the heat conductivity (λ) must be also considered. It is reflected in the second Hasselman parameter (R')

$$R' = \frac{\lambda \sigma_r (1-\nu)}{E \alpha_{CTE}} \tag{1.13}$$

On the other hand, the R'''' parameter describes the condition necessary for the propagation of thermal shock induced cracks, and is given by:

$$R'''' = \frac{1}{2(1-\nu)} \left(\frac{K_{Ic}}{\sigma_r}\right)^2 \tag{1.14}$$

Within this framework, Mai successfully rationalized thermal shock behaviour of cemented carbides according to resistance parameters extracted from Hasselman's theory for two tool carbides [128]. In doing so, he suggested that the resistance to degradation of carbide tools under thermal shock can be described and correlated according to two different parameters: $\lambda\sigma_r/E\alpha$ for crack initiation and $(K_{Ic}/\sigma_f)^2$ for crack propagation.

In addition to material properties and the critical temperature difference, there are several factors that have a relevant influence on the performance of a body subjected to thermal shock. Buessem proposed a classification of these factors in three groups defining different issues [136]: (1) thermal shock conditions; (2) geometry of the solid body; and (3) material properties. The first group includes temperature difference and heat transfer coefficient. The second one considers size and shape of the body. Finally, the third group accounts for coefficient of thermal expansion, elastic properties, fracture strength and fracture toughness [136,137]. The shape of the body is an extremely important aspect in determining the critical temperature difference. In general, it is recommended to avoid corners and edges, since they can act as thermal stress concentrators [137]. Hence, the critical temperature difference to crack a specimen can be defined as the crack initiation resistance parameter, either R or R', multiplied by a shape factor (S') (i.e. $\Delta T_c = R \cdot S'$ or $\Delta T_c = R' \cdot S'$) [137].

From a physical viewpoint, thermal shock damage in cemented carbides principally proceeds through the nucleation of microcracks at the carbide/binder interface which tend to propagate avoiding the hard phase [131,132,134]. This is due to the large difference between coefficients of thermal expansion of WC and Co phases as well as to the high elastic modulus of the composite material. Thus, severe temperature changes generate significant large thermal stresses that may induce the formation of

microcracks at the carbide/binder interface [131,132]. Maximum cooling tensile stresses are concentrated at the surface [133,140], and the magnitude of these induced stresses is a direct function of: coefficient of thermal expansion, elastic modulus and temperature difference [133].

1.5. Focused Ion Beam system

The commercial use of FIB systems started about 30 years ago for their use in the microelectronics industry, but it was not until the early 90s that become popular in a broader range of Material Science topics [141]. When equipped with an additional SEM column, it can be used for a large number of applications including TEM foils preparation, micromachining of specimens, cross-section milling, atom probe post preparation, and 3D FIB/FESEM tomography [141].

The operation principle of the FIB microscope consists of sputtering atoms onto a target material, with a high energetic gallium ion beam. The ions are generated from a Ga liquid metal ion source composed of a Ga reservoir mounted above of a tungsten needle. Ga source is heated up to its melting point and then it flows to the tip of the needle. An intense electric field is produced at the source tip that ionizes the gallium, draws the liquid metal into the fine tip, of about 2-5 nm in diameter, and extract ions from that narrow tip. The Ga ions are accelerated down the column in an electrical field of about 30 KeV and sputtered over the region of interest [141,142]. Initial FIB systems were equipped with a single beam that was used for both imaging and preparing microstructural cross-sections. However, this system had several limitations and nowadays a great number of FIB systems are equipped with an additional SEM column, which allows an improved flexibility by using the FIB column preferentially to cross-section and the SEM one to image [141].

1.5.1. 3D FIB/FESEM Tomography

Tomography is a method to obtain a three-dimensional (3D) image of the internal structures of a solid object through the reconstruction of ‘slices’ (i.e. a tomographic image) of sequential cross sections. This technique is used in a large number of sciences, such as medicine, biology and archaeology, besides materials science. In recent years, this technique has received an increasing interest for the characterization of materials, as it allows acquiring and analysing a large amount of microstructural data that cannot be gathered using 2D imaging. Specifically, 3D tomography is really useful for studying spatial distribution of phases, real feature shapes and sizes and feature connectivity [141]. Furthermore, generated data can be exported to finite element analysis software’s to simulate real microstructures.

There exist several methods to generate 3D visualization currently used in material science, such as serial sectioning, X-ray tomography, TEM-based tomography and atom probe tomography [141]. The selection of the proper method depends on the desired spatial resolution and on the sample length scale [143]. The tomographic technique of interest for this thesis consists of the combined use of focused ion beam and field emission scanning electron microscopy techniques for reconstructing 3D volumes (i.e. FIB/FESEM tomography).

FIB-based tomography is the appropriate technique to reconstruct volumes of several microns per slide with submicron resolution. It has the advantage of requiring little sample preparation and a wide range of materials can be employed. Generally the first step is to deposit a metal layer over the surface of interest, normally platinum-based or tungsten-based, to protect it from damage during subsequent milling and imaging, and also to minimize ‘curtaining’ effects. The next step consists of sputtering a trench normal to the surface of the sample adjacent to the area of interest. Once the cross-section is prepared, thin serial sections can be sputtered by FIB and subsequently imaged with the SEM. The process is repeated several times until the volume of interest has been milled and imaged. General stack of images contains between 100 and 300 micrographs that are finally aligned and treated for the 3D reconstruction. This process is generally performed using a commercial software package, and can be tedious depending on the time required to process and correct the images [141,142]. Once the 3D volume is reconstructed, software packages allow visualizing particular cross-sections in different orientations and to obtain and analyse a large amount of data on the reconstructed bulk [141].

Chapter 2

Aims and scope of the work

As previously commented, the industry of cemented carbides is immersed in a highly dynamic and competitive marked, continuously seeking for more efficient products. In addition, there is a major interest in replacing W and Co because they are classified as critical materials for the "industrial world", as well as due to the healthy issues related to Co powder [17]. Given this situation, a higher degree of expertise is demanded for the development and suitable design of new hardmetal products with improved performance, increased reliability and longer working-life. Thus, it is indispensable to acquire a deep understanding of service degradation phenomena in cemented carbides in order to discern the key microstructural aspects to consider for improving their behaviour. Within this context, **the main target of this Ph.D. thesis is to improve the performance and enhance the reliability of cemented carbides tools and components in rupture-limited applications, on the basis of improved damage tolerance and reduced fatigue sensitivity through an optimal microstructural design.**

Following the above ideas, and taking into account that rupture-limited applications include cases associated with variable combinations of stress state and operating environments, the objectives of this thesis include the evaluation, analysis and understanding of microstructural effects on the fracture and fatigue behaviour of cemented carbides, as well as the assessment of the evolution of microstructure-property-performance interrelations of these materials when damage is induced during service, either by localised corrosion or thermal shock.

2.1. Fracture behaviour of cemented carbides

A higher relevance of fracture toughness is required in order to increase damage tolerance and reliability of cemented carbides. Main goal behind that is to diminish the sensitivity of these materials to critical flaw size [3]. Main toughening mechanism in hardmetals derives from plastic stretching of crack-

bridging ductile enclaves at the crack wake [1,2,59,61]. Hence, hardmetals exhibit a rising crack growth resistance (R-curve) behaviour related to the development of an effective multiligament zone [67,68]. In this regard, damage tolerance capability is intimately related to development of such R-curve behaviour, which is dependent upon the width and strength of the metallic bridges; and therefore, on the microstructural characteristics. Within this framework, **the first objective of this Ph.D. thesis is to document and analyse the toughening phenomenon in cemented carbides as the main foundation for understanding their fracture mechanisms, with the purpose of proposing a model for the description of their R-curve behaviour.** As mentioned above, R-curve characteristics, which are strongly influenced by the microstructure, greatly impact the strength and reliability of hardmetals. Accordingly, **the second objective is to assess microstructural effects on the R-curve behaviour of hardmetals and to evaluate the implications of the crack-bridging toughening mechanism on the strength and reliability of these materials.** Both, the constrained binder and the WC/Co interface, play a major role in defining effective toughening in cemented carbides. Within this context, it is also the **purpose of this thesis to assess the deformation mechanisms and failure strength of the constrained ligaments and their interface through compression of micropillars consisting of Co-binder ligaments constrained by their surrounding WC carbides.**

2.2. Fatigue mechanics and mechanisms of cemented carbides

Although fatigue is recognized to play an active and relevant role as a service degradation mechanism in most of cemented carbides applications, literature surveys devoted to investigate the influence of the microstructure on the fatigue behaviour are relatively scarce and mainly focused to Co-base cemented carbides [82]. Fatigue damage is principally associated with mechanisms occurring in the metallic binder phase and mainly consists of preventing the formation of ductile enclaves at the crack wake [4]. Thus, opposite to fracture toughness, fatigue threshold values are rather independent on the binder content and therefore, straight WC–Co grades exhibit increasing fatigue sensitive as binder content rises [4,91]. Fatigue damage accumulation in the cobalt binder is speculated on the basis of a martensitic transformation from the fcc to the hcp phase as a consequence of high induced stresses and strains [5]. However, fatigue-induced damage mechanisms shift from the fcc to hcp phase transformation to slip and twinning when modifying the binder chemical nature from cobalt to nickel; raising then queries on the effective fatigue susceptibility of binders with distinct chemical nature [6,7]. Therefore, based on the above comments and on the manifest interest of replacing cobalt by alternative binders [17], it is one of the objectives of this thesis **to investigate and understand the fatigue mechanics and mechanisms of cemented carbides consisting of binders with non-transforming deformation mechanisms.**

On the other hand, crack-deflection is an additional operative toughening mechanism in cemented carbides. However, opposite to crack-bridging toughening mechanism, it is immune to fatigue loads [8].

Therefore, lower fatigue sensitive levels are expected for hardmetals exhibiting high crack-deflection toughness enhancement. In this sense, coarse microstructures are envisaged to possess a more effective action of this toughening mechanism. Within the above framework, it is also the **purpose of this doctoral thesis to evaluate the influence of the carbide mean grain size on the crack-deflection toughening mechanism in cemented carbides.**

2.3. Damage tolerance of cemented carbides under service-like conditions: corrosion and thermal shock

A large portion of hardmetal research is devoted to evaluate and analyse microstructure-property relations. However, although it is a valid approach, it is strongly convenient for hardmetal industry to move one step further towards the evaluation of how these microstructure-property relations evolve through the service-life of hardmetal tools and components. In this regard, a change of perspective in the direction of understanding the microstructure-property-performance interrelations in cemented carbides would certainly enable major advances. In this sense, a successful approach was presented by Góez *et al.* [50] on the basis of the assessment of the residual strength of hardmetals after the inducement of controlled damage by means of spherical indentation (i.e. Hertzian contact). Following these ideas, this thesis aims to investigate the relevance of the microstructure in the tolerance of cemented carbides to damage induced by localised corrosion or thermal shock. These two service degradation phenomena are found in a large number of cemented carbide applications [12]. Thus, **a final goal of this thesis is to conduct a systematic study on the influence of the microstructure on the tolerance of cemented carbides to damage-related features induced either by localised corrosion or thermal shock.** In both cases, toughness and R-curve characteristics are assumed to be dominant properties for enhanced performance and reliability.

Chapter 3

Experimental details

The experimental details of each part of this thesis are presented in the respective articles. Nonetheless, some additional details are provided in this chapter for easier follow-up. Concretely, the nomenclature and the experimental process followed to measure the microstructural parameters and the "basic" mechanical properties of all cemented carbide grades studied and presented in the thesis are summarized below. Furthermore, experimental details on the 3D FIB/FESEM reconstruction process are also given.

3.1. Materials: nomenclature and microstructural characterization

In this Ph.D. thesis a total of 14 different hardmetal grades are investigated. All materials are experimental grades supplied by Sandvik Hyperion. In order to select a criterion enabling a fast and easy recognition of the microstructural characteristics, a nomenclature consisting of three different indexes is proposed. The first index is composed by one or two digits that represent the binder weight content. The second one refers to the chemical nature of the binder (i.e. Co, Ni or CoNi). Finally, the third index is associated with the mean grain size of the carbide phase: UF for ultrafine, F for fine, M for medium and C for coarse. Please note that in some articles if the grade is composed by plain Co, the second index is not explicitly indicated.

The main microstructural parameters used in this investigation include: binder weight content (V^{wt}_{binder}), binder composition, carbide mean grain size (d_{WC}), carbide contiguity (C_{WC}) and binder mean free path (λ_{binder}). Binder content values refer to the nominal composition, as given by the supplier. Carbide mean grain size is measured following the linear intercept method in FESEM micrographs acquired using a Jeol JSM-7001F unit [144]. Prior to the acquisition of the micrographs, samples were mounted in Bakelite, then ground and diamond polished up to mirror-like surface finish following a 6, 3 and 1 μm sequence, with a final colloidal silica stage. The magnification of the micrographs was selected

so that they contained around twenty carbides in the horizontal direction. Furthermore, in order to reduce grain size uncertainty, at least 400 grains were measured for each investigated hardmetal grade. On the other hand, two-phase parameters, C_{WC} and λ_{binder}, were estimated from best-fit empirical equations given in literature [10,42,145]. Nomenclature and key microstructural parameters for the hardmetal grades studied in this Ph.D. thesis are given in **Table 3.1**.

Specimen code	Binder Composition	Additives	V^{wt}_{binder} ($\%_{wt.}$)	d_{WC} (μm)	C_{WC}	λ_{binder} (μm)
3CoUF	Co	Cr_3C_2	3	0.37 ± 0.22	0.74 ± 0.04	0.09 ± 0.05
6CoUF	Co	Cr_3C_2	6	0.40 ± 0.21	0.61 ± 0.12	0.12 ± 0.06
10CoUF	Co	Cr_3C_2	10	0.39 ± 0.19	0.46 ± 0.06	0.16 ± 0.06
11CoM	Co	Cr_3C_2	11	1.12 ± 0.71	0.38 ± 0.07	0.42 ± 0.28
10CoC	Co	-	10	2.33 ± 1.38	0.31 ± 0.11	0.68 ± 0.48
15CoUF	Co	Cr_3C_2	15	0.47 ± 0.22	0.36 ± 0.02	0.24 ± 0.11
15CoM	Co	-	15	1.15 ± 0.92	0.30 ± 0.07	0.55 ± 0.46
15CoC	Co	-	15	1.70 ± 1.08	0.27 ± 0.07	0.77 ± 0.54
22CoM	Co	-	22	1.64 ± 0.75	0.19 ± 0.04	1.13 ± 0.56
9NiF	Ni	Cr_3C_2	9	0.83 ± 0.49	0.44 ± 0.08	0.29 ± 0.18
10CoNiM	$8\%_{wt.}$Co - $2\%_{wt.}$Ni	-	10	1.04 ± 0.83	0.41 ± 0.08	0.36 ± 0.29
10CoNiC	$8\%_{wt.}$Co - $2\%_{wt.}$Ni	-	10	1.44 ± 0.86	0.38 ± 0.08	0.47 ± 0.30
15CoNiM	$12\%_{wt.}$Co - $3\%_{wt.}$Ni	-	15	1.26 ± 0.81	0.29 ± 0.06	0.60 ± 0.40
15CoNiC	$12\%_{wt.}$Co - $3\%_{wt.}$Ni	-	15	1.50 ± 1.00	0.28 ± 0.07	0.68 ± 0.49

Table 3.1. Specimen code, binder composition, additives, binder content, carbide mean grain size, carbide contiguity and binder mean free path for the investigated cemented carbides.

3.2. Mechanical characterization

Mechanical characterization includes the assessment of hardness (*HV30*), flexural strength (σ_r), Weibull characteristic strength (σ_0) and modulus (m), and fracture toughness (K_{Ic}). Hardness was measured using a Vickers diamond pyramidal indenter and applying a load of 294 N. In all the others cases, testing was conducted using a four-point bending fully articulated test jig, with inner and outer spans of 20 and 40 mm, respectively. Flexural strength tests were performed on an Instron 8511 servohydraulic machine at load rates of 100 N/s [146]. Bars of 45 mm x 3 mm x 4 mm (i.e. length x thickness x width) dimensions were used as tested specimens, and the number of specimens broken varied between 10 and 15 per grade. The surface subjected to the maximum tensile loads was polished to mirror-like finish and the edges were chamfered to reduce their effect as stress raisers. Flexural strength results were analysed using Weibull statistics and the Weibull characteristics strength and modulus assessed

[80]. Fracture toughness was determined using 45 mm x 5 mm x 10 mm single edge pre-cracked beam (SEPB) specimens following the procedure proposed by Torres *et al.* [147]. In doing so, a notch was introduced by electrical discharge machining (EDM) up to a length-to-specimen width ratio of 0.3, and a sharp crack was generated from the notch tip by subjecting the specimens to cyclic compressive loads. Then, the crack was propagated by applying tensile cyclic loads until reaching a crack length-to-specimen width ratio of about 0.5. The sides of SEPB specimens were polished to follow stable crack growth using a high-resolution laser scanning confocal microscopy. Fracture toughness was determined by testing SEPB specimens to failure at stress-intensity factor load rates of about 2 $MPa \cdot m^{1/2}/s$. At least five samples were tested per studied hardmetal grade [148]. Determined mechanical properties for the investigated cemented carbides are given in **Table 3.2**.

Specimen code	***HV30* (GPa)**	**σ_r (MPa)**	**σ_0 (MPa)**	**Weibull modulus**	**K_{Ic} (MPa)**
3CoUF	18.9 ± 0.8	2214 ± 313	2351	8	7.3 ± 0.7
6CoUF	16.9 ± 0.2	3287 ± 473	3506	7	8.4 ± 0.3
10CoUF	15.7 ± 0.6	3422 ± 512	3598	11	10.4 ± 0.3
11CoM	12.8 ± 0.2	3101 ± 102	3149	36	13.9 ± 0.3
10CoC	11.4 ± 0.2	2489 ± 85	2522	35	15.8 ± 0.3
15CoUF	13.2 ± 0.1	3869 ± 109	3919	42	11.3 ± 0.6
15CoM	11.2 ± 0.1	2912 ± 88	2912	39	15.2 ± 0.4
15CoC	10.2 ± 0.1	2570 ± 54	2570	54	17.0 ± 0.2
22CoM	7.7 ± 0.1	2431 ± 124	2487	24	19.4 ± 1.4
9NiF	13.2 ± 0.2	3080 ± 210	3175	17	11.5 ± 0.2
10CoNiM	12.3 ± 0.1	2720 ± 198	2823	23	14.2 ± 0.4
10CoNiC	11.6 ± 0.1	2534 ± 94	2576	32	15.3 ± 0.3
15CoNiM	10.2 ± 0.1	2634 ± 101	2814	33	15.8 ± 0.4
15CoNiC	9.45 ± 0.1	2716 ± 101	2726	31	17.3 ± 0.4

Table 3.2. Hardness, flexural strength, Weibull characteristic strength, Weibull modulus and fracture toughness values for the investigated cemented carbides.

3.3. 3D FIB/FESEM Tomography

Throughout this thesis several 3D FIB/FESEM tomographic reconstructions of different damage-related features in cemented carbides are presented. In particular, this technique is implemented to characterize fracture and fatigue phenomena and corrosion process in hardmetals. Within this context, an explanation of the followed process is detailed hereafter.

The first step consists of selecting the region of interest with dimensions of about 15 µm x 15 µm for the tomographic reconstruction. Before ion milling, a platinum thin protective layer was deposited over the surface of interest to reduce milling damage and to avoid “curtaining” effects. This undesirable effect is very common when milling materials containing several phases, especially when having pores or void regions such as cracks. Two mark lines were milled, having an angle of 45º between them and sharing one contact point at one of the square vertices of the platinum layer, in order to facilitate further alignment of the micrographs. Subsequently, a U-shaped trench with one cross-sectional surface (perpendicular to specimen surface) was sputtered by FIB. Normally high currents in the nA range are used in this step to reduce milling times. Next step consists of the combined use of FIB and FESEM systems to serial sectioning and imaging the surface of interest. At this stage much lower currents were operated (i.e. in the range of pA) with the purpose of obtaining well-polished surfaces and to lessen redeposition. Sections of about 20 nm in width were milled and more than 500 images were recorded per tomography.

Once micrographs of interest are gathered, next step consists of carrying out the 3D reconstruction of the volume of interest. Aiming to do so, the commercial software Avizo® was used in this investigation. First, the images were aligned using the line marks on the top of the micrographs (coming from the ones milled in the platinum layer). Then, the region of interest was selected and cropped. Subsequently, a series of image filters were applied to the images, in order to differentiate grey levels associated with each phase. In some cases, particularly when having curtaining effects, this process was not straightforward and some manual corrections were required. Finally the 3D volume was reconstructed.

Chapter 4

Articles presentation

This Ph.D. thesis is divided in three sections covering: (1) fracture and (2) fatigue behaviour of hardmetals, and (3) tolerance of these materials to damage-related features, induced either by thermal shock or corrosion. First section consists of four published articles, referred to as **Articles I, II, III** and **IV**. The second chapter is composed of two additional papers, **Articles V and VI**. Finally, the third part contains two papers, **Articles VII and VIII**. An additional contribution to the third section is included in **Annex I**. The contribution made by the author of this thesis to these papers is detailed in **Table 4.1**.

Paper	Design and planning	Literature survey	Experiments	3D Reconstruction	Data collection and analysis	Writing
I	S.R.	P.R.	P.R.	S.R.	P.R.	P.R.
II	P.R.	P.R.	S.R.	N/A	P.R.	P.R.
III	P.R.	P.R.	P.R.	N/A	P.R.	P.R.
IV	P.R.	P.R.	P.R.	N/A	P.R.	P.R.
V	S.R.	P.R.	P.R.	N/A	P.R.	P.R.
VI	P.R.	P.R.	P.R.	N/A	P.R.	P.R.
VII	S.R.	P.R.	S.R.	S.R.	P.R.	P.R.
VIII	P.R.	P.R.	P.R.	N/A	P.R.	P.R.

Table 4.1. Contribution statement of the author to the appended papers. Note that P.R. refers to “principal role” and S.R. to “secondary role”. N/A= Not applicable.

4.1. Fracture behaviour of cemented carbides

The primary objective of this section is the acquisition of a deep knowledge of the fracture mechanics and mechanisms in cemented carbides. Main outcome of this study is to discern the critical role played by the microstructure in defining the fracture strength and reliability of these materials. In doing so, special attention is devoted to reveal key microstructural features of cemented carbides for optimizing their fracture behaviour by means of enhanced crack growth resistance (R-curve) behaviour. This section is composed of four published articles.

Article I carries out a comprehensive study of the toughening and fatigue micromechanisms operative in WC–Co hardmetals when subjected to monotonic (toughness) and cyclic (fatigue) loading conditions. Here, crack-microstructure interactions at the crack-tip of stably grown and arrested cracks, propagated under the application of monotonic and cyclic loads, are analysed by means of 3D FIB/FESEM serial sectioning and imaging technique. Following the above investigation, main purpose of **Article II** is to bring new insights on mechanical deformation and failure behaviour of hardmetals through the compression of micropillars consisting of Co-binder ligaments constrained by their surrounding WC carbides. In this study particular focus is placed on documenting and analysing deformation mechanisms and failure strength of the ductile binder (i.e. yield strength and constraining degree of the soft phase) and the WC/Co interface, as key features for determining effective toughening in cemented carbides. On the other hand, in **Article III** the micrographs gathered in **Article I** of crack–microstructure interaction in cracks arrested after stable extension under monotonic loading (i.e. multiligament zone) are analytically assessed, and a model for the description of R-curve behaviour of hardmetals is proposed. Finally, **Article IV** evaluates the influence of microstructure on the R-curve behaviour of cemented carbides; and in turn, addresses the impact of R-curve characteristics on the strength and reliability of these materials.

Article I. Fracture and fatigue behavior of cemented carbides: 3D Focused Ion Beam Tomography of crack-microstructure interactions

Reference: J.M. Tarragó, E. Jimenez-Piqué, M. Turón-Viñas, L. Rivero, I. Al-Dawery, L. Schneider, L. Llanes, Int. J. Powder Metall. 50 (2014) 1–10. "*Best paper award in the 2014 World Tungsten, Refractory & Hardmaterials Conference"*

This work provides a significant contribution to the understanding of fracture and fatigue failure processes in cemented carbides. It includes a 3D characterization of crack-microstructure interaction in the process zone (i.e. crack-tip) of stably propagated and arrested cracks, under the application of monotonic and cyclic loads. This investigation stands out the critical role played by the constrained binder as both the toughening and fatigue susceptible agent. Hence, unequivocal proof of the multiligament zone as main foundation for understanding toughness and R-curve behaviour in cemented carbides is provided. In addition, clear evidence of fracture and fatigue mechanisms within the binder metallic phase are given, and the differences between both failure mechanisms are analysed and discussed.

Article II. Mechanical deformation of WC–Co composite micropillars under uniaxial compression

Reference: J.M. Tarragó, J.J. Roa, E. Jiménez-Piqué, E. Keown, J. Fair, L. Llanes, Int. J. Refract. Met. Hard Mater. 54 (2016) 70–74.

The effective strength and ductility of the constrained binder together with the interface properties between carbide and binder are critical features for rationalizing microstructural effects on toughening and fatigue sensitivity of cemented carbides. Within this context, the compression behaviour of micropillars consisting of a binder ligament constrained by the surrounding carbides is assessed, with the purpose of gaining a deeper understanding of such features. In doing so, micropillars are machined using FIB milling and uniaxially compressed ex-situ using a nanoindenter equipped with a diamond flat punch. Following the compression tests, deformation and failure micromechanisms are examined by FESEM and FIB cross-sectioning. Experimental results indicate that boundaries between either carbide and binder or carbide crystals are preferential sites for irreversible deformation and failure phenomena. Moreover, plasticity is mostly evidenced within the softer metallic binder in the regions adjacent to carbide-binder interface, where maximum triaxiality stress conditions prevail. Stress-strain curves are analysed and several strain bursts are evidenced at different stress levels, revealing different damage mechanisms on the basis of different crystal orientation and local phase assemblage. Furthermore, this investigation provides a new insight into the microstructural design of ductile metal reinforced ceramic-base composites, on the basis of micropillar compression tests as a valid and effective experimental procedure for the evaluation of mechanical response of these materials at the microscopic level.

Article III. FIB/FESEM experimental and analytical assessment of R-curve behavior of WC–Co cemented carbides

Reference: J.M. Tarragó, E. Jiménez-Piqué, L. Schneider, D. Casellas, Y. Torres, L. Llanes, Mater. Sci. Eng. A 645 (2015) 142–149.

The principal objectives of this work are to analyse the toughening mechanics and mechanisms of cemented carbides and to propose a model for the description of their R-curve behaviour. In doing so, the R-curve behaviour of a WC–11%$_{wt.}$Co cemented carbide is assessed by critical analysis of the FIB/FESEM micrographs gathered in **Article I**, containing evidence of crack-microstructure interaction at the wake of stably grown cracks under monotonic loading. Experimental results point out that cemented carbides exhibit a steep but short R-curve behaviour, due to the large stresses supported by the highly constrained and strongly bonded bridging ligaments. Relevant strength and reliability enhancements can be attributed to this toughening scenario.

Article VI. Microstructural effects on the R-curve behavior of WC–Co cemented carbides

Reference: J.M. Tarragó, D. Coureaux, Y. Torres, D. Casellas, I. Al-Dawery, L. Schneider and L. Llanes, Microstructural effects on the R-curve behavior of WC–Co cemented carbides, Mater. Des. 97 (2016) 492–501.

This article addresses an investigation on the microstructural effects on the R-curve characteristics of cemented carbides. Special attention is paid to evaluate the influence of the crack-bridging mechanism on the strength and reliability of hardmetals. To this end, the model proposed in **Article III** for R-curve description is implemented for rationalizing the fracture behaviour of WC–Co cemented carbides with different microstructural arrangements. Strength and reliability enhancements are discussed on the basis of the effective developed toughness and the subcritical crack extension reached before unstable growth is triggered. Both phenomena are considered to be dependent on microstructural length scale and initial flaw size.

4.2. Fatigue mechanics and mechanisms in cemented carbides

The vast majority of hardmetal tools and components are subjected to repeated loads, and fatigue is recognized as one of the most common failure mechanism in their industrial application [82]. Due to its metallic nature, the binder is the principal fatigue susceptible agent in hardmetals and fatigue phenomenon is mainly based on the inhibition or degradation of the crack-bridging toughening mechanism. Therefore, fatigue response of hardmetals is highly sensitive to their microstructural characteristics, especially to the binder content and chemical nature. Within this context, this chapter covers to main topics: (1) acquisition of a deeper knowledge on the fatigue micromechanisms of hardmetals (**Article I**) and, (2) evaluation of the influence of the microstructure, including the binder chemical nature and carbide mean grain size, on the FCG behaviour and fatigue sensitivity of cemented carbides (**Articles V and VI**).

As explained previously, **Article I** is addressed to investigate the toughening and fatigue micromechanisms of cemented carbides through the implementation of the 3D FIB/FESEM tomographic technique. On the other hand, **Articles V** and **VI** are focused to study the fatigue mechanics and mechanisms of hardmetals with Ni-containing binders, and to compare them with respect to WC–Co hardmetals. Indeed, hardmetal producers are devoting great efforts in replacing Co binder by alternative binders [17]. Main reasons behind such trend include: (1) health issues related with cobalt powder [19,20], (2) high and fluctuating prices of Co due to its scarcity related to the difficult access to the ore mines, and (3) intention of improving the performance of cemented carbides under certain harsh work conditions such as corrosive environments. Among possible Co substitutes, nickel has received the most attention as an alternative binder because of its similarity in structure and properties, besides its good corrosion resistance. **Article V** includes a detailed study of the fatigue behaviour of a fine grain-sized WC–Ni cemented carbide, and results are compared to that expected for a WC–Co hardmetal with alike microstructural parameters. On the other hand, **Article VI** consists of a systematic study on the influence of the mean carbide grain size and the binder chemical nature (i.e. Co vs. CoNi) on the FCG behaviour of cemented carbides.

Article V. Mechanics and mechanisms of fatigue in a WC–Ni hardmetal and a comparative study with respect to WC–Co hardmetals

Reference: J.M. Tarragó, C. Ferrari, B. Reig, D. Coureaux, L. Schneider, L. Llanes, Mechanics and mechanisms of fatigue in a WC–Ni hardmetal and a comparative study with respect to WC–Co hardmetals, Int. J. Fatigue. 70 (2015) 252–257.

As mentioned in the introduction, fatigue degradation of Co-base cemented carbides has been frequently rationalized on the basis of a cyclic-induced accumulation phase transformation within the Co binder [5,90,91]. It raises then queries on the effective fatigue susceptibility of binders with distinct chemical nature (e.g. Ni-containing ones). Accordingly, in this paper the fatigue behaviour of a WC–Ni hardmetal consisting of a binder with non-transforming deformation mechanisms (i.e. slip and twinning [6,7]) is evaluated. In doing so, the FCG behaviour and fatigue life limit (stair-case method) values are assessed. Fatigue sensitivity is also addressed and found to be similar to that speculated for a Co based grade with similar microstructural characteristics. Up to the knowledge of the authors, this is the first paper on the open literature about fatigue strength and fatigue crack growth behaviour of WC–Ni cemented carbides. This investigation also includes a detailed inspection of fatigue micromechanisms within the binder, where step-like crystallographic features similar to that evidenced in WC–Co hardmetals are discerned. Such fatigue failure mode is postulated to be a direct consequence of comparable size length scales of microstructure and cyclic plastic zone in front of the crack-tip. Hence, the finding of both similar fatigue fractographic faceted features and fatigue sensitivity for Ni- and Co-base hardmetals call into question the speculated role played by the fcc to hcp martensitic phase transformation as a critical fatigue micromechanism in Co-base hardmetals.

Article VI. Fracture and fatigue behavior of WC–Co and WC–CoNi cemented carbides

Reference: J.M. Tarragó, J.J. Roa, V. Valle, J.M. Marshall, L. Llanes, Fracture and fatigue behavior of WC–Co and WC–CoNi cemented carbides, Int. J. Refract. Met. Hard Mater. 49 (2015) 184–191.

The main purpose of this work is to evaluate the fatigue behaviour of Ni-containing binder hardmetals (concretely 74 $\%_{wt.}$ Co and 26 $\%_{wt.}$ Ni), and to compare such behaviour with the one exhibited by cemented carbides containing plain Co as a binder. Furthermore, in this paper the influence of the binder content and the carbide mean grain size on the fatigue response is assessed. Therefore, the experimental protocol followed in this investigation is broadly equivalent to that pursued in **Article V**. Results indicate a negligible influence of the binder chemical nature on the FCG behaviour and fatigue sensitivity of studied cemented carbides. On the other hand, the FCG threshold is found to linearly increase when rising carbide mean grain size, due to a more effective action of the crack-deflection mechanism. Similar faceted fatigue features were evidenced for Co and CoNi binders.

4.3. Structural integrity of cemented carbides subjected to service-like damage: corrosion and thermal shock

As previously commented, cemented carbides tools and components suffer from several damage-related features induced during service, such as occasional hard body impacts, contact-related degradation, thermal shock or corrosion. Such damage, when combined with the high monotonic and cyclic loads to which engineering parts are generally subjected, limits the service life and may induce premature and unexpected failures. Generally, in-service real degradation is not merely associated with a unique type of damage, but rather consists on a synergic action among several types of them. However, in order to understand the real operational degradation conditions, it is first necessary to isolate individual elements and to acquire a deep knowledge on the effective action of each one of them. Within this context, the main purpose of this chapter is to study the corrosion and thermal shock damage related features in cemented carbides, and to evaluate the critical role played by the microstructure in tolerating such damage. In doing so, microstructural effects are assessed on the basis of their resistance to damage, the latter as given by either microcracking induced by thermal shock [134] or pits formed due to localized corrosive attack [48,102]. With that purpose, damage tolerance is accounted by using residual strength as a critical "limit state" parameter according to the induced damage level. In both cases, toughness and R-curve characteristics are assumed to be dominant properties for enhanced performance and reliability.

This chapter consists of two papers, one of them devoted to study corrosion damage in cemented carbides (**Article VII**), and a second one committed to the thermal shock behaviour of hardmetals (**Article VIII**). An additional contribution to investigate the influence of the microstructure on the corrosion damage in hardmetals is given in **Annex I**. **Article VII** studies the corrosion behaviour of an ultrafine-sized WC–Co cemented carbide immersed in a synthetic mine water solution. The paper includes a detailed characterization of corrosion damage by means of the 3D FIB/FESEM technique. Moreover, the effect of corrosion damage on the structural integrity is assessed through the measurement of residual strength. Also, a detailed FESEM inspection is conducted to discern critical corrosion pits that promote failure. In **Article VIII** the influence of the microstructure on the thermal shock behaviour of hardmetals is assessed. In doing so, the samples are subjected to single and repetitive sudden temperature changes, and the induced damage is evaluated by measuring the retained strength. Attained results are correlated with those estimated from Hasselman parameters for describing crack initiation and propagation in structural materials when subjected to thermal shock [138,139]. In addition, a detailed fractographic inspection is carried out to discern possible damage induced by thermal shock.

Article VII. Corrosion damage in WC–Co cemented carbides: residual strength assessment and 3D FIB-FESEM tomography characterisation

Reference: J.M. Tarragó, G. Fargas, E. Jimenez-Piqué, A. Felip, L. Isern, D. Coureaux, J.J. Roa, I. Al-Dawery, J. Fair, L. Llanes, Corrosion damage in WC–Co cemented carbides: residual strength assessment and 3D FIB-FESEM tomography characterisation, Powder Metall. 57 (2014) 324–330. *"Keynote paper award in the Euro PM 2014 Congress & Exhibition"*

This work investigates the corrosion damage resulting after immersion of a WC–15%$_{wt.}$Co hardmetal in a synthetic mine water solution. It includes a detailed characterization of induced damage carried out by means of a 3D FIB/FESEM tomographic reconstruction. In addition, damage tolerance to corrosion is assessed by measuring residual strength according to the induced damage level, the latter given by the immersion time in the corrosive media. A strong strength reduction with exposure time is evidenced, directly associated with localised corrosion damage, i.e. corrosion pits acting as stress raisers, concentrated in the binder phase. Moreover, a detailed description of corrosion process is provided in accordance with the information gathered from the tomographic reconstruction. This is the first contribution employing the 3D FIB/FESEM technique to study corrosion phenomena in cemented carbides. As a consequence, it represents the first step to further and wider research employing similar techniques [149].

Article VIII. Influence of the microstructure on the thermal shock behaviour of cemented carbides

Reference: J.M. Tarragó, S. Dorvlo, J. Esteve and L. Llanes, Influence of the microstructure on the thermal shock behavior of cemented carbides, Ceramics International 42 (2016) 12701–12708.

It is the purpose of this work to evaluate microstructural effects on the thermal shock resistance (i.e. through the measurement of the residual strength) of cemented carbides when subjected to single and repetitive abrupt temperature changes. It is also the aim of this investigation to rationalize the thermal shock behaviour of hardmetals on the basis of Hasselman's parameters for quantifying their resistance to either crack initiation or propagation induced by thermal shock. Results reveal that harder cemented carbides tend to exhibit a higher resistance to thermal shock damage nucleation, but a lower damage tolerance to repeated thermal shocks than tougher hardmetals, and vice versa. These trends are in agreement with Hasselman's parameters for quantifying the resistance to either crack initiation or propagation induced by thermal shock. Furthermore, thermal shock damage is associated with subcritical growth of the intrinsic flaws resulting from localised microcracking in the vicinity of pre-existing defects.

Chapter 5

Fracture behaviour of cemented carbides

Article I

Fracture and fatigue behavior of cemented carbides: 3D Focused Ion Beam Tomography of crack-microstructure interactions

Tarragó JM, Jimenez-Piqué E, Turón-Viñas M, Rivero L, Al-Dawery I, Schneider L, Llanes L

International Journal of Powder Metallurgy 50, 1–10 (2014)

Article II

Mechanical deformation of WC–Co composite micropillars under uniaxial compression

Tarragó JM, Roa JJ, Jiménez-Piqué E, Keown E, Fair J, Llanes L

International Journal of Refractory Metals and Hard Materials 54, 70–74 (2016)

Article III

FIB/FESEM experimental and analytical assessment of R-curve behaviour of WC–Co cemented carbides

Tarragó JM, Jiménez-Piqué E, Schneider L, Casellas D, Torres Y, Llanes L

Materials Science & Engineering A 645, 142–149 (2015)

Article IV

Microstructural effects on the R-curve behaviour of WC–Co cemented carbides

Tarragó JM, Coureaux D, Torres Y, Casellas D, Al-Dawery I, Schneider L and Llanes L

Materials & Design 97, 492–501 (2016)

Chapter 6

Fatigue mechanics and mechanisms in cemented carbides

Article V

Mechanics and mechanisms of fatigue in a WC–Ni hardmetal and a comparative study with respect to WC–Co hardmetals

Tarragó JM, Ferrari C, Reig B, Coureaux D, Schneider L, Llanes L

International Journal of Fatigue 70, 252–257 (2015)

Article VI

Fracture and fatigue behavior of WC–Co and WC–CoNi cemented carbides

Tarragó JM, Roa JJ, Valle V, Marshall JM, Llanes L

International Journal of Refractory Metals and Hard Materials 49, 184–191 (2015)

Chapter 7

Structural integrity of cemented carbides subjected to service-like damage: corrosion and thermal shock

Article VII

Corrosion damage in WC–Co cemented carbides: residual strength assessment and 3D FIB-FESEM tomography characterisation

Tarragó JM, Fargas G, Jimenez-Piqué E, Felip A, Isern L, Coureaux D, Roa JJ, Al-Dawery I, Fair J, Llanes L

Powder Metallurgy 57, 324–330 (2014)

Article VIII

Influence of the microstructure on the thermal shock resistance of cemented carbides

Tarragó JM, Dorvlo S, Esteve J, Llanes L

Ceramics International 42, 12701–12708 (2016).

Chapter 8

Results and conclusions

8.1. Summary of the results and discussion

This thesis is devoted to study the influence of the microstructure on the mechanical response of hardmetals, including tolerance to service-like induced damage. It has been structured in three main sections related to relevant service degradation phenomena in cemented carbide: fracture, fatigue and damage tolerance to corrosion and thermal shock. In this chapter, the main findings of the research work are outlined.

8.1.1. Fracture and fatigue processes in cemented carbides: crack-microstructure interactions

This thesis includes a detailed characterization of fracture process in cemented carbides when subjected to monotonic and cyclic loads by means of fractographic inspection and 3D FIB/FESEM tomography. This subject is discussed in several of the presented papers, concretely in **Articles I, III, IV, V and VI**. In line with previous investigations, clear differences have been discerned between the fractographic aspects related to crack growth under monotonic (fracture) and cyclic (fatigue) loads. While in the former the binder exhibits a ductile fracture mechanism consisting of well-defined dimples, in the latter "step-like" fatigue damage features are discerned within the binder, indicative of a crystallographic fracture mode (**Figure 8.1**). Furthermore, tomographic reconstructions of crack-microstructure interactions of both processes have been carried out, allowing a comprehensive visualization and description of these phenomena.

On the one hand, stable crack growth under monotonic loads in cemented carbides can be described as follows: initially crack starts propagating through the carbide phase; and therefore, binder bridges are formed at the crack wake which hamper crack-opening and propagation. As crack opens, ductile enclaves

elongate, and microvoids start to form to compensate this deformation. When increasing further the crack opening displacement, microvoids growth and localised plastic deformation by necking occurs at the ligaments formed between the voids, leading to final failure by microcavities coalescence. Binder regions where maximum triaxiality conditions prevail, such as binder zones close to carbide corners as well as carbide/binder interface regions are preferential zones for microvoid nucleation. The plastic zone is always confined within the binder pools crossed by the crack path, and local blunting is evidenced when the crack front ends inside the binder phase. In addition, interface strength appears to be extremely high as no metal/ceramic debonding is observed. This mechanism implies an increase of fracture toughness as the crack propagates. It is then the main foundation for the existence of a rising crack growth resistance (R-curve) behaviour in hardmetals.

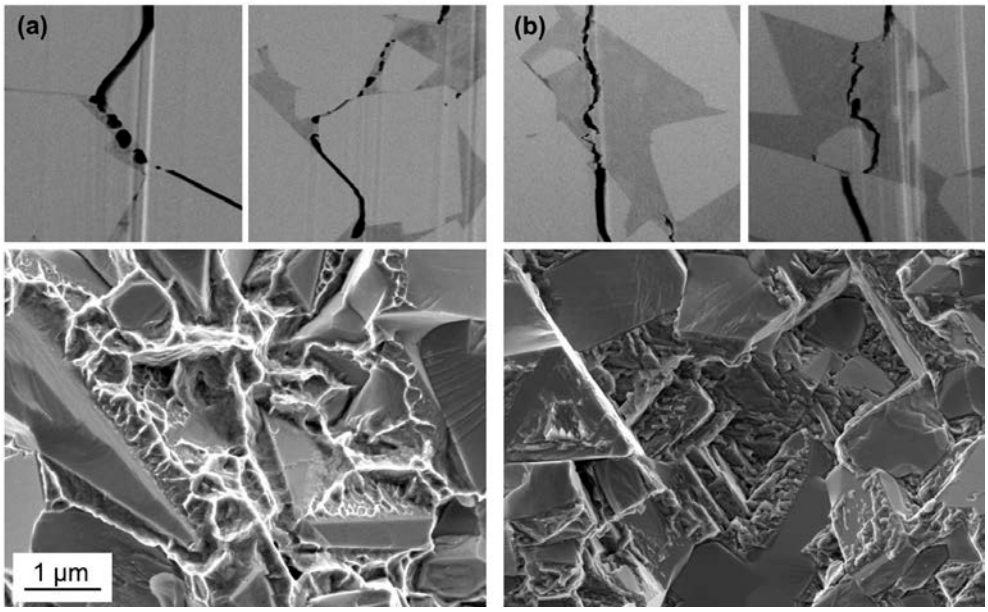

Figure 8.1. FESEM micrographs corresponding to (a) unstable crack growth under monotonic loading and (b) stable crack growth under cyclic loads for Co-base hardmetals. The top images correspond to serial sections obtained by FIB/FESEM tomography whereas the bottom ones correspond to fractographic micrographs.

On the other hand, under cyclic loading the crack follows a crystallographic-like path within the binder. In this case subcritical FCG is more predominantly located at the binder phase, in comparison with stable crack growth under monotonic loads. Although it is obvious that fatigue mechanisms are of crystallographic nature, it remains unclear the exact damage origin of the evidenced steps-like features. However, such fatigue failure mode is assumed to be related to comparable size length scales between the microstructure and the cyclic plastic zone in front of the crack-tip. This scenario is characteristic of the Stage I in the FCG curves of metals, corresponding to the near-threshold regime [83].

8.1.2. Influence of the microstructure on the R-curve behaviour of cemented carbides: implications on strength and reliability

One of the main purposes of this thesis is to propose an analytical model for the description of the R-curve behaviour of hardmetals, capable of capturing microstructural effects. In doing so, in **Article III** the R-curve behaviour of a Co based cemented carbide is assessed by critical analysis of FIB/FESEM micrographs of crack-microstructure interactions taken place at the wake of stably grown cracks (e.g. **Figure 8.1a**). Hence, R-curve behaviour of cemented carbides can be represented according to the following equation:

$$K_R = K_{Ic} - (K_{Ic} - K_t)exp\left[-\frac{\Delta a}{t}\right] \qquad (8.1)$$

where K_R is the crack-tip resistance stress intensity factor, K_t is the critical crack-tip stress intensity factor required for crack initiation, Δa is the subcritical crack growth, and t is a crack length normalizing parameter assumed to be proportional to the microstructural size. According to this equation, cemented carbides exhibit a steep but short R-curve behaviour associated with the large stresses imparted by the highly constrained and strongly bonded bridging ligaments.

Moreover, microstructural effects on R-curve behaviour of cemented carbides and their impact on the strength and reliability of these materials are investigated and discussed in **Article IV**. In doing so, R-curve characteristics of cemented carbides are found to be strongly influenced by the microstructure. In this regard, R-curves decrease in length but become steeper when diminishing the microstructural size. This trend is related to a decrease of the width and an increase of the unitary strength (due to a rise of the constraint level exerted by the carbides on the metal phase) of the metallic bridges as the binder mean free path decreases. It is important to highlight the substantial impact of the R-curve characteristics on the strength and reliability of cemented carbides. Hence, the fracture strength is not only found to be dependent on the fracture toughness and the starting initial flaw size, but also notably influenced by the effectively developed toughness level and the subcritical crack extension reached before unstable growth. Furthermore, stable crack extension before failure results in a size homogenization of existing defects, and consequently in an enhanced reliability.

8.1.3. Response of WC–Co micropillars to uniaxial compression

In **Article II** the response to uniaxial compression of WC–Co composite micropillars (of about 3 μm in diameter) consisting of Co binder regions surrounded by the contiguous ceramic particles is

assessed. Main purpose behind it is to acquire a deeper knowledge on the deformation behaviour and fracture process of the ductile metallic ligaments and the binder/carbide interface.

Compression curves (stress-strain relationships) are characterised by several pop-in events (strain bursts) with stress values from 0.6 up to 3.1 GPa, and probably related to the activation of shearing/cracking events. Very interesting, these stress values range between the flow stresses expected for an unconstrained cobalt binder-like alloy and a highly constrained metallic binder. The large stress difference evidenced between strain bursts arises on the basis of different crystal orientation and local phase assemblage, the latter directly related to constraining degree within tested micropillars.

The fractographic inspection reveals that the boundaries, either between WC and Co or between WC particles, are the weakest points for failure phenomena and microcrack nucleation. On the other hand, although some signs of plasticity are evidenced in the WC phase, the biggest concentration of plastic deformation is accumulated by the binder phase. In accordance to the observations done in **Article I**, deformation within the binder tends to settle in regions close to the carbide-binder interface or at carbides angularities, where triaxiality stress conditions reach their maximum values.

8.1.4. Fatigue sensitivity of hardmetals with Ni-containing binders

The FCG behaviour and fatigue sensitivity of a Ni-base and a series of CoNi-base hardmetals are investigated in **Articles V and VI**, respectively. Results point out that cemented carbides with similar microstructural characteristics (i.e. carbide size and binder content) exhibit similar fatigue behaviour and fatigue sensitivity values regardless of the binder chemical nature. Therefore, for the studied materials there exists a negligible influence of the binder chemical nature for studied hardmetals on the degradation susceptibility of the toughening crack-bridging mechanism when subjected to fatigue loads. This fact, in addition to the similar crystallographic fatigue failure scenario evidenced for Co- and Ni-containing hardmetals, questions the effective action of the fcc to hcp martensitic phase transformation found in WC–Co hardmetals as the main fatigue micromechanism.

8.1.5. Carbide mean grain size effects on crack-deflection

As previously commented, crack-deflection is an additional toughening mechanism in cemented carbides. However, contrary to the case of crack-bridging, it is immune to fatigue loads. The effective action of this mechanism increases for coarser microstructures and accordingly, a linear rise of the FCG threshold with the carbide mean grain size is established in **Article VI**. This relation comprises carbide mean grain sizes from 0.2 up to 4 μm, and is as follows:

$$K_{th} = 5.75 + 1.27 d_{WC} \quad (8.2)$$

Therefore, coarse-grained hardmetals are expected to exhibit lower fatigue sensitive values than fine-grained ones with similar binder mean free path values.

8.1.6. Damage tolerance of cemented carbides to localised corrosion: microstructural effects

In **Article VII** a testing protocol for inducing controlled corrosion damage in cemented carbides is presented. In doing so, samples are immersed in an aerated synthetic mine water solution for different corrosion times, and tolerance to induced damage is assessed by measuring residual strength. Finally, a detailed fractographic inspection is carried out with the purpose of identifying critical corrosion damage that promoted failure. In **Annex I** the testing protocol described in **Article VII** is implemented in a set of hardmetal grades having different microstructural characteristics (i.e. carbide mean grain size and binder content). Results reveal that corrosion damage may result in relevant strength degradation in cemented carbides on the basis of stress raising effects associated with the formation of surface corrosion pits. Thus, as immersion time increases strength gradually decreases. However, relative changes in residual strength become less pronounced with exposure time. Interesting, medium-sized grades exhibit much higher damage tolerance to corrosion damage than ultrafine ones. This behaviour can be attributed to two main factors. First, different corrosion pits geometries are evidenced between medium- and ultrafine-sized hardmetals. In this regard, medium-sized hardmetals show semi-elliptical corrosion pits, whereas ultrafine grades exhibit very sharp corrosion pits at the corrosion front. Second, the higher damage tolerance levels expected for medium-sized grades as related to their higher toughness levels.

8.1.7. Corrosion phenomena in cemented carbides

A detailed description of corrosion process in cemented carbides is provided in **Article VII** and **Annex I** through the characterization of corrosion damage-microstructure interactions by means of the 3D FIB/FESEM serial sectioning and imaging technique. Based on the observation an analysis of gathered micrographs, corrosion damage evolution may be described as follows: initially corrosion proceeds through the nucleation of microcracks at the centre of binder pools, related to stress corrosion cracking effects. Then, as corrosion time increases these microcracks tend to expand in radial directions towards the binder/carbide interface, resulting in vast binder leaching which finally leaves an unsupported WC grain skeleton at the surface.

8.1.8. Damage tolerance of cemented carbides to thermal shock: microstructural effects

The influence of the microstructure on the thermal shock resistance of cemented carbides is studied in **Article VIII,** through the assessment of the residual strength of hardmetal beams after being subjected to single and repetitive severe temperature changes by water quenching. Attained results evidence that the inducement of thermal shock damage may result in relevant strength degradation. Thermal shock damage is speculated to be related to the nucleation of microcracks at the carbide-binder interfaces in the vicinity of pre-existing flaws. Therefore, microcracking promotes a subcritical growth of intrinsic defects, and consequently a strength reduction. Harder cemented carbides grades are found to exhibit a higher resistance to the nucleation of thermal shock induced-damage. However, they also present a lower resistance to the propagation of such damage, as compared to tougher hardmetals. These trends are in agreement with those expected from the relative difference between their initiation (R) and propagation (R'''') Hasselman's parameters. Hence, in **Article VIII** thermal shock indexes are invoked, in terms of strength- and toughness-controlled scenarios, as figures of merit for structural design with these materials. Finally, an improved thermal shock resistance when increasing carbide mean grain size is also evidenced, as related to higher thermal conductivity as well as enhanced damage tolerance (i.e. due to a more prominent R-curve behaviour).

8.2. General conclusions

- Unequivocal proof of the development of a multiligament zone consisting of ductile metallic enclaves at the crack wake is provided. This toughening mechanism is the main foundation for understanding toughness and R-curve behaviour of cemented carbides.

- A model for the description of the R-curve behaviour of hardmetals is proposed. This relation captures microstructural effects on the R-curve characteristics of these materials. On the basis of this model, a strong microstructural influence on the R-curve behaviour of cemented carbides is documented. It is related to the width and strength of the ductile ligaments, the latter directly associated with the effective constraint level exerted by the surrounding carbides over the ductile phase.

- R-curve characteristics have a relevant impact on the strength and reliability of cemented carbides. On the one hand, fracture strength of hardmetals is substantially affected by the effectively developed toughness level and the subcritical crack growth triggered before unstable fracture. On the other hand, crack-bridging toughening mechanism has a beneficial effect on the reliability of hardmetals, due to

size homogenization of existing flaws, as related to stable crack extension before failure. Consequently, the existence of such R-curve behaviour also promotes enhanced damage tolerance.

- WC–Co composite micropillars consisting of few Co binder regions surrounded by hard particles have been successfully tested under uniaxial compression. Experimental results indicate that the interfaces between carbide particles and between binder and carbide phases are the principal points for irreversible deformation and failure phenomena. Stress-strain curves reveal several strain bursts at strength values comprised between the flow stress values expected for an unconstrained Co-binder like alloy and a highly constrained binder region in bulk WC–Co composites. This high strength scatter is rationalised on the basis of different crystal orientation and local phase assemblage.

- Strength degradation of cemented carbides under the application of cyclic loads is principally related to the inhibition of the crack-bridging toughening mechanism. Thus, the metallic phase is the fatigue susceptible agent in hardmetals.

- Stable crack growth under cyclic loads follows a crystallographic path through the metallic binder. This damage mode is speculated to be a direct consequence of the comparable size length scales for the microstructure and the cyclic plastic zone at the crack-tip front.

- Co, CoNi and Ni binders exhibit a similar mechanical degradation as toughening agents in cemented carbides when subjected to cyclic loads, regardless the fact that they have different damage micromechanisms. Accordingly, Co-, CoNi- and Ni-base cemented carbides show similar fatigue sensitivity trends.

- Crack-deflection is an additional toughening mechanism in cemented carbides immune to fatigue loads. The effectiveness of this mechanism increases for coarser microstructures. Consequently, the FCG threshold linearly rises with carbide mean grain size, and as a result fatigue sensitivity decreases.

- Both, localised corrosion and thermal shock damage may result in relevant strength degradation in cemented carbides. Within this context, the microstructure plays a principal role in defining the effective tolerance to the induced damage level.

- Strength loss associated with corrosion damage is rationalised on the basis of stress raising effects related to corrosion pits. Semi-elliptical and sharp angular corrosion pits were identified as critical corrosion damage for medium- and ultrafine-sized hardmetals, respectively. The latter have more

pronounced stress rising effects; and consequently, ultrafine graded cemented carbides exhibit higher strength losses when subjected to corrosion damage.

- Thermal shock strength reduction in cemented carbides is speculated to be associated with subcritical crack growth of pre-existing flaws, as related to localised microcracking. Harder cemented carbides grades tend to exhibit superior resistance to thermal shock damage nucleation but lower resistance to the propagation of such damage than tougher hardmetals. Within this context, thermal shock indexes in terms of strength- and toughness-controlled scenarios are invoked as figures of merit for the structural design with these materials.

8.3. Impact and perspectives

One of the main outcomes of this Ph.D. thesis comes from the realisation of the requirement for hardmetal community to gain a deeper understanding of the role of the microstructure on the evolution of material properties and performance when inducing damage during real service-life of tools and components. Accordingly, the basic approach based on the evaluation of microstructure-property relations should advance towards a more realistic and application based concept. It includes the assessment of the evolution of microstructure-property-performance interrelations as material degrades due to the harsh working conditions to which it is subjected. Although a decisive step forward in this direction is presented in this thesis, further and wider research should be addressed to this purpose with the aim of covering new materials and service-like conditions. Within this context, one step further in the near future should also include the consideration of the synergic effects between different damage mechanisms.

Following above comments, it should be underlined the breakthrough presented in this thesis concerning the acquisition of a deep knowledge on the crack-bridging toughening mechanism in cemented carbides, as the main foundation for understanding the fracture behaviour and damage tolerance of these materials. In this regard, the model proposed for the description of the R-curve behaviour of hardmetals according to their microstructural characteristics could certainly have a great impact for the proper structural design with these materials. However, this advance only represents a closer approximation to reality, and future efforts should be devoted to study the effects of the geometry of critical defects on their effective action as stress raisers. That would allow rationalising the fracture behaviour of cemented carbides on the basis of a simultaneous consideration of (1) their R-curve characteristics, and (2) the stress raising effects associated with flaw geometry.

This Ph.D. thesis also emphasises the importance of understanding microstructure-damage relations in hardmetals in order to set up the basis for an improved microstructural design which minimises the

adverse effects of damage-related features on the performance of engineering components. In this regard, this work provides a detailed description of microstructure-damage interactions under the consideration of monotonic (fracture) and cyclic (fatigue) loads as well as corrosion and thermal shock damage. Within this context, it would be of real interest to explore other types of damage-related features and material configurations by employing similar techniques.

There exists a growing interest on the hardmetal community to move from cobalt to alternative binders. Nickel has attracted considerable attention as Co substitute and therefore the efforts dedicated in this thesis to investigate the fatigue and thermal shock behaviour of cemented carbides with Ni-containing binders would certainly be of interest to this research community. Future research should be addressed to evaluate new binder alloys that could potentially improve the performance and life-time of hardmetal tools and components.

Acknowledgments

I would like to thank to all the people that in different ways have contributed and paid interest to the work I have been carrying out during my last four years. It has been a great life experience, during which I have had the opportunity to make really good friends and live unforgettable experiences. I'm fortunate of having such incredible family, friends and colleagues. Especially, I would like to thank:

- My supervisor Luis Miguel Llanes Pitarch who gave me the opportunity to pursuit this Ph.D. I have learned a lot from him during all these years. His support, enthusiasm, leadership and encouragement have truly been a driving force. Even if he was extremely busy, he always found a moment to give me advice. He gave me an excellent introduction to the art of enjoying research.

- My colleagues for all the good moments and discussions that we shared during the last years. Special attention is given to Astrid, Carlos, Daniela, David, Erik, Erica, Giuseppe, Ina, Jing, Joana, Miquel, Mireia, Natalia, Quentin, Roberta, Romain, Sara and Yassine. I will miss our long coffees and Jungle Speed plays!!!

- All the members of the CIEFMA group. Above all I would like to thank Gemma Fargas, Emilio Jiménez and Joan Josep Roa for all the fruitful collaborations and discussion we had during this time.

- All the members of the Sandvik Hyperion R&D group for the good moments and fruitful discussions that we always had during my visits. I sincerely appreciate the help received from my Sandvik co-advisors, Ihsan Al-Dawery and Ludvig Schneider.

- Isaac Lopez and Trifon Trifonov for their immeasurable support with the SEM and FIB equipment.

- My family and friends, for all their love and support.

This work was financially supported by the Spanish Ministerio de Economía y Competitividad (Grant MAT2012-34602 and MAT2015- 70780). Additionally, I would like to acknowledge the Ph.D. scholarship received from the collaborative Industry-University program between Sandvik Hyperion and Universitat Politècnica de Catalunya.

Bibliography

[1] L.S. Sigl, H.E. Exner, Experimental study of the mechanics of fracture in WC–Co alloys, Metall. Trans. A. 18A (1987) 1299–1308.

[2] L.S. Sigl, H.F. Fischmeister, On the fracture toughness of cemented carbides, Acta Metall. 36 (1988) 887–897.

[3] A.G. Evans, Perspective on the development of high-toughness ceramics, J. Am. Ceram. Soc. 73 (1990) 187–206.

[4] L. Llanes, Y. Torres, M. Anglada, On the fatigue crack growth behavior of WC–Co cemented carbides: kinetics description, microstructural effects and fatigue sensitivity, Acta Mater. 50 (2002) 2381–2393.

[5] U. Schleinkofer, H.G. Sockel, K. Gorting, W. Heinrich, Microstructural processes during subcritical crack growth in hard metals and cermets under cyclic loads, Mater. Sci. Eng. A. 209 (1996) 103–110.

[6] E.F. Drake, A.D. Krawitz, Fatigue damage in a WC–Nickel cemented carbide composite, Metall. Mater. Trans. A. 12A (1981) 505–513.

[7] C.H. Vasel, A.D. Krawitz, E.F. Drake, E.A. Kenik, Binder deformation in WC–(Co, Ni) cemented carbide composites, Metall. Mater. Trans. A. 16A (1985) 2309–2317.

[8] Y. Torres, J.M. Tarragó, D. Coureaux, E. Tarrés, B. Roebuck, P. Chan, M. James, B. Liang, M. Tillman, R.K. Viswanadham, K.P. Mingard, A. Mestra, L. Llanes, Fracture and fatigue of rock bit cemented carbides: Mechanics and mechanisms of crack growth resistance under monotonic and cyclic loading, Int. J. Refract. Met. Hard Mater. 45 (2014) 179–188.

[9] H.E. Exner, Physical and chemical nature of cemented carbides, Int. Met. Rev. 24 (1979) 149–173.

[10] B. Roebuck, E.A. Almond, Deformation and fracture processes and the physical metallurgy of WC–Co hardmetals, Int. Mater. Rev. 33 (1988) 90–110.

[11] A.V. Shatov, S.S. Ponomarev, S.A. Firstov, Fracture and strength of hardmetals at room temperature, in: V.K. Sarin, D. Mari, L. Llanes (Eds.), Comprehensive Hard Materials, Elsevier, UK, 2014: pp. 301–343.

[12] L. Prakash, Fundamentals and general applications of hardmetals, in: V.K. Sarin, D. Mari, L. Llanes (Eds.), Comprehensive Hard Materials, Elsevier, UK, 2014: pp. 29–90.

[13] G.S. Upadhyaya, Cemented tungsten carbides: production, properties, and testing, Noyes Publications, New Jersey, USA, 1998.

[14] P. Ettmayer, H. Kolaska, H.M. Ortner, History of hardmetals, in: V.K. Sarin, D. Mari, L. Llanes (Eds.), Comprehensive Hard Materials, Elsevier, UK, 2014: pp. 3–27.

[15] H.F. Fischmeister, Development and present status of the science and technology of hard materials, in: R.K. Viswanatham, D.J. Rowcliffe, J. Gurland (Eds.), Proceedings of the 1st International Conference on the Science of Hard Materials, Plenum Press, New York, 1983: pp. 1–45.

[16] C.M. Fernandes, A.M.R. Senos, Cemented carbide phase diagrams: A review, Int. J. Refract. Met. Hard Mater. 29 (2011) 405–418.

[17] S. Norgren, J. García, A. Blomqvist, L. Yin, Trends in the P/M hard metal industry, Int. J. Refract. Met. Hard Mater. 48 (2015) 31–45.

[18] W. Schubert, E. Lassner, W. Böhlke, Cemented carbides - A success story, Tungsten. (2010).

[19] Registration, Evaluation, Authorisation and Restriction of Chemicals (REACH), http://ec.europa.eu/environment/chemicals/reach/reach_en.htm (accessed January 5, 2016).

[20] National Toxicology Program (NTP), http://ntp.niehs.nih.gov/ (accessed January 12, 2016).

[21] K. Brookes, There's more to hard materials than tungsten carbide alone, Met. Powder Rep. 66 (2011) 36–45.

[22] K.J.A. Brookes, 3D-printing style additive manufacturing for commercial hardmetals, Met. Powder Rep. 70 (2015) 137–140.

[23] A Petersson, Cemented carbide sintering: constitutive relations and microstructural evolution. PhD Thesis, Stockholm: Royal Institute of Technology, 2004.

[24] B. Roebuck, M.G. Gee, E.G. Bennett, R. Morrell, Mechanical tests for hardmetals. NPL report, Teddington, UK, 1999.

[25] S. Lay, HRTEM investigation of dislocation interactions in WC, Int. J. Refract. Met. Hard Mater. 41 (2013) 416–421.

[26] A. Duszová, R. Halgaš, M. Bľanda, P. Hvizdoš, F. Lofaj, J. Dusza, J. Morgiel, Nanoindentation of WC–Co hardmetals, J. Eur. Ceram. Soc. 33 (2013) 2227–2232.

[27] S. Lay, J.-M. Missiaen, Microstructure and morphology of hardmetals, in: V.K. Sarin, D. Mari, L. Llanes (Eds.), Comprehensive Hard Materials, Elsevier, UK, 2014: pp. 91–120.

[28] B. Roebuck, E.A. Almond, The influence of composition, phase transformation and varying the relative F.C.C. and H.C.P. phase contents on the properties of dilute Co-W-C Alloys, Mater. Sci. Eng. 66 (1984) 179–194.

[29] K.P. Mingard, B. Roebuck, J. Marshall, G. Sweetman, Some aspects of the structure of cobalt and nickel binder phases in hardmetals, Acta Mater. 59 (2011) 2277–2290.

[30] V. Bounhoure, S. Lay, M. Loubradou, J.-M. Missiaen, Special WC/Co orientation relationships at basal facets of WC grains in WC–Co alloys, J. Mater. Sci. 43 (2007) 892–899.

[31] J. Weidow, H.-O. Andrén, Binder phase grain size in WC–Co-based cemented carbides, Scr. Mater. 63 (2010) 1165–1168.

[32] V.A. Tracey, Nickel in hardmetals, Int. J. Refract. Met. Hard Mater. 11 (1992) 137–149.

[33] E.O. Correa, J.N. Santos, A.N. Klein, Microstructure and mechanical properties of WC Ni–Si based cemented carbides developed by powder metallurgy, Int. J. Refract. Met. Hard Mater. 28 (2010) 572–575.

[34] K. Shi, K. Zhou, Z. Li, X. Zan, S. Xu, Z. Min, Effect of adding method of Cr on microstructure and properties of WC–9Ni–2Cr cemented carbides, Int. J. Refract. Met. Hard Mater. 38 (2013) 1–6.

[35] Z.Z. Fang, Correlation of transverse rupture strength of WC–Co with hardness, Int. J. Refract. Met. Hard Mater. 23 (2005) 119–127.

[36] J. Gurland, The measurement of grain contiguity in two-phase alloys, Trans AIME. 212 (1958) 452–455.

[37] A.V. Shatov, S.A. Firstov, I.V. Shatova, The shape of WC crystals in cemented carbides, Mater. Sci. Eng. A. 242 (1998) 7–14.

[38] V.T. Golovchan, N. V Litoshenko, On the contiguity of carbide phase in WC–Co hardmetals, Int. J. Refract. Met. Hard Mater. 21 (2003) 241–244.

[39] B. Roebuck, E.G. Bennett, Phase size distribution in WC-Co hardmetal, Metallography. 19 (1986) 27–47.

[40] A.V. Shatov, S.S. Ponomarev, S.A. Firstov, R. Warren, The contiguity of carbide crystals of different shapes in cemented carbides, Int. J. Refract. Met. Hard Mater. 24 (2006) 61–74.

[41] J.W. Lee, D. Jaffrey, J.D. Browne, Influence of process variables on sintering of WC–25 wt%Co, Powder Metall. 23 (1980) 57–64.

[42] J.M. Tarragó, D. Coureaux, Y. Torres, F. Wu, I. Al-Dawery, L. Llanes, Implementation of an effective time-saving two-stage methodology for microstructural characterization of cemented carbides, Int. J. Refract. Met. Hard Mater. 55 (2016) 80–86.

[43] Sandvik new developments and applications, http://www2.sandvik.com/SANDVIK/0130/Internet/SE03460.NSF/Index/4321fa9f60f7f648c125721300411c4c/$FILE/CCRD.pdf. (accessed October 30, 2015).

[44] Z.Z. Fang, M.C. Koopman, H. Wang, Cemented tungsten carbide hardmetal-an introduction, in: V.K. Sarin, D. Mari, L. Llanes (Eds.), Comprehensive Hard Materials, Elsevier, UK, 2014: pp. 123–137.

[45] P. Kenny, The application of fracture mechanics to cemented tungsten carbides, Powder Metall. 14 (1971) 22–38.

[46] H. Suzuki, K. Hayashi, The strength of WC–Co cemented carbide in relation to structural defects, Trans. Japan Inst. Met. 16 (1975) 353–360.

[47] B. Casas, X. Ramis, M. Anglada, J.M. Salla, L. Llanes, Oxidation-induced strength degradation of WC–Co hardmetals, Int. J. Refract. Met. Hard Mater. 19 (2001) 6–12.

[48] V.A. Pugsley, G. Korn, S. Luyckx, H.G. Sockel, W. Heinrich, M. Wolf, H. Feld, R. Schulte, The influence of a corrosive wood-cutting environment on the mechanical properties of hardmetal tools, Int. J. Refract. Met. Hard Mater. 19 (2001) 311–318.

[49] B. Casas, Y. Torres, L. Llanes, Fracture and fatigue behavior of electrical-discharge machined cemented carbides, Int. J. Refract. Met. Hard Mater. 24 (2006) 162–167.

[50] A. Góez, D. Coureaux, A. Ingebrand, B. Reig, E. Tarrés, A. Mestra, A. Mateo, E. Jiménez-Piqué, L. Llanes, Contact damage and residual strength in hardmetals, Int. J. Refract. Met. Hard Mater. 30 (2012) 121–127.

[51] J.-L. Chermant, A. Deschanvres, A. Iost, R. Meyer, Tenacite de WC–Co 15 %, Mater. Res. Bull. 8 (1973) 925–934.

[52] H.E. Exner, A. Walter, R. Pabst, Zur ermittlung und darstellung der Fehlerverteilungen von spröden werkstoffen, Mater. Sci. Eng. 16 (1974) 231–238.

[53] N. Ingleström, H. Nordberg, The fracture toughness of cemented carbides, Eng. Fract. Mech. 6 (1974) 597–607.

[54] G.R. Irwin, Fracture, in: Handbuch Der Physics, Springer-Verlag, Berlin, 1958.

[55] R.O. Ritchie, The conflicts between strength and toughness, Nat. Mater. 10 (2011) 817–822.

[56] A.G. Evans, A.H. Heuer, D.L. Porter, The fracture toughness of ceramics, in: D.M.R. Taplin (Ed.), Proceedings of the 4th International Conference in Fracture, Pergamon, Waterloo, Canada, 1977: pp. 529–556.

[57] R.K. Viswanadham, T.S. Sun, E.F. Drake, J. Peck, Quantitative fractography of WC-Co cermets by Auger spectroscopy, J. Mater. Sci. 16 (1981) 1029–1038.

[58] V.D. Krstic, On the fracture of brittle-matrix/ductile-particle composites, Philos. Mag. A. 48 (1983) 695–708.

[59] A.G. Evans, R.M. McMeeking, On the toughening of ceramics by strong reinforcements, Acta Metall. 34 (1986) 2435–2441.

[60] L.S. Sigl, P.A. Mataga, B.J. Dalgleish, R.M. McMeeking, A.G. Evans, On the toughness of brittle materials reinforced with a ductile phase, Acta Metall. 36 (1988) 945–953.

[61] M.F. Ashby, F.J. Blunt, M. Bannister, Flow characteriztics of highly constrained metal wires, Acta Metall. 37 (1989) 1847–1857.

[62] H.F. Fischmeister, S. Schmauder, L.S. Sigl, Finite element modelling of crack propagation in WC–Co hard metals, Mater. Sci. Eng. A. 105/106 (1988) 305–311.

[63] C. McVeigh, W.K. Liu, Multiresolution modeling of ductile reinforced brittle composites, J. Mech. Phys. Solids. 57 (2009) 244–267.

[64] O. Raddatz, G.A. Schneider, N. Claussen, Modelling of R-curve behavior in ceramic/metal composites, Acta Metall. 46 (1998) 6381–6395.

[65] D. Munz, What can we learn from R-curve measurements?, J. Am. Ceram. Soc. 90 (2007) 1–15.

[66] H.G. Schmid, The mechanisms of fracture of WC–11wt%Co between 20^{o}C and 1000^{o}C, Mater. Forum. 10 (1987) 184–197.

[67] P.A. Mataga, Deformation of crack-bridging ductile reinforcements in toughened brittle materials, Acta Metall. 37 (1989) 3349–3359.

[68] Y. Torres, D. Casellas, M. Anglada, L. Llanes, Fracture behavior of hardmetals: implementation of flaw configuration modeling and R-Curve concepts, in: H. Danninger, R. Ratzi (Eds.), Proceedings of the EuroPM 2004, EPMA, Vienna, Austria, 2004: pp. 551–556.

[69] Y. Torres, R. Bermejo, L. Llanes, M. Anglada, Influence of notch radius and R-curve behaviour on the fracture toughness evaluation of WC–Co cemented carbides, Eng. Fract. Mech. 75 (2008) 4422–4430.

[70] G.R. Odette, B.L. Chao, J.W. Sheckherd, G.E. Lucas, Ductile phase toughening mechanisms in a TiAl-TiNb laminate composite, Acta Metall. Mater. 40 (1992) 2381–2389.

[71] R.O. Ritchie, K.J. Koester, S. Ionova, W. Yao, N.E. Lane, J.W. Ager, Measurement of the toughness of bone: a tutorial with special reference to small animal studies, Bone. 43 (2008) 798–812.

[72] M.E. Launey, R.O. Ritchie, On the fracture toughness of advanced materials, Adv. Mater. 21 (2009) 2103–2110.

[73] D. Rubes, B. Smoljan, R. Danzer, Main features of designing with brittle materials, J. Mater. Eng. Perform. 12 (2003) 220–228.

[74] E.A. Almond, B. Roebuck, Defect-initiated fracture and the bend strength of WC–Co hardmetals, Met. Sci. 11 (1977) 458–461.

[75] T. Klünsner, S. Wurster, P. Supancic, R. Ebner, M. Jenko, J. Glätzle, A. Püschel, R. Pippan, Effect of specimen size on the tensile strength of WC–Co hard metal, Acta Mater. 59 (2011) 4244–4252.

[76] Y. Torres, R. Bermejo, F.J. Gotor, E. Chicardi, L. Llanes, Analysis on the mechanical strength of WC-Co cemented carbides under uniaxial and biaxial bending, Mater. Des. 55 (2014) 851–856.

[77] R. Danzer, T. Lube, P. Supancic, R. Damani, Fracture of ceramics, Adv. Eng. Mater. 10 (2008) 275–298.

[78] W. Weibull, A statistical distribution function of wide applicability, J. Appl. Mech. 18 (1951) 293–297.

[79] J.B. Wachtman, Mechanical properties of ceramics, 2nd ed., John Wiley & Sons, New York, 1996.

[80] ASTM C 1239-00: Standard practice for reporting uniaxial strength data and estimating Weibull distribution parameters for advanced ceramics, USA, 2000.

[81] R. Danzer, P. Supancic, J. Pascual, T. Lube, Fracture statistics of ceramics – Weibull statistics and deviations from Weibull statistics, Eng. Fract. Mech. 74 (2007) 2919–2932.

[82] L. Llanes, M. Anglada, Y. Torres, Fatigue of cemented carbides, in: V.K. Sarin, D. Mari, L. Llanes (Eds.), Comprehensive Hard Materials, Elsevier, UK, 2014: pp. 345–362.

[83] S. Suresh, Fatigue of materials, 2nd ed., Cambridge University press, New York, 1998.

[84] W. Dawihl, Die wissenschaftlichen und technischen grudlagen der pulvermetallurgic und ihrer anwendungsbereiche, Stahl U. Eisen. 61 (1941) 909–919.

[85] U. Schleinkofer, H.G. Sockel, K. Gorting, W. Heinrich, Fatigue of hard metals and cermets, Mater. Sci. Eng. A. 209 (1996) 313–317.

[86] U. Schleinkofer, H.G. Sockel, K. Görting, W. Heinrich, Fatigue of hard metals and cermets - new results and a better understanding, Int. J. Refract. Met. Hard Mater. 15 (1997) 103–112.

[87] P. Schlund, P. Kindermann, H.-G. Sockel, U. Schleinkofer, W. Heinrich, K. Görting, Mechanical behaviour of PVD- and CVD-coated hard metals under cyclic loads, Int. J. Refract. Met. Hard Mater. 17 (1999) 193–199.

[88] P. Kindermann, P. Schlund, H.-G. Sockel, M. Herr, W. Heinrich, K. Görting, U. Schleinkofer, High-temperature fatigue of cemented carbides under cyclic loads, Int. J. Refract. Met. Hard Mater. 17 (1999) 55–68.

[89] G. Erling, S. Kursawe, S. Luyck, H.G. Sockel, Stable and unstable fracture surface features in WC–Co, J. Mater. Sci. Lett. 19 (2000) 437–438.

[90] S. Kursawe, P. Pott, H.G. Sockel, W. Heinrich, M. Wolf, On the influence of binder content and binder composition on the mechanical properties of hardmetals, Int. J. Refract. Met. Hard Mater. 19 (2001) 335–340.

[91] T. Sailer, M. Herr, H.-G. Sockel, R. Schulte, H. Feld, L.J. Prakash, Microstructure and mechanical properties of ultrafine-grained hardmetals, Int. J. Refract. Met. Hard Mater. 19 (2001) 553–559.

[92] R.K. Viswanadham, T.S. Sun, E.F. Drake, A. Peck, J. Peck, Quantitative fractography of WC–Co cermets by Auger spectroscopy, J. Mater. Sci. 16 (1981) 1029–1038.

[93] R. V Marrey, R. Burgermeister, R.B. Grishaber, R.O. Ritchie, Fatigue and life prediction for cobalt-chromium stents: A fracture mechanics analysis, Biomaterials. 27 (2006) 1988–2000.

[94] R.O. Ritchie, Mechanisms of fatigue-crack propagation in ductile and brittle solids, Int. J. Fract. 100 (1999) 55–83.

[95] E.A. Almond, B. Roebuck, Fatigue-crack growth in WC–Co hardmetals, Met. Technol. 2 (1980) 83–85.

[96] P.R. Fry, G.G. Garret, Fatigue crack growth behaviour of tungsten carbide-cobalt hardmetals, J. Mater. Sci. 23 (1988) 2325–2338.

[97] Y. Torres, M. Anglada, L. Llanes, Fatigue mechanics of WC–Co cemented carbides, Int. J. Refract. Met. Hard Mater. 19 (2001) 341–348.

[98] Y. Torres, M. Anglada, L. Llanes, Fatigue limit - fatigue crack growth threshold correlation for hardmetals: influence of microstructure, in: A.F. Blom (Ed.), Proceedings of the 8th International Fatigue Congress, EMAS, Stockholm, 2002.

[99] Y. Torres, V.K. Sarin, M. Anglada, L. Llanes, Loading mode effects on the fracture toughness and fatigue crack growth resistance of WC–Co cemented carbides, Scr. Mater. 52 (2005) 1087–1091.

[100] U. Beste, T. Hartzell, H. Engqvist, N. Axén, Surface damage on cemented carbide rock-drill buttons, Wear. 249 (2001) 324–329.

[101] R. Lu, L. Minarro, Y.-Y. Su, R.M. Shemenski, Failure mechanism of cemented tungsten carbide dies in wet drawing process of steel cord filament, Int. J. Refract. Met. Hard Mater. 26 (2008) 589–600.

[102] V.A. Pugsley, H.-G. Sockel, Corrosion fatigue of cemented carbide cutting tool materials, Mater. Sci. Eng. A. 366 (2004) 87–95.

[103] M. Lagerquist, A study of the thermal fatigue crack propagation in WC–Co cemented carbide, Powder Metall. 18 (1975) 75–87.

[104] H. Chandrasekaran, Fracture of carbide tools in intermittent cutting, in: R.K. Viswanadham, D.J. Rowcliffe, J. Gurland (Eds.), Proceedings of the 1st International Conference on the Science of Hard Materials, Plenum Press, New York, 1983: pp. 735–755.

[105] A.C.A. Melo, J.C.G. Milan, M.B. Silva, A.R. Machado, Some observations on wear and damages in cemented carbide tools, J. Brazilian Soc. Mech. Sci. Eng. 28 (2006) 269–277.

[106] W.J. Tomlinson, C.R. Linzell, Anodic polarisation and corrosion of cemented carbides with cobalt and nickel binders, J. Mater. Sci. 23 (1988) 914–918.

[107] A.M.M. Human, H.E.E. Exner, The relationship between electrochemical behaviour and in-service corrosion of WC based cemented carbides, Int. J. Refract. Met. Hard Mater. 15 (1997) 65–71.

[108] S. Hochstrasser(-Kurz), Y. Mueller, C. Latkoczy, S. Virtanen, P. Schmutz, Analytical characterization of the corrosion mechanisms of WC–Co by electrochemical methods and inductively coupled plasma mass spectroscopy, Corros. Sci. 49 (2007) 2002–2020.

[109] W.J. Tomlinson, N.J. Ayerst, Anodic polarization and corrosion of WC–Co hardmetals containing small amounts of Cr_3C_2 and/or VC, J. Mater. Sci. 24 (1989) 2348–2352.

[110] H. Engqvist, U. Beste, N. Axén, The influence of pH on sliding wear of WC-based materials, Int. J. Refract. Met. Hard Mater. 18 (2000) 103–109.

[111] F.J.J. Kellner, H. Hildebrand, S. Virtanen, Effect of WC grain size on the corrosion behavior of WC–Co based hardmetals in alkaline solutions, Int. J. Refract. Met. Hard Mater. 27 (2009) 806–812.

[112] A.M. Human, I.T. Northrop, S. Luyckx, M.N. James, A comparaison between cemented carbides containing Cobalt- and Nickel-based binders, J. Hard Mater. 2 (1991) 245–256.

[113] H. Scholl, B. Hofman, A. Rauscher, Anodic polarization of cemented carbides of the type [(WC,M): M = Fe, Ni or Co] in sulphuric acid solution, Electrochim. Acta. 37 (1992) 447–452.

[114] B. Bozzini, G.P. De Gaudenzi, M. Serra, A. Fanigliulo, F. Bogani, Corrosion behaviour of WC–Co based hardmetal in neutral chloride and acid sulphate media, Mater. Corros. 53 (2002) 328–334.

[115] F.J.J. Kellner, M.S. Killian, G. Yang, E. Spiecker, S. Virtanen, TEM and ToF-SIMS studies on the corrosion behavior of vanadium and chromium containing WC–Co hard metals in alkaline solutions, Int. J. Refract. Met. Hard Mater. 29 (2011) 376–383.

[116] S. Sutthiruangwong, G. Mori, R. Kösters, Passivity and pseudopassivity of cemented carbides, Int. J. Refract. Met. Hard Mater. 23 (2005) 129–136.

[117] A. Bock, W.D. Schubert, B. Lux, Inhibition of grain growth on submicron cemented carbides, Powder Met. 24 (1992) 20–26.

[118] B. Wittmann, W.-D. Schubert, B. Lux, WC grain growth and grain growth inhibition in nickel and iron binder hardmetals, Int. J. Refract. Met. Hard Mater. 20 (2002) 51–60.

[119] C.W. Morton, D.J. Wills, K. Stjernberg, The temperature ranges for maximum effectiveness of grain growth inhibitors in WC–Co alloys, Int. J. Refract. Met. Hard Mater. 23 (2005) 287–293.

[120] Z. Guo, J. Xiong, M. Yang, X. Song, C. Jiang, Effect of Mo_2C on the microstructure and properties of WC–TiC–Ni cemented carbide, Int. J. Refract. Met. Hard Mater. 26 (2008) 601–605.

[121] Q. Zhang, N. Lin, Y. He, Effects of Mo additions on the corrosion behavior of WC–TiC–Ni hardmetals in acidic solutions, Int. J. Refract. Met. Hard Mater. 38 (2013) 15–25.

[122] A.M. Human, H.E. Exner, Electrochemical behaviour of tungsten-carbide hardmetals, Mater. Sci. Eng. A. 209 (1996) 180–191.

[123] S. Sutthiruangwong, G. Mori, Corrosion properties of Co-based cemented carbides in acidic solutions, Int. J. Refract. Met. Hard Mater. 21 (2003) 135–145.

[124] E.J. Wentzel, C. Allen, Erosion-corrosion resistance of tungsten carbide hard metals with different binder compositions, Wear. 181-183 (1995) 63–69.

[125] A.J. Gant, M.G. Gee, A.T. May, The evaluation of tribo-corrosion synergy for WC–Co hardmetals in low stress abrasion, Wear. 256 (2004) 500–516.

[126] M.R. Thakare, J.A. Wharton, R.J.K. Wood, C. Menger, Exposure effects of alkaline drilling fluid on the microscale abrasion–corrosion of WC-based hardmetals, Wear. 263 (2007) 125–136.

[127] W.J. Tomlinson, I.D. Molyneux, Corrosion, erosion-corrosion, and the flexural strength of WC–Co hardmetals, J. Mater. Sci. 26 (1991) 1605–1608.

[128] Y.W. Mai, Thermal-shock resistance and fracture-strength behavior of two tool carbides, J. Am. Ceram. Soc. 59 (1976) 1–4.

[129] C.W. Merten, Response of a WC–Co alloy to thermal shock, in: R.K. Viswanadham, D.J. Rowcliffe, J. Gurland (Eds.), Proceedings of the 1st International Conference on the Science of Hard Materials, Plenum Press, New York, 1983: pp. 757–774.

[130] D. Hand, J.J. Mecholsky, Strength and toughness degradation of a tungsten carbide-cobalt due to thermal shock, J. Am. Ceram. Soc. 73 (1990) 3692–3695.

[131] S. Ishihara, T. Goshima, K. Miyao, T. Yoshimoto, S. Takehana, Study on the thermal shock behavior of cermets and cemented carbides, Japan Soc. Mech. Eng. Solid Mech. Mater. Eng. 34 (1991) 490–495.

[132] S. Ishihara, T. Goshima, K. Nomura, T. Yoshimoto, Crack propagation behavior of cermets and cemented carbides under repeated thermal shocks by the improved quench test, J. Mater. Sci. 34 (1999) 629–636.

[133] T. Yoshimoto, S. Ishihara, T. Goshima, A.J. McEvily, T. Ishizaki, An improved method for the determination of the maximum thermal stress induced during a quench test, Scr. Mater. 41 (1999) 553–559.

[134] S. Ishihara, H. Shibata, T. Goshima, A.J. McEvily, Thermal shock induced microcracking of cermets and cemented carbides, Scr. Mater. 52 (2005) 559–563.

[135] ASTM C1525 - 04: Standard test method for determination of thermal shock resistance for advanced ceramics by water quenching, USA, 2014.

[136] W.R. Buessem, Thermal shock testing, J. Am. Ceram. Soc. 38 (1955) 15–17.

[137] W.D. Kingery, Factors affecting thermal stress resistance, J. Am. Ceram. Soc. 38 (1955) 3–15.

[138] D.P. Hasselman, Elastic energy at fracture and surface energy as design criteria for thermal shock, J. Am. Ceram. Soc. 46 (1963) 535–540.

[139] D.P. Hasselman, Unified theory of thermal shock fracture initiation and crack propagation in brittle ceramics, J. Am. Ceram. Soc. 52 (1969) 600–604.

[140] Z.-H. Jin, Y.-W. Mai, Effects of damage on thermal shock strength behavior of ceramics, J. Am. Ceram. Soc. 78 (1995) 1873–1881.

[141] P.R. Munroe, The application of focused ion beam microscopy in the material sciences, Mater. Charact. 60 (2009) 2–13.

[142] R. Wirth, Focused Ion Beam (FIB) combined with SEM and TEM: Advanced analytical tools for studies of chemical composition, microstructure and crystal structure in geomaterials on a nanometre scale, Chem. Geol. 261 (2009) 217–229.

[143] N. Yao, Focused Ion Beam systems: basics and applications, Cambridge University Press, Cambridge, 2007.

[144] ISO 4499 - 2 Hardmetals. Metallographic determination of microstructure. Part 2: Measurement of WC grain size, Switzerland, 2008.

[145] D. Coureaux, Comportamiento mecánico de carburos cementados WC–Co: Influencia de la microestructura en la resistencia a la fractura, la sensibilidad a la fatiga y la tolerancia al daño inducido bajo solicitaciones de contacto. PhD Thesis, Universitat Politècnica de Catalunya, 2012.

[146] ASTM C1161 - 02c: Standard test method for flexural strength of advanced ceramics at ambient temperatures, USA, 2008.

[147] Y. Torres, D. Casellas, M. Anglada, L. Llanes, Fracture toughness evaluation of hardmetals: influence of testing procedure, Int. J. Refract. Met. Hard Mater. 19 (2001) 27–34.

[148] ASTM E399 - 09: Standard test method for linear-elastic plane-strain fracture toughness K_{Ic} of metallic materials, USA, 2009.

[149] K.J.A. Brookes, Corrosion damage in WC/Co, Met. Powder Rep. 70 (2015) 82–87.

Annex I

Microstructural influence on tolerance to corrosion-induced damage in hardmetals

1. Introduction

Cemented carbides, also referred to as hardmetals, are a group of ceramic-metal composite materials that exhibit an outstanding combination of hardness, wear resistance and toughness [1–3]. Their unique combination of properties has made of them the preferential choice in a large number of industrial applications demanding high performance under harsh working conditions, e.g. cutting and forming tools, mining bits and mechanical seals [4,5]. Hardmetals composite nature consists of hard and brittle ceramic particles (generally WC) embedded into a ductile metallic matrix forming two interpenetrating networks. The preferential choice for the ductile binder is Co but binders of different chemical nature (e.g. Ni, CoNi) are used in applications demanding enhanced performance under certain severe working conditions, such as corrosive environments and high temperatures [6].

Cemented carbides tools and components are frequently exposed to chemically aggressive media including a large variety of corrosive environments, such as lubricants, chemical and petrochemical products as well as mine- and sea- water (e.g. Refs. [7–10]). Therefore, it is of crucial importance to improve the corrosion resistance of cemented carbides in order to increase their service life and to prevent premature failure of tools and components. In acidic and neutral pH solutions, hardmetals corrosion process consists on a galvanic couple where the binder is selectively attacked due to its anodic role [11–14], whereas WC particles are cathodically protected [13]. In addition, due to the larger surface area covered by ceramic particles, corrosion in the anodic sites gets enhanced [13]. The opposite trend is found in basic solutions, where ceramic particles dissolve and the binder phase passivates [15,16]. Corrosion mechanisms in cemented carbides are really complex and depend on a large number of factors such as surface state, corrosive medium, hardmetal microstructure and binder chemical nature. Furthermore, corrosion system is in constant evolution due to the continuous changes produced by the cathodic and anodic reactions taking place at the surface [13].

In-service performance of cemented carbides is not only dependent on their intrinsic mechanical properties but also is highly influenced by their resistance to the aggressive medium to which they are exposed. Within this context, corrosion attack exposes WC grains, resulting in a noticeable increase of wear rates. Accordingly, several studies have been focused on studying the synergic effects between erosion/abrasion and corrosion on the wear rates of cemented carbides (e.g. Refs. [15–19]). Cemented carbides exhibit brittle fracture behaviour related to the propagation of pre-existing flaws which may be processing-, shaping- or service- induced defects (e.g. Refs. [2,8,20–24]). Therefore, corrosion damage may also induce a detrimental effect on the strength and fatigue resistance of hardmetals due to the formation of corrosion pits with pronounced stress rising effects [8,9,25–27]. Thus, localized corrosion damage may have a critical role as a critical flaw, promoting a premature and un-expected failure [8,9,25,27]. However, to the best knowledge of the authors, only two studies have been addressed to correlate strength reduction and corrosion damage in cemented carbides, and both of them point out relevant strength degradation due to the stress rising effects produced by localized corrosion damage [8,27]. Thus, from a structural integrity perspective, it is essential to understand the detrimental impact that corrosion damage may induce in the performance of cemented carbides components.

The combined use of Focused Ion Beam (FIB) and Field Emission Scanning Electron Microscopy (FESEM) has been proved as an extremely useful technique for characterizing microstructure [28,29] and damage phenomena [19,27,28,30–32] in cemented carbides. Following the above ideas, the aim of this investigation is two-fold: (1) to provide a thorough characterization of corrosion damage in cemented carbides immersed in a mine water solution, and (2) to study the detrimental effects of corrosion as a degrading factor of their mechanical performance. Within this purpose, the corrosion behaviour of five WC-Co cemented carbide grades having different microstructural characteristics was first investigated by means of electrochemical measurements. Then, retained strength after the inducement of corrosion damage was assessed and a corresponding fractographic analysis was conducted. Finally, a detailed characterization of corrosion damage-microstructure interactions in cemented carbides was done from tomographic reconstructions obtained by means of 3D FIB/FESEM serial sectioning and imaging.

2. Materials and experimental aspects

Carbide mean grain size (d_{WC}) and the binder content ($\%_{wt.}$), are the principal parameters involved in the definition of the microstructural assemblage of WC-Co hardmetals. Thus, in order to investigate the influence of the microstructure on the corrosion damage of cemented carbides, five experimental WC-Co hardmetal grades having different combinations of binder content and mean grain size were studied. All materials were supplied by Sandvik Hyperion. Main microstructural characteristics, including specimen designations, binder content, carbide mean grain size, contiguity (C_{WC}) and binder mean free path (λ_{Co}) are detailed in **Table 1**. Mean grain size was measured following the linear intercept method, using field

emission scanning electron microscopy (FESEM) micrographs. On the other hand, carbide contiguity and binder mean free path were deduced following empirical relationships given in the literature [2,33]. A small amount of Cr_3C_2 (i.e. around a $5\%_{wt.}$ of the binder content) was added to the composition of 11M, 15UF, 10UF and 3UF grades as a grain growth inhibitor.

Specimen Code	Binder content ($\%_{wt.}$)	d_{WC} (μm)	C_{WC}	λ_{binder} (μm)
15M	15	1.15 ± 0.92	0.30 ± 0.07	0.55 ± 0.46
11M*	11	1.12 ± 0.71	0.38 ± 0.07	0.42 ± 0.28
15UF*	15	0.47 ± 0.22	0.36 ± 0.02	0.24 ± 0.11
10UF*	10	0.39 ± 0.19	0.46 ± 0.06	0.16 ± 0.06
3UF*	3	0.37 ± 0.09	0.59 ± 0.12	0.08 ± 0.03

Table 1. Nomenclature and microstructural parameters for investigated cemented carbides. *Presence of Cr_3C_2 in the composition as a grain growth inhibitor.

Corrosion behaviour was first studied on the basis of electrochemical response of the grades under consideration. Corrosive media consisted on synthetic mine water solution (SMW) (pH = 6.3) containing dissolved salts whose composition is detailed in **Table 2** [12,34]. The potentiodynamic polarization technique was applied to study the corrosion resistance of the investigated cemented carbides in the aerated SMW solution at room temperature. The electrochemical tests were carried out using a standard three electrode system in which the test specimen was the working electrode, a platinum plate was the counter electrode and a silver/silver chloride electrode was used as the reference electrode. After immersion in the electrolyte, the open circuit potential was stabilized during 30 minutes. Subsequently, the sample was polarized into the cathodic region at -500 mV. Then, the potential was increased towards the anodic region with a scan rate of 600 mV/h in the positive direction up to 500 mV.

Compound	Concentration (mg/L)
$CaCl_2$	1058
Na_2SO_4	1237
$MgSO_4$	199
NaCl	1380

Table 2. Synthetic mine water solution composition [11].

Different levels of corrosion damage were induced through simple immersion of specimens in the stirred synthetic mine water corrosive media. Weight loss was measured after immersion tests performed from 24 to 360 h. Before and after immersion tests, the specimens were first hand-cleaned by using soapy

water and then ultrasonically cleaned for 15 min in ethanol, subsequently dried with a pure air, and weighted in an electronic balance having a resolution of ± 0.1 mg. Corrosion rates were estimated using the following equation:

$$Corrosion\ rate\ (mm/year) = 87.6\left(\frac{w}{A\rho t}\right) \quad (1)$$

where w is the weight loss in mg; A is the surface area of the specimen in cm^2; ρ is the density of the material in g/cm^3; and t is the corrosion time in hours.

After immersion tests, retained flexural strength (σ_r) was assessed. At least three samples were tested per investigated material and corrosion time. Flexural strength was determined by subjecting 4 mm x 3 mm x 45 mm specimens to failure using a four-point bending fully articulated test jig with inner and outer spans of 20 and 40 mm, respectively. Subsequently, a detailed FESEM fractographic inspection was conducted with the purpose of characterizing corrosion damage as well as to discern critical failure sites. Strength data was also assessed for non-corroded specimens (reference) and at least 15 samples were tested per studied grade. Here, the surface which was later subjected to the maximum tensile load was polished to mirror-like finish and the edges were chamfered to reduce their effect as stress raisers. Besides fracture strength, each grade was mechanically characterized in terms of hardness and fracture toughness. Hardness (*HV30*) was measured using a Vickers indenter and applying a load of 294N. Fracture toughness (K_{Ic}) was determined using 5 mm x 10 mm x 45 mm single edge pre-cracked beam (SEPB) specimens and details on the procedure may be found elsewhere [35]. In this case, five samples were tested per material.

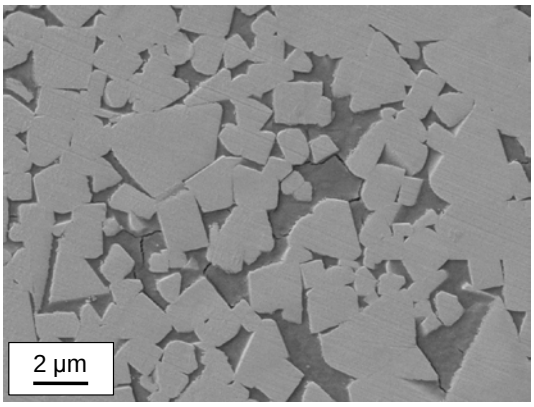

Figure 1. FESEM micrograph corresponding to the selected region of interest for 3D reconstruction on the 15M hardmetal corroded for 7 days.

One of the main goals of this investigation is to conduct a detailed characterization of corrosion damage in cemented carbides by performing a 3D reconstruction of corrosion damage-microstructure interactions. In doing so, the serial sectioning and imaging technique was implemented in a FIB/FESEM (Zeiss Neon 40) equipment. Two samples were selected for the tomographic reconstruction, corresponding to the 15M grade immersed in the synthetic mine water solution for 7 and 15 days. Initially, an inspection of the corroded surface was carried out in order to select a small area of interest (of about 12 μm x 12 μm) for the reconstruction (e.g. **Figure 1**). Before ion milling, a thin protective platinum layer was deposited on the area of interest. Then, a U-shaped trench with one cross-sectional surface (perpendicular to specimen surface) was produced by FIB (**Figure 2**). Subsequently, a series of micrographs were obtained by periodic removal of the material by FIB, within the U-shaped crater parallel to the cross-sectional surface. An example of obtained micrographs is shown for both, 7 and 15 days, in **Figure 3**. A total volume of about 12 μm × 12 μm × 10 μm was ion milled and around 600 images were obtained with a span of about 20 nm between them. The 3D reconstruction of the images was carried out using the commercial Avizo software. Obtained micrographs were aligned and a series of image processing techniques were implemented in order to correct, equalize, and differentiate the grey levels associated with each phase (WC, cobalt, corroded cobalt and microcracks). The next step consisted of segmenting these phases to finally reconstruct the 3D volume.

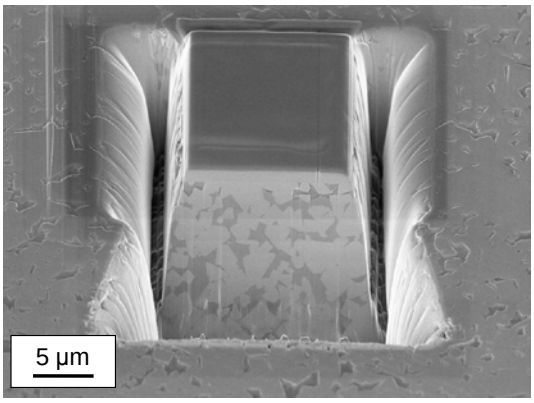

Figure 2. FESEM image of the trench generated by FIB, previous to sequential milling around the region of interest for the 15M hardmetal corroded for 7 days.

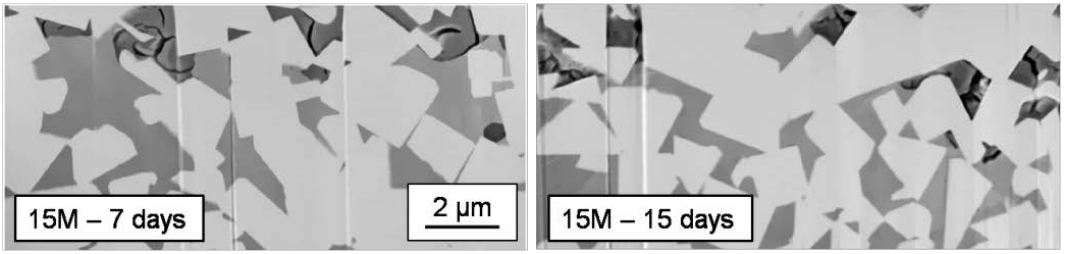

Figure 3. Micrographs showing corrosion damage–microstructure interactions on serial sections obtained by means of FIB/FESEM after being filtered.

3. Results and discussion

3.1. Corrosion behaviour

The measured corrosion rates for the studied materials are shown in **Figure 4**. It can be observed that the investigated 15M hardmetal grade exhibit much higher corrosion rates than the other studied materials. Indeed, during sintering chromium dissolves into the binder and that result in a beneficial effect against corrosion [36,37]. TEM analysis performed by Suttihiruangwong *et al*. demonstrated the formation of a passivating Co-based chromium oxide layer film at the binder surface which strongly decreased the rate of dissolution of the binder, and hence the improved corrosion resistance of Cr-containing cemented carbides [37]. On the other hand, the other materials showed similar corrosion rates. A small decrease of corrosion rates with grain size was evidenced when comparing 11M and 10UF grades. Contradictory results may be found in literature regarding the effect of grain size on the corrosion resistance of hardmetals [12,36]. On one hand Human and Exner [12] documented, on the basis of electrochemical measurements, that the WC mean size does not have a significant effect on the corrosion rates of cemented carbides. On the other hand, Tomlinson and Ayerst pointed out an increase of corrosion rates with grain size [36]. As discussed below, this slightly decrease in corrosion rates observed for the ultrafine grades may be related to the pseudopassive behaviour evidenced for these materials. As expected, a decrease of the corrosion rates when decreasing the binder content was also evidenced. This decrease is related to a lower binder surface area exposed to the corrosive media, even though the decrease of the metallic phase surface area enhances the galvanic couple effect between WC and Co phases [13].

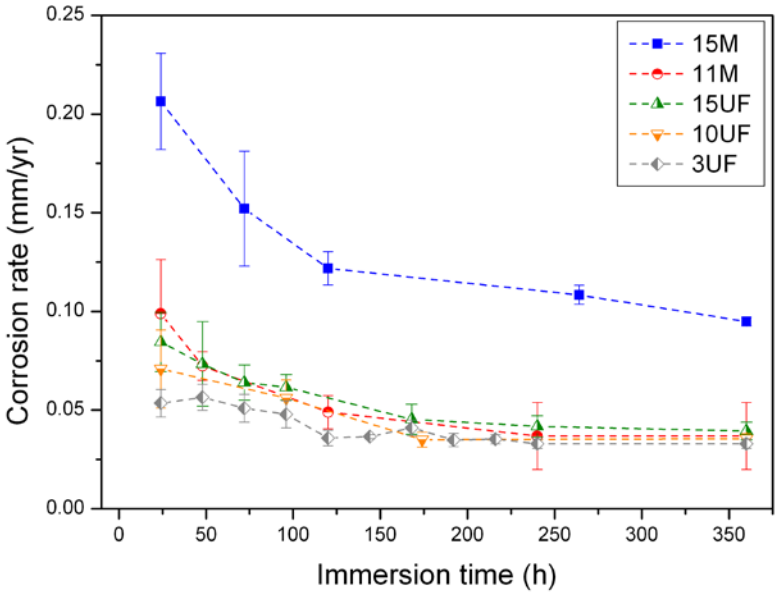

Figure 4. Corrosion rates as a function of immersion time for the studied cemented carbides.

The electrochemical parameters measured for the studied cemented carbides are listed in **Table 3**. They include corrosion potential (E_{corr}), corrosion current density (i_{corr}), critical current density (i_c) and minimum current density in pseudopassive region (i_{pp}). As an example, the potentiodynamic polarisation curves obtained for the 15M and 15UF grades are shown in **Figure 5**. It can be observed that the presence of chromium in the binder leads to lower values of the corrosion current density, as evidenced when comparing 11M and 15M grades [38]. Very interesting, pseudopassivation phenomenon was only discerned for the ultrafine grades. This is particularly clear in **Figure 5**, where a continuous anodic dissolution is observed for the 15M hardmetal, while the current density for the 15UF grade drops to lower values after achieving the critical current density. In agreement with previous results [39], pseudopassivation phenomenon is a consequence of a limitation of the cobalt diffusion that causes a decrease of the current flow. After the dissolution of the cobalt present at the surface, the current flow is limited because cobalt has to diffuse throughout the remaining porous tungsten carbide skeleton. Thus, when the binder mean free path gets shorter, as it is the case for the ultrafine grades, cobalt diffusion gets lessened. On the other hand, 15M did not show a pseudopassivation phenomenon. In addition, it is interesting to notice that ultrafine grades exhibit less negative E_{corr}, i.e. more noble values, than medium ones for similar binder contents (see **Table 3**), which yields lower corrosion current densities.

Specimen code	E_{corr} (mV)	i_{corr} (μA/cm^2)	i_c (mA/cm^2)	i_{pp} (mA/cm^2)
15M	-287	6.23	3.72	-
11M	-291	2.87	3.51	-
15UF	-274	3.64	0.56	0.23
10UF	-264	2.41	0.40	0.18
3UF	-268	1.13	0.51	0.16

Table 3. Electrochemical parameters of the studied cemented carbides. They include corrosion potential (E_{corr}), corrosion current density (i_{corr}), critical current density (i_c) and minimum current density in pseudopassive region (i_{pp}).

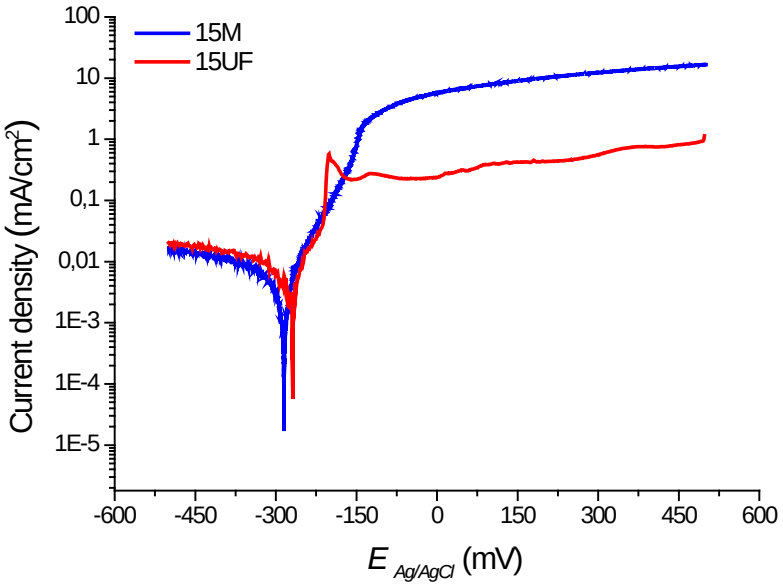

Figure 5. Potentiodynamic polarisation of 15M and 15UF alloys in synthetic mine water.

3.2. Residual strength of corroded hardmetals

The mechanical characterization of investigated materials prior to immersion tests includes the assessment of their hardness, fracture toughness, flexural strength and Weibull modulus. Obtained results are listed in **Table 4**. As expected, hardness rises and fracture toughness decreases when the binder mean free path gets shorter [2]. The tougher grades exhibited extremely high Weibull modulus values, whereas the higher strength scatters were measured for the harder hardmetals.

Specimen Code	*HV30* (GPa)	K_{Ic} (MPa·m$^{1/2}$)	Flexural strength (MPa)	Weibull modulus
15M	11.2 ± 0.1	15.2 ± 0.4	2912 ± 88	39
11M	12.8 ± 0.2	13.9 ± 0.3	3101 ± 102	36
15UF	13.2 ± 0.1	11.3 ± 0.6	3869 ± 109	42
10UF	15.7 ± 0.6	10.4 ± 0.3	3422 ± 512	11
3UF	18.9 ± 0.8	7.4 ± 0.7	2214 ± 313	8

Table 4. Hardness, fracture toughness, flexural strength and Weibull modulus for the investigated cemented carbides.

Retained strength after corrosion is plotted as a function of immersion time in **Figure 6a**. Same experimental data is given in **Figure 6b** as normalized strength loss, using as reference baseline the strength exhibited by non-corroded specimens. These results clearly indicate that; (1) corrosion may produce a relevant strength degradation in cemented carbides that is highly dependent on their microstructure; (2) relative changes of strength loss are pronounced for short exposure times, but tend to stabilize for longer immersion times; and (3) retained strength results are characterized by a high dispersion probably related to significant differences in the size and geometry of corrosion damage acting as a critical flaws for fracture. Attempting to document and analyse corrosion-induced damage promoting failure, a detailed inspection of fractured surfaces was conducted by means of FESEM. In doing so, critical flaws were identified and documented. Fractographic examination reveals that corrosion pits act as critical points for starting fracture. A strong effect of the carbide mean grain size on the size and shape of these pits, and accordingly on strength degradation was evidenced. On one hand, medium-sized hardmetals exhibit semi-elliptical corrosion pits. On the other hand, corrosion in ultrafine grades is characterized by a heterogeneous surface layer, where localized sharp corrosion pits form at the corrosion front. In this sense, after the dissolution of the cobalt directly exposed to the media, the oxidation for ultrafine grades continues within the pit itself. The pits downward growth evidenced for ultrafine grades is speculated to be related to several interacting factors: shorter path between center of binder pools and carbide/binder interface together with higher surface area of interfaces as grain size decreases, gravity effects and a synergic increase of [Cl-] concentration at sharper pits of angular corrosion pits as they grows. Consequently, the formation of such defects could induce a decrease in service life due to their effect as stress concentrators for crack initiation and growth. Some examples are shown in **Figure 7**, corresponding to short and long immersion times, for the investigated 15UF, 15M and 11M hardmetals.

Concerning microstructural effects on strength degradation, the ultrafine-sized studied grades are much more affected by corrosion damage than medium-sized ones. Indeed, they exhibit strength losses of about a 30% after immersion time of 3 days, increasing up to values close to a 50% for longer exposure times. Critical corrosion damage is characterized by a selective attack of the metallic binder that leaves a WC skeleton surface layer [12,13,39,40]. Fractographic examination reveals that for the ultrafine grades,

depth of the corrosion front increases as immersion time into the corrosive media gets longer. Nonetheless, the corrosion front is not homogeneous and localized corrosion pits at the interface between the corrosion front and the un-corroded surface were discerned. Clear examples of such phenomena are given in **Figure 7**. The formation of these corrosion features is of crucial importance for determining effective strength degradation, as they act as preferential sites for crack nucleation and extension [8]. However, as immersion time increases, the ratio between the pit depth and the thickness of the damaged layer decreases. As a consequence, the stress concentration role played by corrosion pits gets geometrically lessened. This fact explains the lower relative changes observed in retained strength for long exposure times.

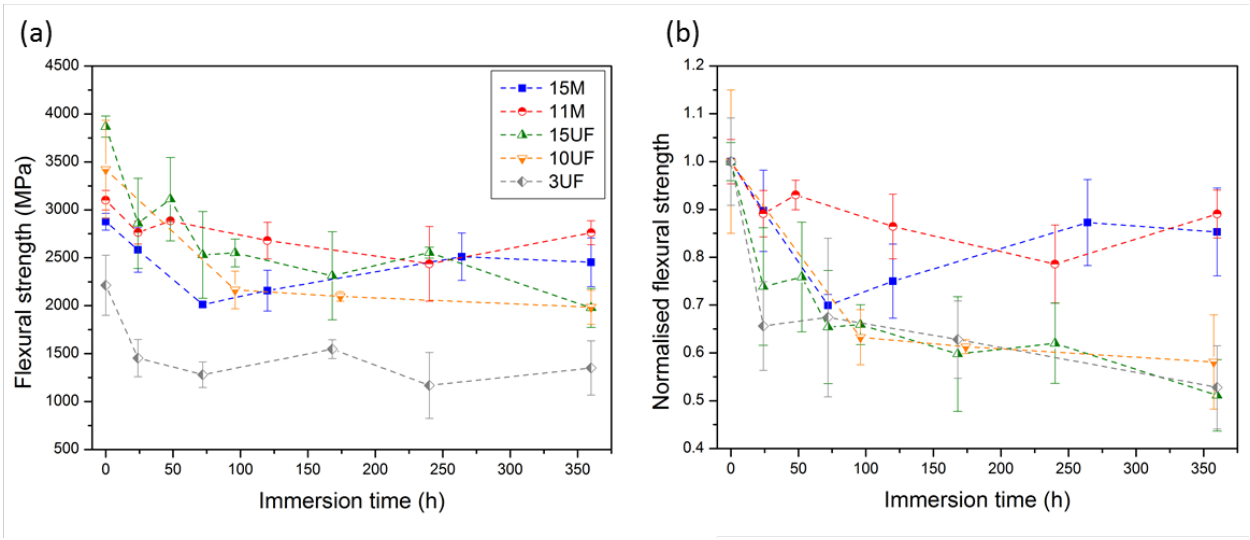

Figure 6. (a) Retained strength and (b) normalized retained strength as a function of corrosion time in the stirred corrosive media for the materials here studied. Strength of non-corroded specimens is used as reference baseline.

Corrosion damage is less critical for the 15M investigated grade and its strength is retained up to 80% level for long immersion times. Two aspects should be considered for explaining the differences found between 15UF and 15M specimens. First, for similar binder content, the medium-sized grade is tougher, and thus a higher damage-tolerance level is to be expected [24,41,42]. Hence, as binder mean free path increases, and likewise fracture toughness, damage mode shifts from fracture to deformation controlled, increasing the tolerance to presence of critical damage [24]. Second, the geometry of corrosion induced critical damage is significantly different for both materials, as it is clearly evidenced in **Figure 7**. In the case of the 15M hardmetal, critical corrosion damage consists of surface semi-elliptical corrosion pits. The depth of these pits slowly growths as immersion time increases. However, this is not the case for their length, which increases with corrosion time. Thus, as exposure time gets longer, the ellipse eccentricity of corrosion induced pits increases. It should be noted that this fact relates to the stabilization of the residual strength of the 15M grade for long immersion times. In agreement with previous

experiments carried out in acidic solutions, binder surface area distribution plays a decisive role on the corrosion behavior of cemented carbides [39]. For hardmetals with large binder mean free paths corrosion develops homogenously at the surface. On the other hand, corrosion becomes localized when the exposed area to corrosive media is reduced (i.e. ultrafine cemented carbides).

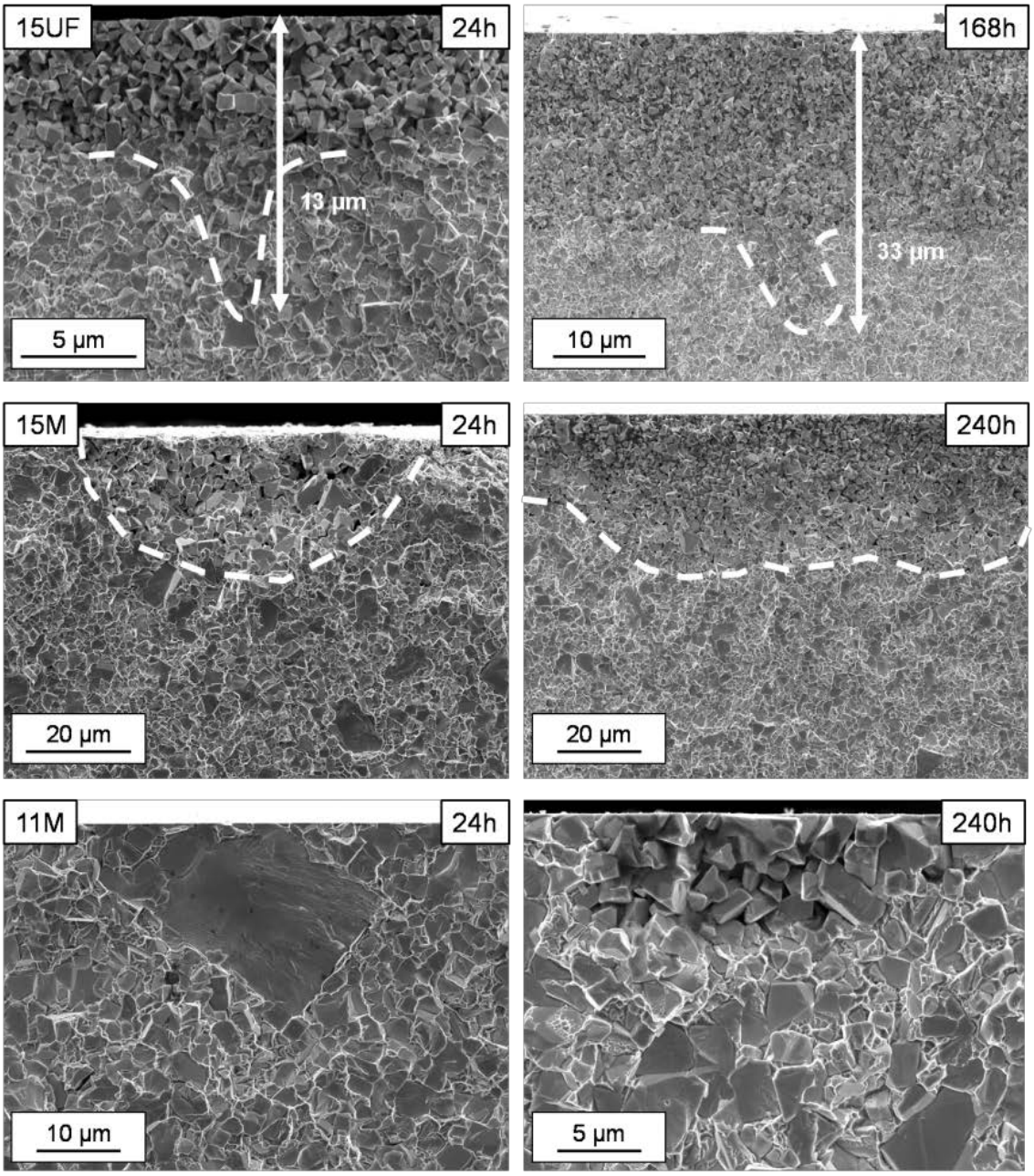

Figure 7. Critical corrosion damage promoting failure for different corrosion times the 15UF, 15M and 11M investigated WC-Co cemented carbides.

The strength of the 11M grade is barely reduced due to corrosion damage. In fact, identified critical flaws for short exposure times were mainly not corrosion-related, but rather pre-existing flaws inherent to

the manufacturing process (**Figure 7**). Therefore, in such cases corrosion pits were less critical than pre-existing manufacturing defects and the strength was evidently retained. For longer corrosion times, semi-elliptical corrosion flaws were discerned (**Figure 7**). Thus, it could be concluded that 11M hardmetal exhibits the best compromise between corrosion resistance and damage tolerance.

3.3. 3D FIB/FESEM characterization of corrosion-induced damage

A detailed characterization of corrosion damage was conducted by means of the FESEM/FIB technique for the 15M hardmetal after being immersed for 7 (168h) and 15 (360h) days in the corrosive medium. Examples of obtained micrographs after the application of image processing techniques showing corrosion damage-microstructure interactions are shown in **Figure 3** for both investigated conditions. In **Figure 8** such phases were segmented and appear as yellow (WC carbides), blue (cobalt), green (corroded cobalt) and red (microcracks). The whole 3D reconstructed volume for both analysed conditions is shown in **Figure 9**. In addition, an illustrative **video** detailing the 3D FIB/FESEM reconstruction, segmentation and analysis process is provided. To access to the **video** component, simply click the image visible below (online version only). From the observation of these figures and the video, corrosion damage may be described by a selective attack of the metallic binder consisting on the nucleation of microcracks, probably associated with binder dissolution [12,13,39,40] and the formation of new cobalt phases [9,15,39]. As immersion time increases, corrosion damage evolves form microcrack formation to vast binder leaching, the latter resulting then in unsupported carbide grains throughout the affected surface (see **Figure 10**).

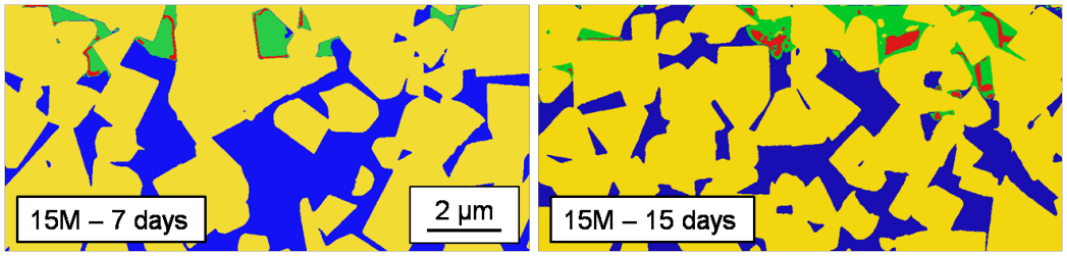

Figure 8. Filtered and segmented FESEM micrographs attained by FIB tomography, four phases were identified: WC carbides (yellow), metallic binder (blue), attacked cobalt (green) and microcracks (red).

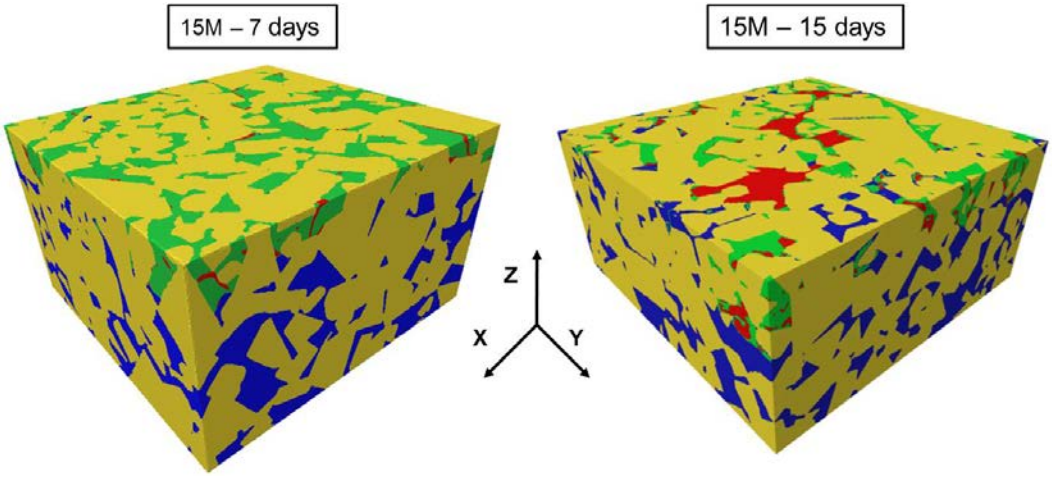

Figure 9. 3D reconstructed image describing corrosion damage-microstructure interactions for the 15M hardmetal here studied (after 7 and 15 days of exposure time).

The direct inspection of transversal cut micrographs indicates that corrosion process is mainly the result of selective dissolution of metallic binder, which initially is located at the centre of the binder pools and growth towards the carbide/binder interface. Thus, corrosion induced microcracks were mostly observed in the core of binder pools rather than at binder/carbide interfaces (e.g. **Figure 10**). With the purpose of obtaining a qualitative estimation of this fact, and in order to study the evolution of corrosion damage-microstructure interactions as immersion time gets longer, the R_c index was proposed:

$$R_c = \frac{A_{m/Co}}{A_{m/WC}} \qquad (2)$$

where $A_{m/Co}$ and $A_{m/WC}$ are the contact areas between the microcracks and the cobalt binder (**Figure 10b**) and the WC phase (**Figure 10c**), respectively. Therefore, R_c index takes high values if the microcracks are mainly concentrated at the binder pools centres without direct contact with the WC skeleton. Current estimates yield R_c values of 74 and 16 for 7 and 15 immersion days, respectively. As expected, high R_c values were obtained, confirming above presented ideas. Interesting, R_c decreases as immersion time gets longer for the 15M hardmetal, indicating that corrosion damage nucleates at the binder pool cores but expands in the radial direction as corrosion time increases. It validates the above presented ideas.

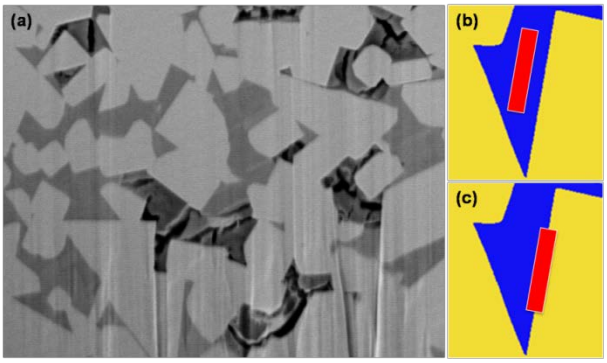

Figure 10. (a) Micrograph detailing the formation of microcracks within the binder; images illustrating (b) microcracks/binder and (c) microcracks/carbides contact areas.

From the observation of obtained micrographs, and according to previous investigations (e.g. Ref. [13,40]), it is evident that the binder phase controls the corrosion behaviour of WC-Co composites. It is therefore reasonable to assume the binder itself, the corroded binder and the microcrack 'phases' as the pertinent features for describing corrosion damage–microstructure interactions in hardmetals. With this purpose, a study of the relative distribution and interconnectivity degree of those phases was attempted by means of the image analysis technique of skeletonization. This process involves the simplification of the phase of interest by transforming it in filaments whose diameter and colour are related to its local size. In this study, local regions corresponding to large volumes occupied at the small length scale are characterized by thick ligaments coloured in red. Conversely, if presence of the phase at the local level becomes scarcer, cords become thinner and blue. This enables the assessment of certain distribution properties such as the interconnectivity degree and the length and local thickness of each phase. The skeleton of the binder, the attacked binder (i.e. corresponding to the addition of the corroded binder and the corrosion-induced microcracked phases) and of the corrosion-induced microcracked phases is shown in **Figure 11**. A first observation reveals a long range and fully interconnected cobalt binder, whereas the microcracked phase forms short range and locally interconnected networks. These results indicate that the binder phase is composed by a single group (i.e. the cobalt phase is fully interconnected), suggesting that WC and binder phases form two networks that are fully interconnected. This perfectly interpenetrated structure is attributable to the very low interfacial energy, excellent wetting and very good adhesion for the WC and Co couple, and is the main reason for explaining the outstanding fracture toughness levels exhibited by cemented carbides [42,43].

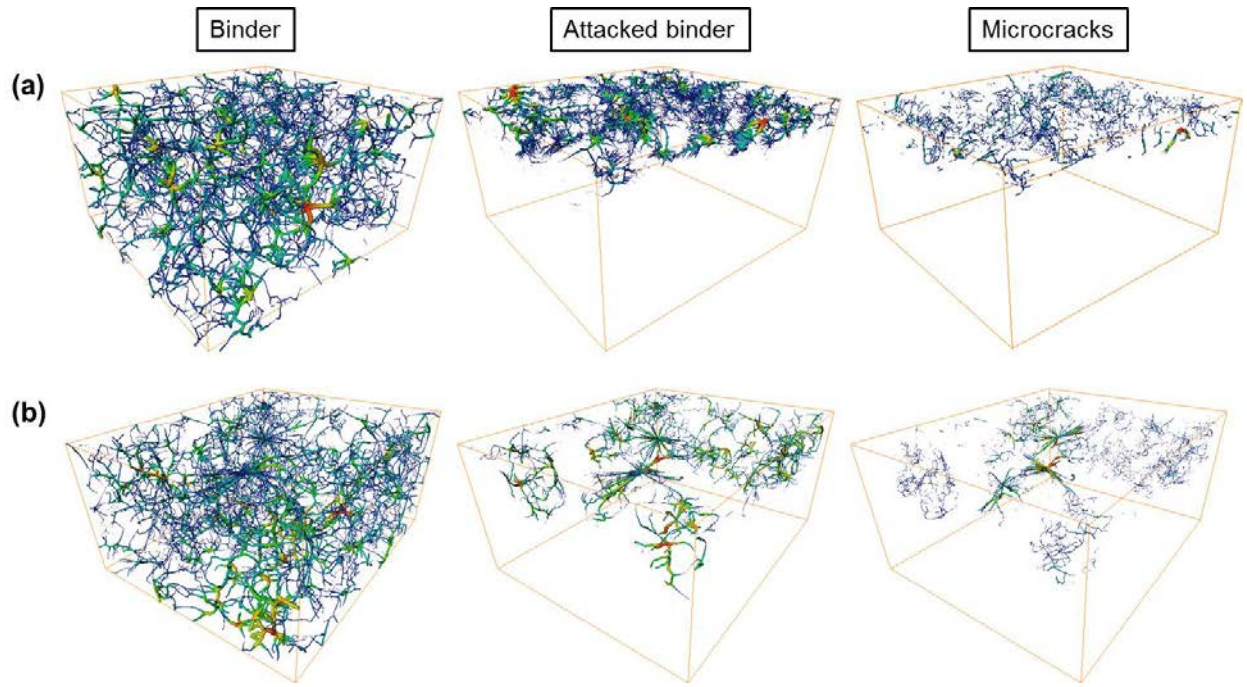

Figure 11. Skeletonization of the binder, attacked binder and microcrack phases for the reconstructed volumes corresponding to the 15M samples immersed for 7 (a) and 15 (b) days.

4. Conclusions

In this study the influence of microstructure on the tolerance to damage induced by corrosion in WC-Co cemented carbides has been investigated. Corrosion media used was an agitated mine water solution, and damage tolerance was assessed on the basis of the retained strength after corrosion exposure. The investigation also included a characterization of corrosion damage-microstructure interactions by means of the 3D FIB/FESEM technique. Based on obtained results, the following conclusions may be drawn:

1. Strong microstructural effects on the corrosion behaviour of cemented carbides when immersed in a synthetic mine water solution were evidenced. A pseudopassive behaviour was determined for ultrafine grades which slightly decreases corrosion rates due to a limitation of the diffusion of cobalt from the surface. Medium grain sized hardmetals do not exhibit this pseudopassive regime.

2. Corrosion damage may result in relevant strength degradation in cemented carbides. However, relative changes in residual strength become less pronounced with exposure time, as corrosion damage gets homogenized. Within this context, the microstructure plays a principal role in defining the effective tolerance to the induced damage level.

3. Strength loss associated with corrosion damage is rationalized on the basis of stress raising effects related to corrosion pits. Semi-elliptical and sharp angular corrosion pits were identified as critical corrosion damage for medium- and ultrafine-sized hardmetals, respectively. The latter have much more pronounced stress rising effects and consequently, ultrafine graded cemented carbides exhibit higher strength losses in the presence of corrosion damage.

4. 3D FIB/FESEM tomography reveals localized corrosion pits with variable and partial interconnectivity (as a function of depth). Corrosion damage starts at the center of the binder pools by microcracking. Microcracks growth with exposure time in radial directions resulting in pronounced binder removal, which finally leaves a WC skeleton.

Bibliography

[1] H.E. Exner, Physical and chemical nature of cemented carbides, Int. Met. Rev. 24 (1979) 149–173.

[2] B. Roebuck, E.A. Almond, Deformation and fracture processes and the physical metallurgy of WC–Co hardmetals, Int. Mater. Rev. 33 (1988) 90–110.

[3] G.S. Upadhyaya, Materials science of cemented carbides - an overview, Mater. Des. 22 (2001) 483–489.

[4] G.S. Upadhyaya, Cemented tungsten carbides: production, properties, and testing, Noyes Publications, New Jersey, USA, 1998.

[5] L. Prakash, Fundamentals and general applications of hardmetals, in: V.K. Sarin, D. Mari, L. Llanes (Eds.), Compr. Hard Mater., Elsevier, UK, 2014: pp. 29–90.

[6] V.A. Tracey, Nickel in hardmetals, Int. J. Refract. Met. Hard Mater. 11 (1992) 137–149.

[7] U. Beste, T. Hartzell, H. Engqvist, N. Axén, Surface damage on cemented carbide rock-drill buttons, Wear. 249 (2001) 324–329.

[8] V.A. Pugsley, G. Korn, S. Luyckx, H.G. Sockel, W. Heinrich, M. Wolf, H. Feld, R. Schulte, The influence of a corrosive wood-cutting environment on the mechanical properties of hardmetal tools, Int. J. Refract. Met. Hard Mater. 19 (2001) 311–318.

[9] V.A. Pugsley, H.-G. Sockel, Corrosion fatigue of cemented carbide cutting tool materials, Mater. Sci. Eng. A. 366 (2004) 87–95.

[10] R. Lu, L. Minarro, Y.-Y. Su, R.M. Shemenski, Failure mechanism of cemented tungsten carbide dies in wet drawing process of steel cord filament, Int. J. Refract. Met. Hard Mater. 26 (2008) 589–600.

[11] W.J. Tomlinson, C.R. Linzell, Anodic polarisation and corrosion of cemented carbides with cobalt

and nickel binders, J. Mater. Sci. 23 (1988) 914–918.

[12] A.M.M. Human, H.E. Exner, The relationship between electrochemical behaviour and in-service corrosion of WC based cemented carbides, Int. J. Refract. Met. Hard Mater. 15 (1997) 65–71.

[13] S. Hochstrasser(-Kurz), Y. Mueller, C. Latkoczy, S. Virtanen, P. Schmutz, Analytical characterization of the corrosion mechanisms of WC–Co by electrochemical methods and inductively coupled plasma mass spectroscopy, Corros. Sci. 49 (2007) 2002–2020.

[14] D.S. Konadu, J. van der Merwe, J.H. Potgieter, S. Potgieter-Vermaak, C.N. Machio, The corrosion behaviour of WC-VC-Co hardmetals in acidic media, Corros. Sci. 52 (2010) 3118–3125.

[15] H. Engqvist, U. Beste, N. Axén, The influence of pH on sliding wear of WC-based materials, Int. J. Refract. Met. Hard Mater. 18 (2000) 103–109.

[16] F.J.J. Kellner, H. Hildebrand, S. Virtanen, Effect of WC grain size on the corrosion behavior of WC–Co based hardmetals in alkaline solutions, Int. J. Refract. Met. Hard Mater. 27 (2009) 806–812.

[17] A.J. Gant, M.G. Gee, A.T. May, The evaluation of tribo-corrosion synergy for WC–Co hardmetals in low stress abrasion, Wear. 256 (2004) 500–516.

[18] M.R. Thakare, J.A. Wharton, R.J.K. Wood, C. Menger, Exposure effects of alkaline drilling fluid on the microscale abrasion–corrosion of WC-based hardmetals, Wear. 263 (2007) 125–136.

[19] A.J. Gant, M.G. Gee, D.D. Gohil, H.G. Jones, L.P. Orkney, Use of FIB/SEM to assess the tribo-corrosion of WC/Co hardmetals in model single point abrasion experiments, Tribol. Int. 68 (2013) 56–66.

[20] P. Kenny, The application of fracture mechanics to cemented tungsten carbides., Powder Metall. 14 (1971) 22–38.

[21] H. Suzuki, K. Hayashi, The strength of WC–Co cemented carbide in relation to structural defects, Trans. Japan Inst. Met. 16 (1975) 353–360.

[22] B. Casas, X. Ramis, M. Anglada, J.M. Salla, L. Llanes, Oxidation-induced strength degradation of WC–Co hardmetals, Int. J. Refract. Met. Hard Mater. 19 (2001) 6–12.

[23] B. Casas, Y. Torres, L. Llanes, Fracture and fatigue behavior of electrical-discharge machined cemented carbides, Int. J. Refract. Met. Hard Mater. 24 (2006) 162–167.

[24] A. Góez, D. Coureaux, A. Ingebrand, B. Reig, E. Tarrés, A. Mestra, A. Mateo, E. Jiménez-Piqué, L. Llanes, Contact damage and residual strength in hardmetals, Int. J. Refract. Met. Hard Mater. 30 (2012) 121–127.

[25] W.J. Tomlinson, I.D. Molyneux, Corrosion, erosion-corrosion, and the flexural strength of WC–Co hardmetals, J. Mater. Sci. 26 (1991) 1605–1608.

[26] W.J. Przybylowicz, S.B. Luyckx, J.I.W. Watterson, Proton microprobe investigation of the causes of pitting in cemented tungsten carbide, Nucl. Instruments Methods Phys. Res. Sect. B Beam Interact. with Mater. Atoms. 79 (1993) 428–431.

[27] J.M. Tarragó, G. Fargas, E. Jimenez-Piqué, A. Felip, L. Isern, D. Coureaux, J.J. Roa, I. Al-Dawery, J. Fair, L. Llanes, Corrosion damage in WC–Co cemented carbides: residual strength assessment and 3D FIB-FESEM tomography characterisation, Powder Metall. 57 (2014) 324–330.

[28] K.P. Mingard, H.G. Jones, M.G. Gee, B. Roebuck, A. Gholinia, B. Winiarski, P. Withers, 3D Imaging of structures in bulk and surface modified WC-Co hardmetals, in: Proceedings Euro PM 2012, EPMA, Basel, 2012: pp. 155–160.

[29] I. Borgh, P. Hedström, J. Odqvist, A. Borgenstam, J. Ågren, A. Gholinia, B. Winiarski, P. Withers, G.E. Thompson, K.P. Mingard, M.G. Gee, On the three-dimensional structure of WC grains in cemented carbides, Acta Mater. 61 (2013) 4726–4733.

[30] J.M. Cairney, P.R. Munroe, J.H. Schneibel, Examination of fracture surfaces using focused ion beam milling, Scr. Mater. 42 (2000) 473–478.

[31] U. Beste, E. Coronel, S. Jacobson, Wear induced material modifications of cemented carbide rock drill buttons, Int. J. Refract. Met. Hard Mater. 24 (2006) 168–176.

[32] J.M. Tarragó, E. Jimenez-Piqué, M. Turón-Viñas, L. Rivero, I. Al-Dawery, L. Schneider, L. Llanes, Fracture and fatigue behavior of cemented carbides: 3D Focused Ion Beam Tomography of crack-microstructure interactions, Int. J. Powder Metall. 50 (2014) 1–10.

[33] J.M. Tarragó, D. Coureaux, Y. Torres, F. Wu, I. Al-Dawery, L. Llanes, Implementation of an effective time-saving two-stage methodology for microstructural characterization of cemented carbides, Int. J. Refract. Met. Hard Mater. 55 (2016) 80–86.

[34] C.N. Machio, D.S. Konadu, J.H. Potgieter, S. Potgieter-Vermaak, J. Van der Merwe, Corrosion of WC-VC-Co Hardmetal in Neutral Chloride Containing Media, ISRN Corros. 2013 (2013) 506759.

[35] Y. Torres, D. Casellas, M. Anglada, L. Llanes, Fracture toughness evaluation of hardmetals: influence of testing procedure, Int. J. Refract. Met. Hard Mater. 19 (2001) 27–34.

[36] W.J. Tomlinson, N.J. Ayerst, Anodic polarization and corrosion of WC–Co hardmetals containing small amounts of Cr_3C_2 and/or VC, J. Mater. Sci. 24 (1989) 2348–2352.

[37] S. Sutthiruangwong, G. Mori, R. Kösters, Passivity and pseudopassivity of cemented carbides, Int. J. Refract. Met. Hard Mater. 23 (2005) 129–136.

[38] G. Mori, H. Zitter, A. Lackner, M. Schretter, Influencing the corrosion resistance of cemented carbides by addition of Cr_3C_2, TiC and TaC, in: G. Kneringer, P. Rödhammer, H. Wildner (Eds.), Proceedings of the 15th international Plansee seminar, 2001: pp. 222–236.

[39] S. Sutthiruangwong, G. Mori, Corrosion properties of Co-based cemented carbides in acidic solutions, Int. J. Refract. Met. Hard Mater. 21 (2003) 135–145.

[40] S. Hochstrasser-Kurz, D. Reiss, T. Suter, C. Latkoczy, D. Günther, S. Virtanen, P.J. Uggowitzer, P. Schmutz, ICP-MS, SKPFM, XPS, and microcapillary investigation of the local corrosion mechanisms of WC–Co hardmetal, J. Electrochem. Soc. 155 (2008) 415–426.

[41] Y. Torres, R. Bermejo, F.J. Gotor, E. Chicardi, L. Llanes, Analysis on the mechanical strength of WC-Co cemented carbides under uniaxial and biaxial bending, Mater. Des. 55 (2014) 851–856.

[42] J.M. Tarragó, D. Coureaux, Y. Torres, D. Casellas, I. Al-Dawery, L. Schneider, L. Llanes, Microstructural effects on the R-curve behavior of WC-Co cemented carbides, Mater. Des. 97 (2016) 492–501.

[43] L.S. Sigl, H.E. Exner, Experimental study of the mechanics of fracture in WC–Co alloys, Metall. Trans. A. 18A (1987) 1299–1308.

Annex II

Additional Contributions

Work presented in conferences

Oral contributions

- Roa JJ, Jimenez-Pique E, **Tarragó JM** and Llanes L. *Micromechanics of WC–Co composites*. In: 9th European Solid Mechanics Conference, Madrid, Spain, 6-10 July 2015.

- **Tarragó JM**, Schneider L, Al-Dawery I and Llanes L. *Microstructural influence on the fatigue behaviour of cemented carbides*. In: V Congreso Nacional de Pulvimetalurgia, Girona, Spain, 1-3 July 2015.

- **Tarragó JM**, Fargas G, Jiménez-Piqué E, Felip A, Isern L, Coureaux D, Al-Dawery I, Fair J and Llanes L. *Corrosion damage in WC–Co cemented carbides: Residual strength assessment and 3D FIB-FESEM tomography characterization*. In: EuroPM2014, Salzburg, Austria, 21-24 September 2014. ***(Keynote paper)***

- **Tarragó JM**, Serra I, Al-Dawery I and Llanes L. *Residual strength of WC–Co cemented carbides after being subjected to abrupt temperature changes*. In: CIEC14, 14th European Inter-regional Conference on Ceramics, Stuttgart, Germany, 8-10 September 2014.

- Jiménez-Piqué E, **Tarragó JM**, Turón-Viñas M, Fargas G, Al-Dawery L, Schneider L and Llanes L. *Characterization by 3D SEM/FIB tomography of cracks and damage in hardmetals*. In: 2nd International Conference on 3D Material Science, Annecy, France, 29 June – 3 July 2014.

- Roa JJ, Verge C, Jimenez-Pique E, **Tarragó JM** and Llanes L. *Anisotropía plástica y mecanismos de deformación activados mediante nanoindentación en granos de WC*. In: XIII Congreso Nacional de Materiales, Barcelona, Spain, 18-20 June 2014.

- **Tarragó JM**, Jiménez-Piqué E, Turón-Viñas M, Rivero L, Schneider L and Llanes L. *Fracture and Fatigue Behavior of Cemented Carbides: 3-D FIB Tomography of Crack-Microstructure Interactions*. In: World Congress on Powder Metallurgy & Particulate Materials, Orlando, USA, 18-22 May 2014. ***(Best paper award)***

- **Tarragó JM**, Roa JJ, Valle V, Marshall JM and Llanes L. *Fracture and fatigue behavior of WC–Co and WC–CoNi cemented carbides*. In: 10th International Conference on the Science of Hard Materials, Cancun, México, 10-14 March 2014.

- Roa JJ, Jimenez-Pique E, **Tarragó JM**, Zivcec M, Broeckmann C and Llanes L. *Study by AFM and EBSD of plastic deformation mechanisms induced by nanoindentation in a hardmetal binder-like cobalt alloy*. In: Proceedings of the IV Conference on Nanomechanical Testing in Materials Research and Development, Olhao, Portugal, 6-11 October 2013.

- **Tarragó JM**, Jiménez-Piqué E, Turón M, Rivero L, Schneider L and Llanes L. *Toughening and fatigue micromechanisms in hardmetals: SEM/FIB tomography characterization*. In: 18th Plansee Seminar, Reutte, Austria, 3-7 June 2013.

Poster contributions

- **Tarragó JM**, Dorvlo S, Al-Dawery I and Llanes L. *Strength degradation of cemented carbides due to thermal shock*. In: EuroPM2015, Reims, France, 4-7 October 2015.

- **Tarragó JM**, Rizki Z, Schneider L and Llanes L. *Application of image processing and analysis techniques for microstructural characterization of cemented carbides*. In: EuroPM2013, Gothenburg, Sweden, 15-18 September 2013.

- **Tarragó JM**, Ferrari C, Reig B, Coureaux D, Schneider L and Llanes L. *Fatigue behavior of a WC-Ni Cemented Carbide*. In: 18th Plansee Seminar, Reutte, Austria, 3-7 June 2013.

- **Tarragó JM**, Jimenez-Pique E and Llanes L. *3-D Characterization by SEM/FIB tomography of multiligament zones at the crack tip of cemented carbides*. In: 7th EEIGM International Conference on Advanced Materials Research, Luleå, Sweden, 21-22 March 2013.

- **Tarragó JM**, Mir J, Mestra A, Heredero F, Martínez R, Rodríguez R and Llanes L. *Surface damage on PVD TiN and CrN coatings under monotonic and cyclic spherical indentation*. In: CIEC13, 13th European Inter-regional Conference on Ceramics, Barcelona, Spain, 12-14 September 2012.

Additional articles published in International Journals

- **Tarragó JM**, Torres Y, Coureaux D, Wu F, Al-Dawery I and Llanes L. *Implementation of an effective time-saving two-stage methodology for microstructural characterization of cemented carbides.* International Journal of Refractory Metals and Hard Materials 55, (2016) 80–86.

- Roa JJ, Jiménez-Piqué E, **Tarragó JM**, Zivcec M, Broeckmann C and Llanes L. *Intrinsic hardness of constitutive phases in WC–Co composites: Nanoindentation testing, statistical analysis, WC crystal orientation effects and flow stress for the constrained metallic binder*. Journal of the European Ceramic Society 35 [13], (2015) 3419–3429.

- Roa JJ, Jiménez-Piqué E, **Tarragó JM**, Zivcec M, Broeckmann C and Llanes L. *Berkovich nanoindentation and deformation mechanisms in a hardmetal binder-like cobalt alloy*. Materials Science Engineering A 621, (2014) 28–32.

- Torres Y, **Tarragó JM**, Coureaux D, Tarrés E, Roebuck B, Chan P, James M, Liang B, Tillman M, Viswanadham RK, Mingard KP, Mestra A and Llanes L. *Mechanics and mechanisms of crack growth resistance under monotonic and cyclic loading.* International Journal of Refractory Metals and Hard Materials 45, (2014) 179–88.